REDUCTION KINETICS OF IRON ORE CONCENTRATE PARTICLES RELEVANT TO A NOVEL GREEN IRONMAKING PROCESS

by

Haitao Wang

A dissertation submitted to the faculty of
The University of Utah
in partial fulfillment of the requirements for the degree of

Doctor of Philosophy

Department of Metallurgical Engineering

The University of Utah

August 2011

The University of Utah Graduate School

STATEMENT OF DISSERTATION APPROVAL

The dissertation of **Haitao Wang**

has been approved by the following supervisory committee members:

Hong Yong Sohn	, Chair	**5/3/2011** Date Approved
Zhigang Zak Fang	, Member	**5/3/2011** Date Approved
Michael S. Moats	, Member	**5/3/2011** Date Approved
Hang Goo Kim	, Member	**5/3/2011** Date Approved
Edward M. Trujillo	, Member	**5/3/2011** Date Approved

and by **Jan D. Miller** , Chair of

the Department of **Metallurgical Engineering**

and by Charles A. Wight, Dean of The Graduate School.

ABSTRACT

A novel green ironmaking technology is under development at the University of Utah. This technology produces iron directly from fine magnetite concentrates by the suspension reduction by gaseous reductants. The direct use of concentrates allows bypassing the problematic pelletization/sintering and cokemaking steps in conventional blast furnace ironmaking. Hydrogen is the main reducing agent for high reactivity and for reduced carbon dioxide release during ironmaking. Feasibility tests indicated that high reduction degrees above 90% could be achieved within several seconds by this method.

The purpose of this research was to determine comprehensive kinetics of the suspension reduction reaction of magnetite concentrate particles by hydrogen. Experiments were carried out in the temperature range of 1150 - 1400℃ with other experimental variables being hydrogen partial pressure and particle size. The nucleation-and-growth kinetics expression was found to describe the reduction rate in this study. In order to obtain a complete rate expression, a series of experiments were conducted to determine the functional dependence of the rate on partial pressures of hydrogen and water vapor, particle size, and then activation energy value.

The residence time was varied by changing the total gas flowrate. It was determined that the reduction rate has 1/2-order dependence with respect to hydrogen partial pressure. The effect of particle size factor changed with temperature. The reduction rate increased with particle size at 1150℃ and 1200℃, but the effect of

particle size was negligible when reduction temperature was above 1300℃. The activation energy was 464 kJ/mol, indicating that this reaction has a greater dependence on temperature than most reactions. Finally, a complete reaction rate expression was formulated.

Hydrogen is best as a reductant and/or fuel from the environmental and reduction kinetics points of view, but it is currently expensive. Instead, syngas which is mainly composed of H_2 and CO from the reforming of natural gas or coal gasification has been used as a reducing gas mixture for the majority of direct reduction processes. CO was added to replace H_2 and N_2 in the reducing gas mixture to examine the effect of CO addition on the reduction rate on the base of the experimental conditions examined in the kinetics measurement. It was determined that the pure hydrogen reduction was much faster than the syngas reduction. When nitrogen was replaced by CO, the reduction rate increased significantly.

TABLE OF CONTENTS

APPENDICES

LIST OF FIGURES

LIST OF TABLES

CHAPTER 1

INTRODUCTION

1.1 Background

More than 90% of iron is currently produced by the blast furnace (BF) process, while the balance is produced by the Direct Reduction (DR) processes (Wordsteel Committee on Economic Studies, 2010). Despite the improvements in the modern BF processes such as increasing campaign life and productivity, decreasing coke consumption, developing better cokemaking processes, increasing coal injection, and injecting natural gas and plastics, and the fact that the blast furnace is a highly energy efficient and chemically efficient reactor, it still suffers from drawbacks. The process requires the iron ore feed in the form of sinters or pellets and coke produced from high-grade coking coal. Also, the BF process is highly capital and energy intensive, requiring large-scale infrastructure and operation. Those constraints limit the flexibility of the BF process in terms of operation and choice of materials (Chatterjee, 1993). Thus, BF iron production is projected to decrease significantly in the future (Fruehan, 1998). The main factors for this are environmental regulations (Ritt, 2000) and high capital investment cost.

Accordingly, a number of new ironmaking technologies have been developed or are under development (Lockwood Greene Technologies, 2000). Most of these processes, however, are not sufficiently intensive to replace the blast furnace because they cannot be

operated at high temperatures due to the sticking and fusion of particles. Especially, the shaft furnace processes, which are dominant types among others, require pelletization of iron oxide concentrates accompanied with additional cost and environmental problems, and also suffer from pellet disintegration problems.

Therefore, a new technology is under development to produce iron directly from fine concentrates by a gas-solid suspension process, which would be more energy efficient than the blast furnace and drastically lower environmental pollution, especially CO_2 emission, from the steel industry (Sohn, 2007). This is accomplished by adopting H_2-based reductant, together with bypassing pelletization/sintering and cokemaking steps in typical ironmaking processes. Unlike other gas-based alternative ironmaking processes based on shaft furnaces or fluidized-bed reactors, the suspension reduction process is highly intensive because it will not suffer from the problems of particle sticking and fusion that other processes do when operated at high temperatures. Low-temperature disintegration problems encountered in the processes using pellets also will not be present. Therefore, a suspension reduction process presents a high potential for high-intensity alternative ironmaking.

CHAPTER 2

LITERATURE REVIEW AND RESEARCH OBJECTIVES

The present work is a study of reduction kinetics of fine iron ore concentrate particles relevant to a novel green ironmaking process, i.e. gas-solid suspension ironmaking technology. The literature review is primarily concerned with the reduction of iron oxide concentrate particles in the presence of gaseous reductant, H_2, CO and CH_4. Typical research on the gaseous reduction of iron oxide in the form of pellet or sinter whose sizes are much larger than the size of the single fine concentrate particle will not be reviewed.

2.1 Reduction Kinetics of Concentrate Particles by H_2

Themelis and Gauvin (1962a, 1963) derived a rate equation from the published data of twenty independent studies on the reduction of iron oxide particles by hydrogen, for forty particle sizes ranging from 70 to 42000 μm in diameter. Those data were obtained at temperatures of 600 - 1000℃ under conditions of negligible boundary layer resistance to gas transport. Despite the differences in iron oxides tested, the experimental data were in good agreement with the following equation:

$$\frac{[1-(1-X)^{1/3}]\cdot d_p}{t} = 0.15 \cdot \exp\left(-\frac{3000}{RT}\right) \qquad (1)$$

where X is the reduction degree; d_p is the particle size, μm; t is time, sec.; R is the gas-constant, 1.987 cal·mol^{-1}·K^{-1}; T is reduction temperature, K.

The hydrogen reduction of iron oxide was conducted in a gas-conveyed system (Themelis and Gauvin, 1962b). The reactor consisted of a 4.4 in ID X 8.5 ft long tube made of 330 stainless steel, 3/8-in thick, and was supported in a vertical position. The particle size of ferric oxide made from carbonyl iron varied from 5 to 102 μm. The experiments were carried out in the temperature range of 500 - 1100℃ in 1 - 12 seconds. The results obtained during reduction of the larger moving particles confirmed further the validity of the rate equation (1). On the other hand, for particles below 31 μm, this rate equation does not satisfy the experimental results. And the evidence supplied by the electron microscope study supported the theory that the reduction was initiated on the surface of the particles.

Ezz and Wild (1960) reduced fine hematite particles of various sizes (50 - 260 μm). The particles were reduced while suspended as a dispersed cloud in a reducing gas. They found that 80% reduction could be achieved between 20 and 30 seconds in the temperature range of 700 - 1100℃. An increase in temperature exerts a major influence on increasing reduction rate, while ore characteristics, such as porosity, shape factor, and surface condition also affected reduction rate. The concentration of water vapor in the reducing gas which depends on the ore/gas ratio has a major influence on the reduction rate. The time for 100% reduction increased with partial pressure of water vapor in the reducing gas. The reduction rate was almost independent of the kind and the size of ores.

Davis and Feld (1972) studied the flash reduction of fine low grade iron ore (monosized by passing 100, 200 or 400 mesh size) by hydrogen and reformed natural gas

in a dilute phase system at 500 - 900℃ within a heated stainless steel tubular coil. Concurrently flowing with the reducing gases, Alabama brown iron ore and Mesabi semitaconite ore were observed to be reduced rapidly. Although the maximum reduction extent was 77% by hydrogen, the possibility to increase the rate by increasing temperature was anticipated in their report.

Hydrogen reduction of very fine powder of pyrite cinder and a fine hematite ore were examined in a gas conveyed system (Ozawa and Tanaka, 1973). The pyrite cinder contained 57% total iron and the mean particle diameter was about 15 μm. It was reduced with different feeding rates at 750 - 950℃. At 750℃, the reduction degree reached 38% in 4 seconds when the feeding rate was 1.4 g/min and decreased to 32% in 4 seconds when the feeding rate of ore was increased to 21 g/min. When the temperature was raised to 950℃, above 90% reduction was achieved in 2.5 seconds at a feeding rate of 0.7 g/min. The ratio of solid feeding rate S (g/min) to the gas feeding rate G (Nl/min) was chosen as an index of solid concentration. At a relatively low temperature (750℃), the feeding rate did not show any remarkable effect on the reduction rate. About 40% reduction was achieved in 4 seconds at the S/G range of 0.1 - 0.9. At 950℃, the reduction degree decreased from 90% to 76% in 2.3 seconds when S/G ratio was increased from 0.1 to 0.5. The effect of water vapor on the rate of reduction was also examined. Gas conveyed reduction of fine ore seemed to proceed as a 2nd-order reaction with respect to the fraction unreduced when the concentrate of solid was dilute, and the relation between the rate constant and partial pressure of water vapor was formulated as a linear equation.

In order to simulate the gaseous reduction of liquid iron oxide in the lower part of a blast furnace or the smelting reduction processes, a laboratory scale fine particles-gas

conveyed system was utilized to measure the reduction rates of liquid wustite particles with hydrogen at 1450 - 1550℃(Hayashi and Iguchi, 1994). Wustite particles of 53 - 63 μm were prepared after chemical reagent Fe_2O_3 was reduced, melted by arc heating under argon, crushed, and screened. From the cross-sections of the reduced particles, they observed that dense metallic iron particles were entrapped inside a wustite droplet, and no agglomeration of the droplets occurred. The rate constant for hydrogen reduction of liquid wustite was obtained in the form of one empirical equation, which is quite complicated. The activation energy they obtained in their experimental conditions was 110 kJ/mol.

The kinetics of reduction of magnetite by pure hydrogen and the mixture of hydrogen and inert gas (He, N_2, and Ar) were investigated in the temperature range 234 - 620℃(Al-Kahtany and Rao, 1980; Rao and Al-kahtany, 1984a and 1984b). Extremely thin (89 μm) magnetite specimens were used in this investigation in order to avoid any pore-diffusion effects. A rapid flow of the reducing gas was maintained through the reduction system to minimize film mass-transfer effects. The experimental results in this study were examined in light of nucleation and growth phenomena. The data correlated well with the Avrami-Erofeyev equation. The experimental results of wustite (50 μm thick) and hematite (137 μm thick) reduction by hydrogen at similar temperature range showed the same phenomena of nucleation and growth (El-Rahaiby and Rao, 1979 and 1980; Moinpour and Rao, 1988).

2.2 Reduction Kinetics of Concentrate Particles by CO

The kinetics of reduction of molten iron oxide with CO gas at temperature of 1450 and 1600℃ were investigated (Tsukihashi and Kato, 1982). In order to reduce the

influence of mass transfer rate on overall rate, fine powders of iron oxide were used as specimen and were reduced in a transport reactor. After the specimens of fine powder of reagent grade were melted during falling down in the reaction zone, liquid oxide drops thus formed were reduced with CO gas. Reduction rates of molten iron oxide particles (mean diameter is 25 μm) in a CO gas-conveyed system were $2.8x10^{-4}$ g-oxygen/cm^2sec at 1600℃ and $2.0x10^{-4}$ g-oxygen/cm^2sec at 1450℃.The rate constant of reduction of molten iron oxide in a gas-conveyed system was less than the value estimated from the result of experiment of a CO gas blowing system. What is more, the rate of reduction became lower as the particle size becomes smaller from 25 to 16 μm. The product cross-section morphology showed that the molten iron oxide surrounded the reduced spherical iron, and the shape of particle was spherical.

2.3 Reduction Kinetics of Concentrate Particles by CH_4

The mechanism and the kinetics of wustite reduction by CH_4 were studied with rapid in-flight reduction of spherical wustite fine particles with 32 - 35 μm in diameter at the temperatures of 1100 - 1300℃(Takeuchi and Nomura, 2007). They found that the reduction of wustite by CH_4 progressed more efficiently than that by H_2 at the temperature of 1100 - 1300℃. From the cross-section observation of the samples after reduction, the reduction progressed topochemically. The unreacted core model was adapted to the analysis of the reduction rates at the temperatures of 1100 - 1300℃. The reduction rate determining-step of wustite is chemical reaction at the Fe-FeO interface and the reduction of wustite is preceeded by carbon dissolution into the metallic shell.

2.4 Research Objectives

The literature review indicated that most previous work was done on the reduction of iron ore particles at temperature lower than 1100℃, which is much lower than the temperature at which the new process under development is expected to operate (Sohn, 2007; Sohn, et al., 2009). What is more, none of the rate equations reported in the literature could be applied to the conditions of the new process. Thus, it was necessary to develop a comprehensive kinetics expression applicable to the new conditions.

Previous work in this laboratory on the kinetics feasibility tests showed that iron oxide concentrate can be reduced to a high metallization degree within a few seconds of residence time typically available in a suspension process (Sohn, 2007; Sohn and Choi, 2010).

The goal of this research was to perform systematic measurement of the reduction kinetics of the direct gaseous reduction of fine iron oxide concentrates in a suspension reduction process. These include the effects of temperature, partial pressures of hydrogen, particle size, and types of reducing gas. Furthermore, data covering the entire fractional reduction degree vs time are necessary for comprehensive kinetics analysis. Such data, which had not been available for the conditions applicable to the proposed ironmaking process, were generated in this work. Finally, a comprehensive rate expression in terms of those above-mentioned variables, which was currently not available, was formulated. An additional emphasis on the formulation was that such a rate expression should be applicable and usable in developing an overall process model for the design and simulation of an industrial reactor for the proposed novel ironmaking technology.

Hydrogen is best as a reductant and/or fuel from the environmental and reduction kinetics points of view, but it is currently expensive. Instead, syngas which is mainly composed of H_2 and CO from the reforming of natural gas or coal gasification is used as a reducing gas mixture for the majority of current direct reduction processes. Thus, the effect of syngas on the reduction rate was also investigated.

CHAPTER 3

EXPERIMENTAL WORK

3.1 Materials

The iron oxide concentrate used in this work was provided by ArcelorMittal. The concentrate particles are irregularly shaped and angular, as shown in Figure 1. The chemical composition is presented in Table 1. Most of the iron oxide was magnetite and the total iron content ranged from 68 to 71%. The ArcelorMittal concentrate was screened to 25 - 32, 32 - 38, and 45 - 53 μm fractions for kinetics measurements in a drop-tube reactor.

3.2 Experimental Apparatus

It was reported by Sohn (2007) that the reduction rate of fine concentrate particles by hydrogen above 1100℃ took only a few seconds to be completed. It is extremely difficult to record weight change of the sample in such a short reduction time and avoid diffusion resistance among particles in the sample layer in a crucible by using a traditional TGA system. Thus, a high temperature drop-tube reactor system was fabricated (Sohn, 2007) for accurate determination of the rate of individual concentrate particles. It utilizes a dilute fine particles-gas conveyed system to measure the chemical reaction rate of fine particles entrained in a reducing gas. The advantages of this system are: 1) the rate measurement of the rapid in-flight reduction of fine particles is possible,

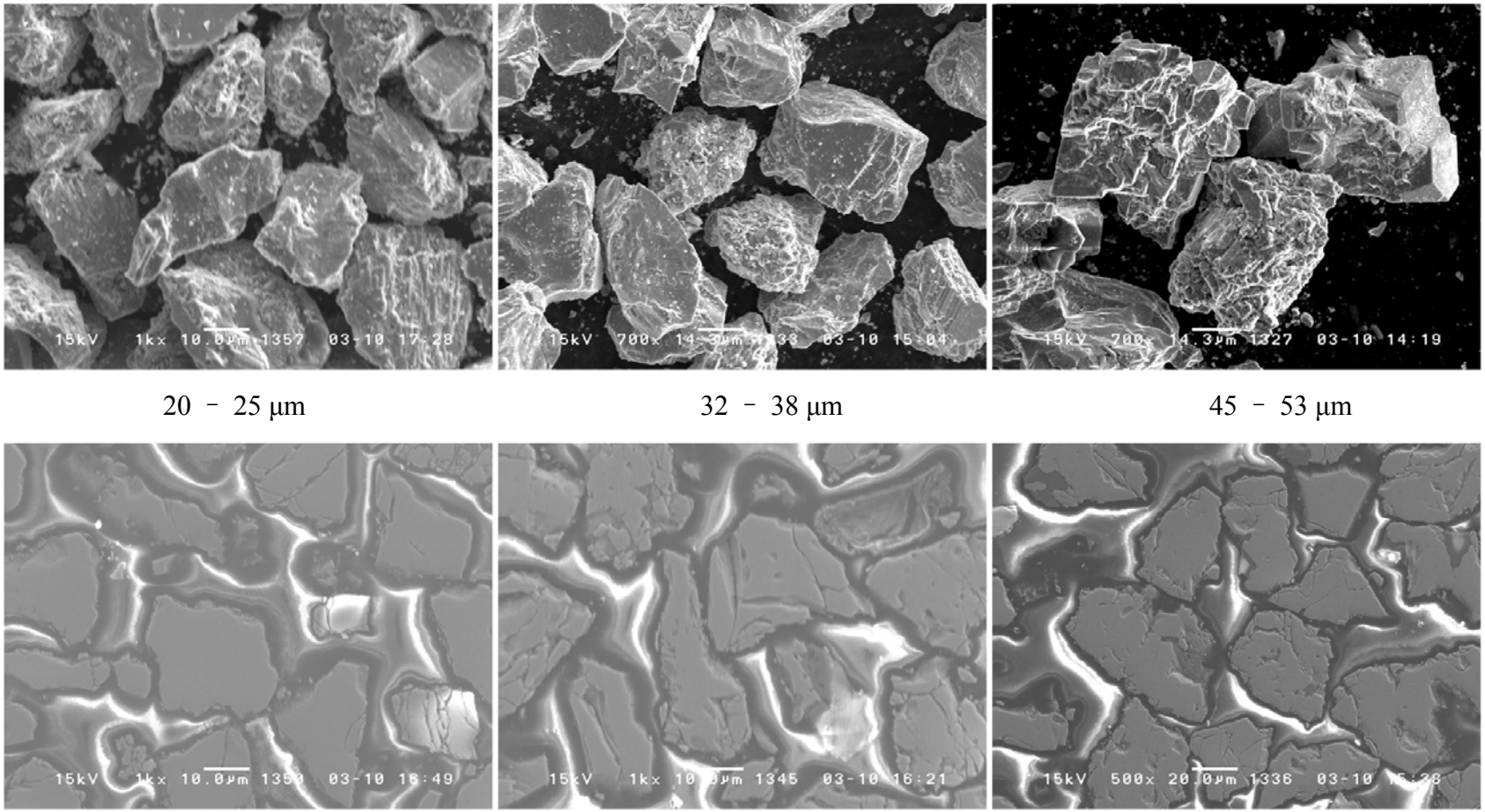

Figure 1. SEM micrographs: (a), (b), and (c) are screened ArcelorMittal concentrate.
Upper Row: SEM micrographs of screened particles; Lower Row: SEM micrographs of screened particles with polished sections

Table 1. Chemical composition (wt%) of iron oxide concentrate from ArcelorMittal.

Component	Particle Size		
	20-25 µm	**32-38 µm**	**45-53 µm**
Total Fe	71.00	70.28	67.62
FeO	30.63	30.18	29.67
P	0.01	0.01	0.01
S	0.02	0.02	0.02
C	0.25	0.28	0.58
Sr	0.02	0.01	0.02
SiO_2	1.68	2.08	4.51
Al_2O_3	0.13	0.10	0.17
CaO	0.21	0.35	0.85
MgO	0.11	0.18	0.49
MnO	0.09	0.12	0.24
Cr_2O_3	0.10	0.07	0.11
K_2O	0.01	0.01	0.01
Na_2O	0.10	0.10	0.10
TiO_2	0.01	0.01	0.01
ZrO_2	0.01	0.03	0.03
CuO	N/A	N/A	N/A

2) high mass and heat transfer between gas and particles is expected, and 3) there is no contamination from external parts because no crucible is used. Similar systems were reported in other investigations (Ezz and Wild, 1960; Themelis and Gauvin, 1962b and 1963; David and Feld, 1972; Ozawa and Tanaka, 1973; Hayashi and Iguchi, 1994 and 1995).

As shown in Figure 2, this apparatus consists of a vertical high temperature drop-tube furnace, a pneumatic powder feeder, gas delivery lines, a powder cooling and collecting system, and an off-gas outlet. The furnace system was made up of a vertical split tube furnace with a maximum working temperature of 1540℃ and a cylindrical alumina tube (5.6 cm ID, 193 cm long). A reaction zone was maintained at a constant temperature of 900 to 1500℃ by bar-type SiC elements. Carefully measured reaction zone was 91 cm long within ± 20 K for typical downward gas flow conditions. A cylindrical alumina honey-comb was inserted in the tube and hung right above the beginning of the reaction zone as a flow straightener and a heat exchanger for the reducing gas.

The pneumatic powder feeding system consisted of a syringe pump, a vibrator, a carrier gas line, a powder container, and a powder delivery line. Dried screened concentrate was charged in a powder container, a disposable test tube, which was held by a bore-through Swagelok and sealed with an O-ring. The mixture of hydrogen and nitrogen was fed as the carrier gas at a total rate of 200 NmL/min into the disposable test tube (0.9 cm ID) and passed through the powder delivery line (0.12 cm ID) at the top of the powder feeder continuously entraining a small amount of the powder. The feeding tube was vibrated by an electric vibrator to prevent clogging. The vial was pushed up by

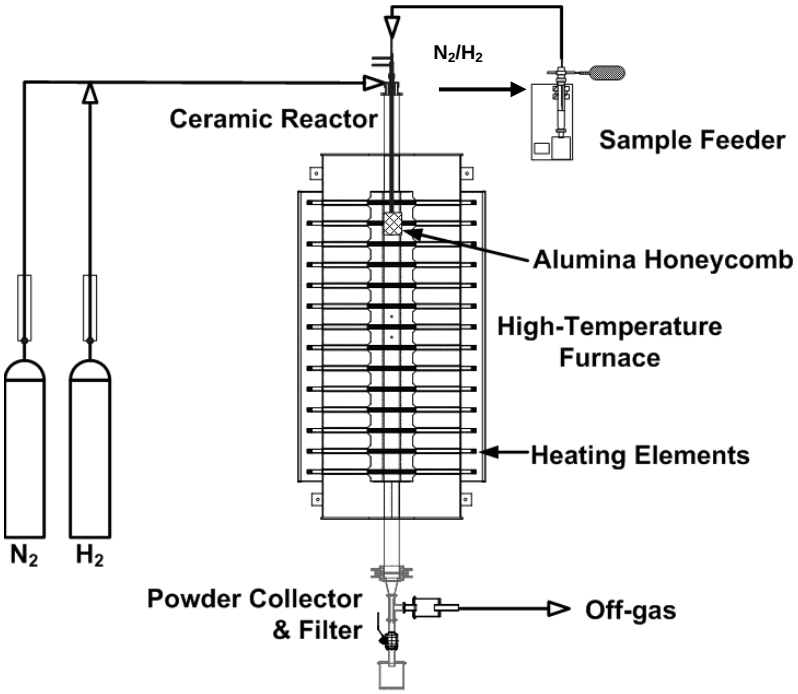

(a) Schematic Diagram of Drop-Tube Reactor System

(b) Photograph of Drop-Tube Reactor System

Figure 2. A high temperature drop-tube reactor system

a motor at a constant target advancing rate which was determined based on the calibration data between the advancing rate of the syringe pump and the powder feed rate. During the experiments, the concentrate feed rate was controlled from 60 to 590 mg/min.

The reacted powder was collected in a powder collector at the bottom of the reactor and the unreacted hydrogen and water vapor were discharged through the off-gas outlet that included a backflow prevention device for safety.

3.3 Experimental Procedure

At a designed experimental temperature, the predetermined amounts of hydrogen and nitrogen were charged into the reactor after the furnace system was purged by nitrogen. The concentrate powder began to be charged into the reactor after the temperature inside the furnace became stable. After all the concentrate contained in the vial was supplied into the reactor, the vibrator was kept running for 3 more minutes to prevent some concentrate particles staying in the powder feeding tube. Then, the reducing gas hydrogen was shut off and replaced by nitrogen to purge the system. After the system was purged by nitrogen for 15~20 minutes, the valve of the powder collection container was closed and the container was disconnected from the reactor. The reduced powder collection container was opened and the reduced sample was collected in a vial sealed by a cap after the sample cooled down. The collected sample was ready for further analysis, including titration, XRD, and SEM.

3.4 Sample Analysis

The determination of the reduction degree from raw concentrate to metallic iron (Fe) in the reaction product was the major purpose of analysis in this work. The total iron

content in the product was determined by titration methods (see Appendix A) based on international standard on the determination of metallic iron in direct reduced iron (DRI) (International Standard, 2006). To confirm the analytical procedure, either hematite or iron powder with over 99% purity supplied by Alfa Aesar was also analyzed along with the samples.

For further characterization, a Siemens D5000 X-ray diffractometer was used for the compositional analysis of samples. A TOPCON SM-300 Scanning Electron Microscope (SEM) equipped with an energy dispersive spectrometer (EDS) was used to examine the microstructure of concentrate and the quantitative elemental analysis. An Optical Microscope was used to check the polished sections of the samples.

3.5 Definition of Parameters

3.5.1 Residence Time Determination

The duration of hydrogen reduction of fine iron oxide concentrate particles is determined by the residence time of particles in the reaction zone (Choi, 2010). The value of residence time is calculated from the length of the reaction zone, which starts from the tip of the powder feeding tube, the linear velocity of the gas, and the terminal falling velocity for the creeping flow region expressed by the Stokes' law assuming that particles fall at a constant velocity in the reaction zone (Szekely and Themelis, 1971, pp. 606-8).

As the gas flow moves downward after the flow straightener, the flow mode change from a plug flow to a fully developed laminar flow ($Re = 0.1 \sim 3$ typically in this work) due to the entrance effects in pipe flow is expected in the very short length of the circular tube. From the normalized development length relationship suggested by Durst et

al. (2005) as indicated in equation (2), it was found (Choi, 2010) that the fully developed state of the flow is reached in less than 5% of the reaction zone length.

$$L/D = [(0.619)^{1.6} + (0.0567Re)^{1.6}]^{1/1.6} \quad (2)$$

where L = length of the reaction zone, D = diameter of tubular reactor, Re = Reynolds number.

Since the solid particles fall along the centerline, the residence time in this work is calculated (Choi, 2010) by varying the centerline velocity, which is twice the average velocity (= volumetric flow rate divided by cross-sectional area), as the linear velocity of gas. The relevant equations for the residence time calculation are:

$$u_t = d_p^2 g(\rho_p - \rho_g)/18\mu \quad (3a)$$

$$u_p = u_g + u_t \quad (3b)$$

$$\tau = L/u_p \quad (3c)$$

where, all in consistent units, d_p = particle size, g = gravitational acceleration, ρ_p = particle density, ρ_g = gas density, μ = viscosity of gas, u_p = particle velocity relative to tube wall, u_g = centerline gas velocity at furnace temperature, u_t = terminal velocity of a falling particle, τ = residence time, and L = length of isothermal zone.

The terminal velocity depends not only on the particle size but also the temperature due to its effect on the gas density and the viscosity of gas. As temperature increases, the density and viscosity of gas increase and the terminal velocity decreases, as shown in Figure 3. This makes the residence time, namely the reduction time, longer in

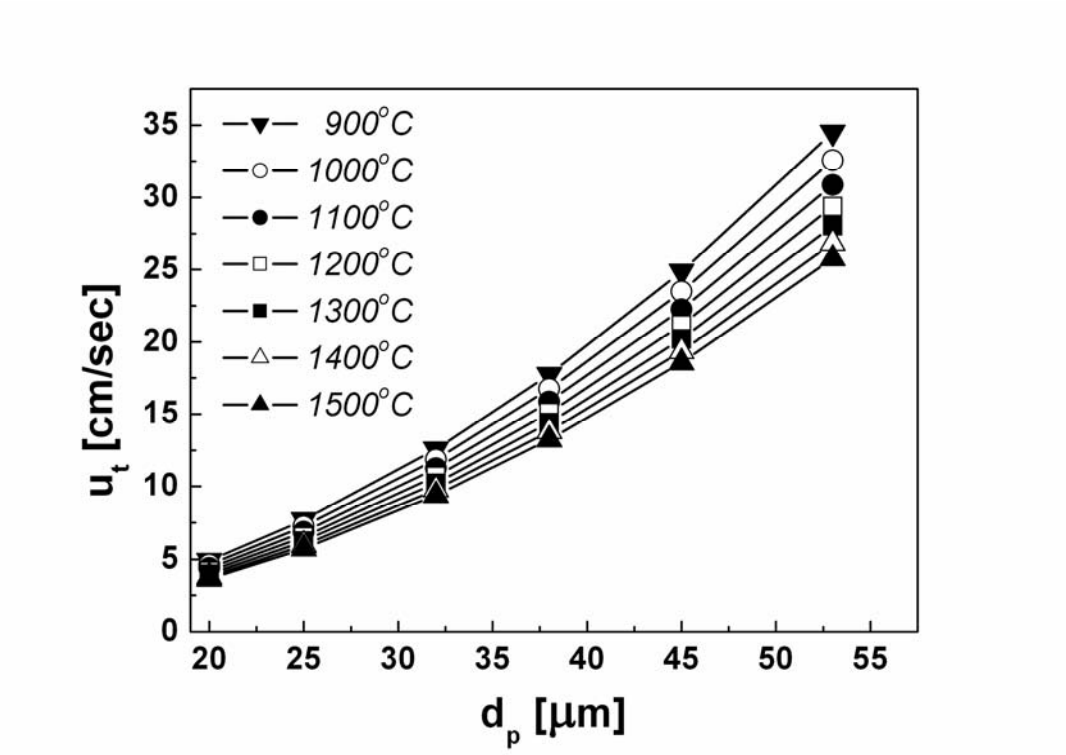

Figure 3. Terminal velocity of a falling spherical particle vs. the particle size. [Adapted from Choi (2010)]

the same length of the reaction zone when other parameters are fixed. On the other hand, a higher temperature causes the gas velocity to decrease at the same molar rate of gas input, which in turn decreases the residence time. Thus, all of these several factors must be taken into consideration when interpreting the effect of temperature on the reduction rate.

To make sure if this approach is reasonable, error analyses were performed examining the deviation of the average residence time of gas in the radial direction (Choi, 2010). The results show that the change in the average residence time of the gas is less than 10% of that at the centerline even if we assume that the particles are spread over the cross-section within the inner half of the reactor radius.

3.5.2 % Excess H_2

A hydrogen-containing gas mixture is fed into the reactor concurrently with the pneumatically transported iron oxide concentrate, of which the carrier gas is a mixture of hydrogen and nitrogen with a total rate of 200 NmL/min. The term % excess H_2 used in this work is defined as follows, especially taking into consideration the fact that the final stage of the iron oxide reduction, i.e. the reaction of FeO with H_2, is significantly limited by equilibrium. For example, at 1400°C

$$\mathrm{FeO(s)+H_2(g)=Fe(s)+H_2O(g)} \quad \Delta G^o \approx +900 cal \;\; (1400^o C) \tag{4a}$$

$$\left[p_{\mathrm{H_2}}/(p_{\mathrm{H_2}} + p_{\mathrm{H_2O)}})\right]_{\mathrm{eq}} = 0.5 \tag{4b}$$

This reaction has a slightly positive standard Gibbs free energy, and the equilibrium gas product has an H_2/H_2O molar ratio of ~ 1 at this temperature, i.e. 50% H_2

and 50% H_2O when pure hydrogen is used as the reductant. Taking the equilibrium composition into consideration, % excess H_2 is defined as follows in this work:

$$Fe_3O_4 + H_2 = 3FeO + H_2O \quad (5a)$$

$$FeO + H_2 = Fe + H_2O \quad (5b)$$

$$\text{Overall: } Fe_3O_4 + 4H_2 = 3Fe + 4H_2O \quad (5c)$$

$$K_{5b} = \left[\frac{p_{H_2O}}{p_{H_2}}\right]_{eq} = \left[\frac{n_{H_2O}}{n_{H_2}}\right]_{eq} \quad (6)$$

$$n_{H_2,\min} = n_o^i + \frac{n_o^i}{K_{5b}} = \left[1 + \frac{1}{K_{5b}}\right] n_o^i \quad (7)$$

$$\%\ excess\ H_2 = \frac{n_{H_2,supplied} - n_{H_2,\min}}{n_{H_2,\min}} \times 100 \quad (8)$$

Reaction (5a), the hydrogen reduction of magnetite to wustite, has a large equilibrium constant, i.e. essentially irreversible, whereas Reaction (5b) is considerably limited by chemical equilibrium. The minimum amount of hydrogen, $n_{H2,min}$, is the amount of hydrogen used to remove the oxygen from the iron oxide, n^i_o, plus the hydrogen required by equilibrium to be present with the water vapor produced by the reduction reaction, n^i_o / K_{R2}. The % excess H_2 is then calculated from the total amount of hydrogen fed into the reactor $(H_2)_{total}$ compared with the minimum amount of hydrogen, $n_{H2,min}$, as indicated in equation (8).

3.5.3 Degree of Reduction

The concentrate particles are transported downward, heated, reduced in-flight, and collected. The total iron content in the particles after reduction is determined by titration

methods and the fractional reduction is obtained by tracing the difference of the mass of oxygen combined with iron in the concentrate particles before and after reduction. The percent reduction is calculated as follows.

$$\%\text{Reduction} = \frac{m_{o(0)} - m_{o(t)}}{m_{o(0)}} \times 100\% \quad (9)$$

$$m_{o(0)} = \frac{m_{TFe(t)}}{(\%TFe)_0} \times (\%O)_0 \quad (10)$$

$$m_{o(t)} = m - m_{TFe(t)} - \frac{m_{TFe(t)}}{(\%TFe)_t} \times [100 - (\%TFe)_0 - (\%O)_0] \quad (11)$$

Here, m is the mass of reduced sample used in the titration, $m_{o(t)}$ and $m_{o(0)}$ are, respectively, the mass of the removable oxygen in the reduced sample collected after reaction for time t, and the corresponding mass of the removable oxygen in the unreduced dry concentrate. $m_{TFe(t)}$ is the mass of total iron in the reduced sample (mass is m), which is determined by titration. $(\%TFe)_0$ and $(\%O)_0$ are the mass percentage of total Fe and removable oxygen of the corresponding unreduced concentrate, which are determined by titration and reduction conducted in the horizontal tubular furnace, respectively. The amount of oxygen in the gangue materials which could be reduced by hydrogen in the experimental temperature range is negligible and the weight change due to the possible volatile species such as phosphorus and sulphur was also neglected based on the small contents as given in Table 1. Weight loss by heating alone was also confirmed to be negligible.

CHAPTER 4

EXPERIMENTAL RESULTS AND DISCUSSION

4.1 Previous Results

The major purpose of the hydrogen reduction rate measurements in the previous work (Choi, 2010) was the investigations on the kinetic feasibility of the proposed technology. Specifically, the rate measurements were mainly aimed at determining whether a high metallization degree could be obtained within a few seconds of residence time that is typically available in a suspension reduction process at a reasonable temperature and with an acceptable amount of excess hydrogen.

In the drop-tube reactor, over 90% reduction was attained in 1.6 seconds and the particles were almost completely reduced in 2.5 seconds at 1200℃ in large excess hydrogen, as shown in Figure 4. However, the reduction degree was significantly lower below 1100℃. Because of the method of experimental operation, the residence time and % excess H_2 were coupled. When feeding rate of the concentrate particles was the same, the residence time was changed with the amount of total flowrate of hydrogen, that is to say, the amount of % excess hydrogen. The reduction degree was decreased slightly in a longer residence time when the amount of % excess hydrogen was decreased to 200, as shown in Figure 4.

As expected for thermally activated processes, increased temperature promotes a higher reduction rate. It is especially noted that there was a considerable increase in the

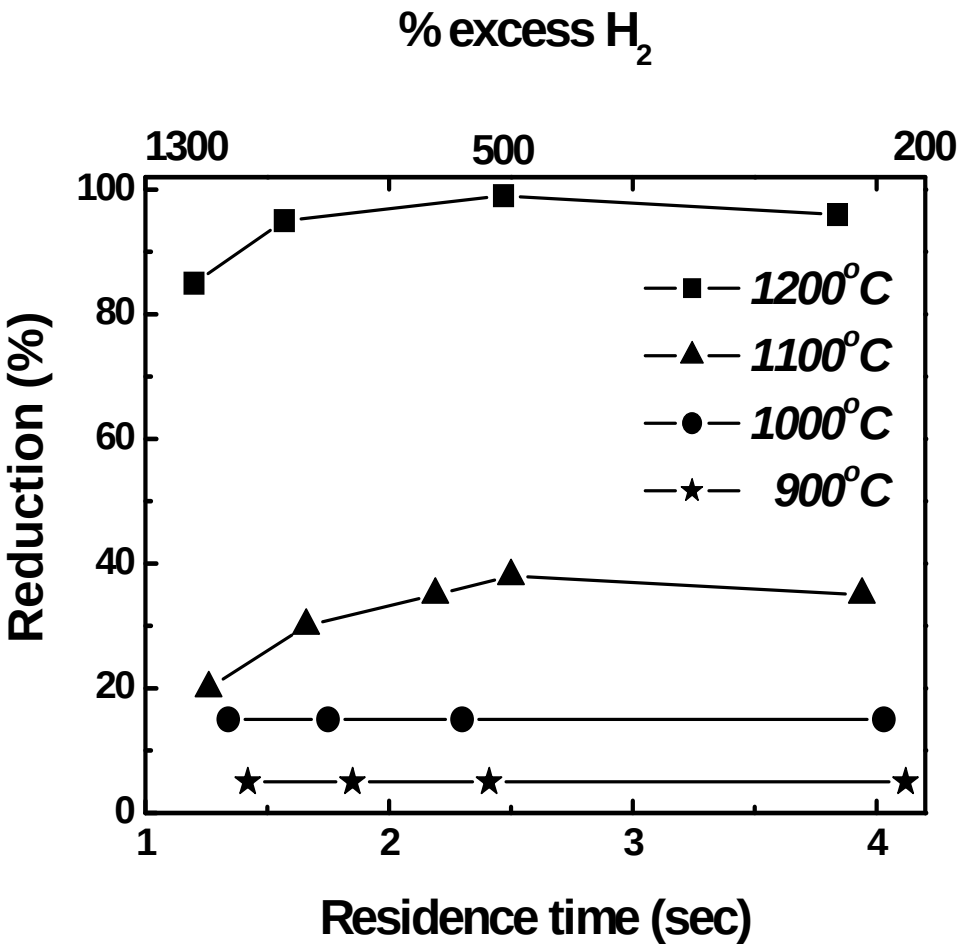

Figure 4. Hydrogen reduction rate of iron oxide concentrate vs. residence time and % excess H_2 at 900 - 1200℃. (particle size: 25 - 32 μm)
[Adapted from Choi (2010)]

hydrogen reduction rate when temperature was increased from 1100 to 1200℃, which essentially establishes the lower limit of the process temperature of the suspension reduction process at approximately 1200℃, given that the residence time in such a process would be in the same range.

Further experiments were performed at temperatures higher than 1200℃ to obtain the temperature effects. Above 1300℃, complete reduction was already accomplished in less than 1.1 seconds, as shown in Figure 5. Even when excess hydrogen was lowered to 40%, complete reduction was reached in less than 6.5 seconds. These results confirmed that the rate was sufficiently fast for the reduction of currently available concentrate to be carried out in the suspension reduction process above 1200℃.

4.2 Results of Main Experiments

4.2.1 Conditions Used in This Study

In this study, magnetite concentrate from ArcelorMittal was used. The amount of removable oxygen was determined by the weight loss in the experiment of concentrate reduction with a large amount of H_2 in the horizontal furnace. The oxygen and total iron contents in the ArcelorMittal concentrate indicated a removable O/Fe ratio was close to 1.33, indicating that essentially all the iron oxide exists as Fe_3O_4 (O/Fe=1.33). The fact that all iron oxide in the concentrate exists essentially as Fe_3O_4 was further confirmed by the XRD pattern, given in Figure 6.

It was demonstrated by detailed calculation (Choi, 2010) that the reduction rate controlled by external-mass-transfer + pore-diffusion is much greater than the measured rates. Under typical conditions designed in this study, a 30 μm particle would be fully

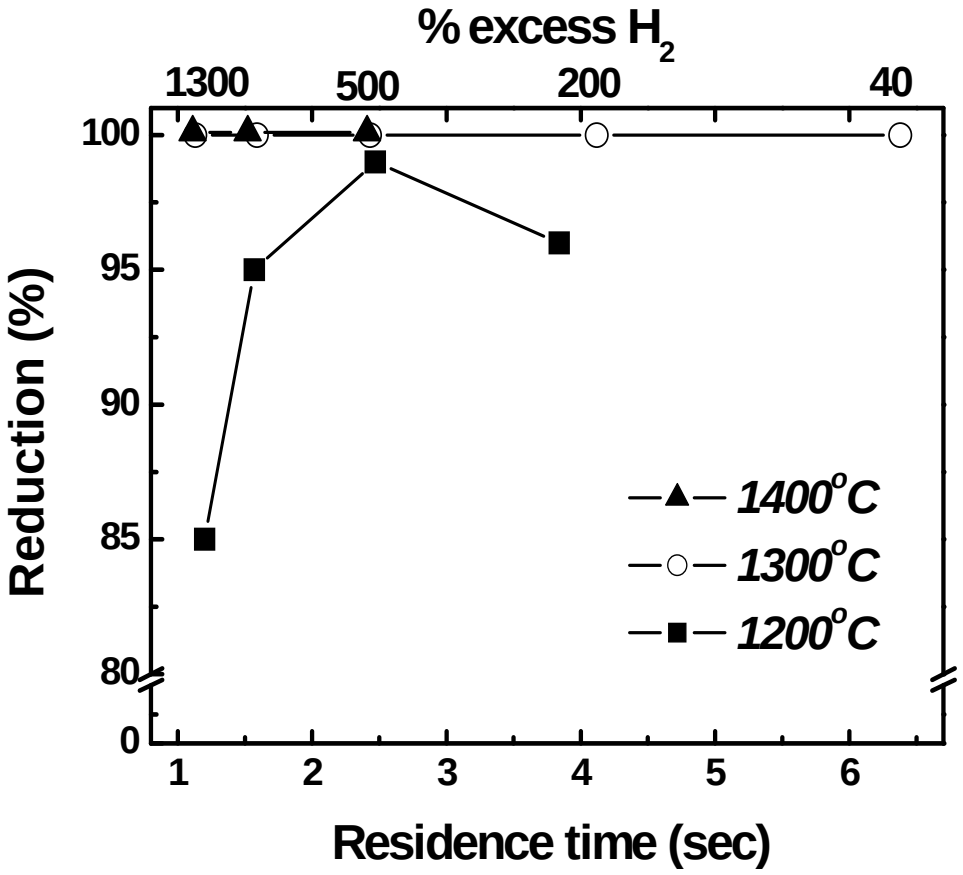

Figure 5. Hydrogen reduction rate of iron oxide concentrate vs. residence time and % excess H_2 at 1200 - 1400℃. (particle size: 25 - 32 μm)
[Adapted from Choi (2010)]

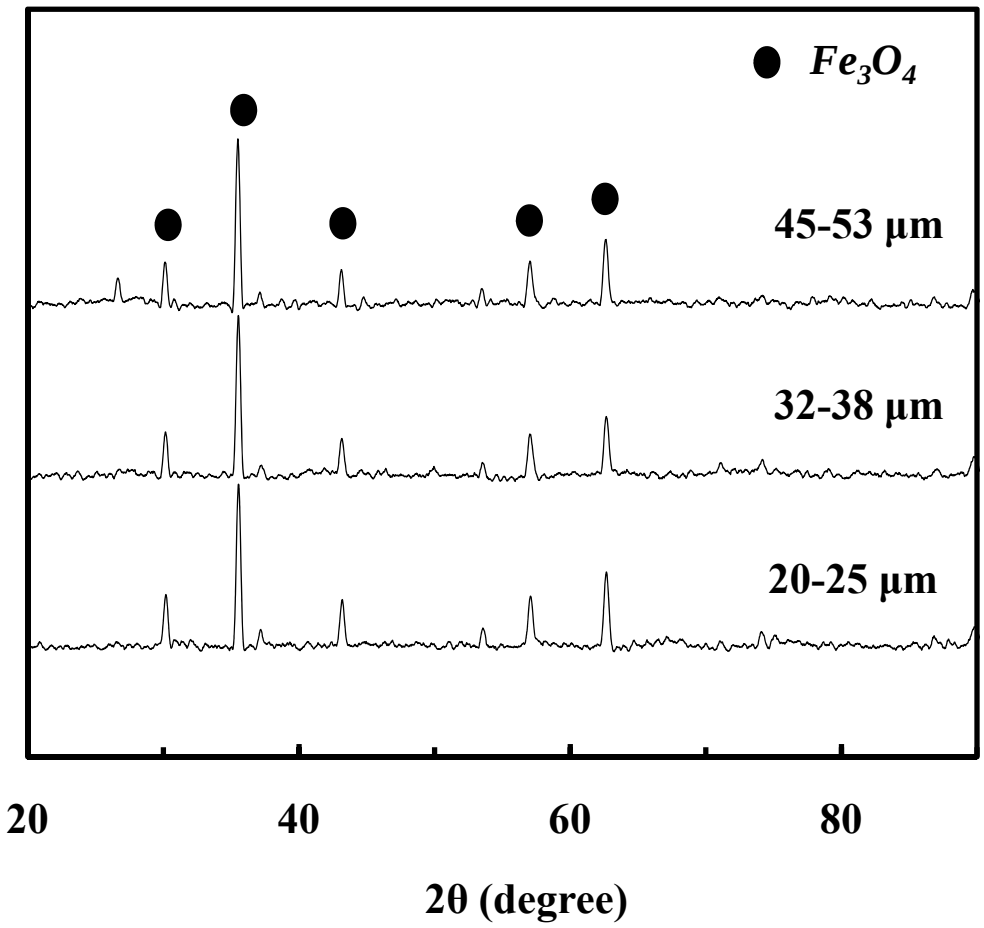

Figure 6. X-Ray patterns of concentrate particles with different sizes.

reduced in milliseconds compared with a few seconds as observed in this study. Therefore, the overall reaction is controlled by the chemical reaction of individual particles and not affected by pore diffusion or external mass transfer. In order to examine the reduction behavior of the concentrate particles, experiments to determine the effect of partial pressure of hydrogen, particle size, and reduction temperature on reduction rate were conducted.

4.2.2 Effect of Experimental Variables

4.2.2.1 Effect of reduction temperature. Previous results (Section 4.1) indicated that the reduction rate was fast enough for a flash reduction system when temperature was higher than 1100℃. In order to examine the effect of temperature on the reduction rate of concentrate particles, experiments were carried out at 1150 - 1400℃ at different partial pressures of hydrogen. The particle size varied from 20 - 53 μm. The effect of temperautre on reduction rate of the sample with 20 - 25μm is presented in Figure 7. The rest is listed in Appendix B. It is observed that the reduction temperature significantly increased the reduction rate of the concentrate particles at different particle pressures of H_2.

4.2.2.2 Effect of hydrogen partial pressure. It was obtained (Choi, 2010) that complete reduction of the concentrate particles was finished in the shortest time that is typically available in the suspension reduction system, even with lower excess pure hydrogen (40%). In order to obtain data to cover the entire range of reduction curve, N_2 was added to change the partial pressure of H_2 and examine the effect of partial pressure of hydrogen on the reduction rate of the samples with different particle sizes at 1200 - 1400℃. After preliminary experiments, partial pressure of hydrogen was set to be 0.1 -

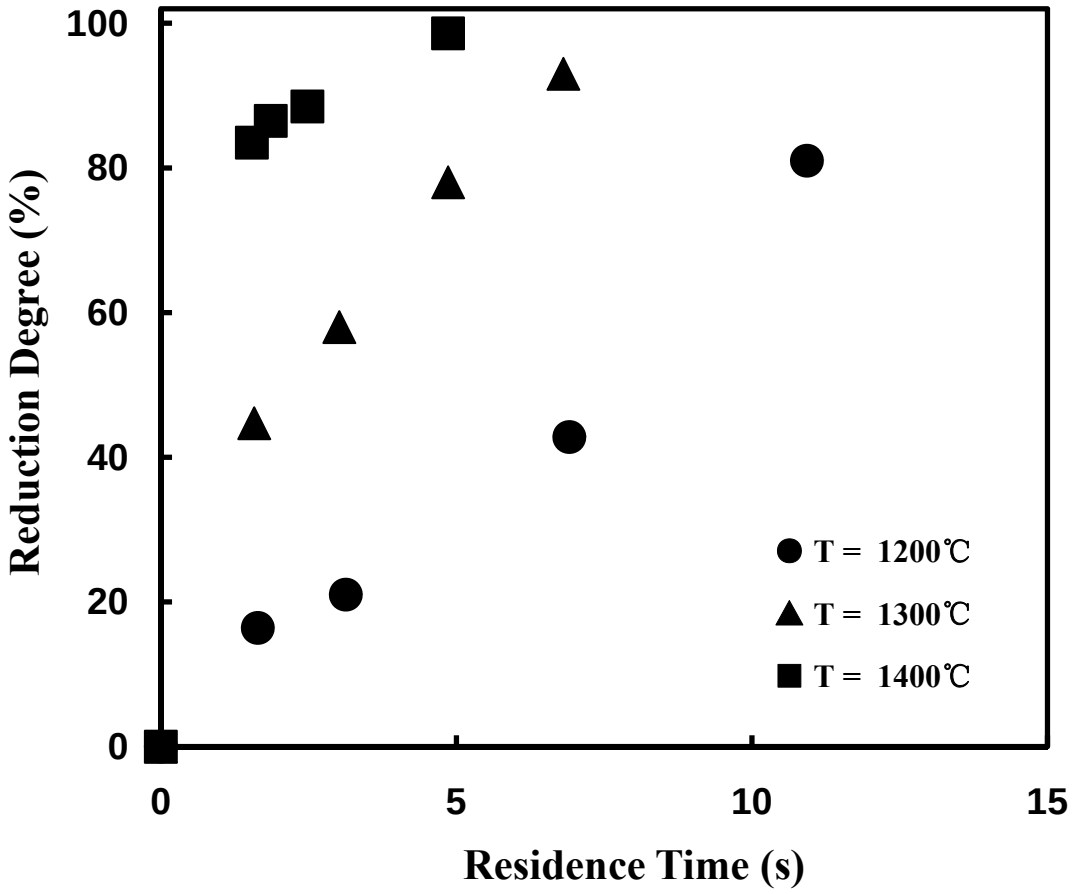

Figure 7. Effect of temperature on the reduction rate of the sample with 20 - 25 μm with 200% excess hydrogen (p_{H2} = 0.2 atm)

0.3 atm to get the entire reduction curve from about 10% to 100%. Suitable partial pressure range of hydrogen varied with reduction temperature, as shown in Figure 8, and the rest were listed in Appendix C.

4.2.2.3 Effect of particle size. The effect of particle size was determined with different partial pressures of H_2 at 1150 - 1400℃, as shown in Figures 9 - 10 (The rest is given in Appendix D). At temperatures below 1300℃, the reduction rate increased with particle size at different partial pressures of H_2. However, the effect became negligible when temperature reached above 1300℃.

4.2.3 Reproducibility of Experimental Results

Due to the specific characteristics of the drop-tube system, it is difficult to obtain a large amount of data as quickly as with a TGA system. Along the entire reduction curve, only distinct points at certain intervals of residence time could be obtained experimentally. Therefore, it is necessary to check the reproducibility of the single point in order to obtain enough confidence that those obtained data can illustrate the whole reduction curve behavior. Experiments were repeated three times at an identical set of conditions for four different residence times. The results are given in Figure 11, which show that every point was reproducible within ± 3% reduction degree. Another indication of the reproducibility of the collected data is given subsequently when the Arrehnius plot is discussed.

4.2.4 Morphologies of Samples Reduced at Different Conditions

Two samples reduced at 1300℃ with different reduction degree were randomly selected to examine their morphological change during the reduction, as shown in Figure

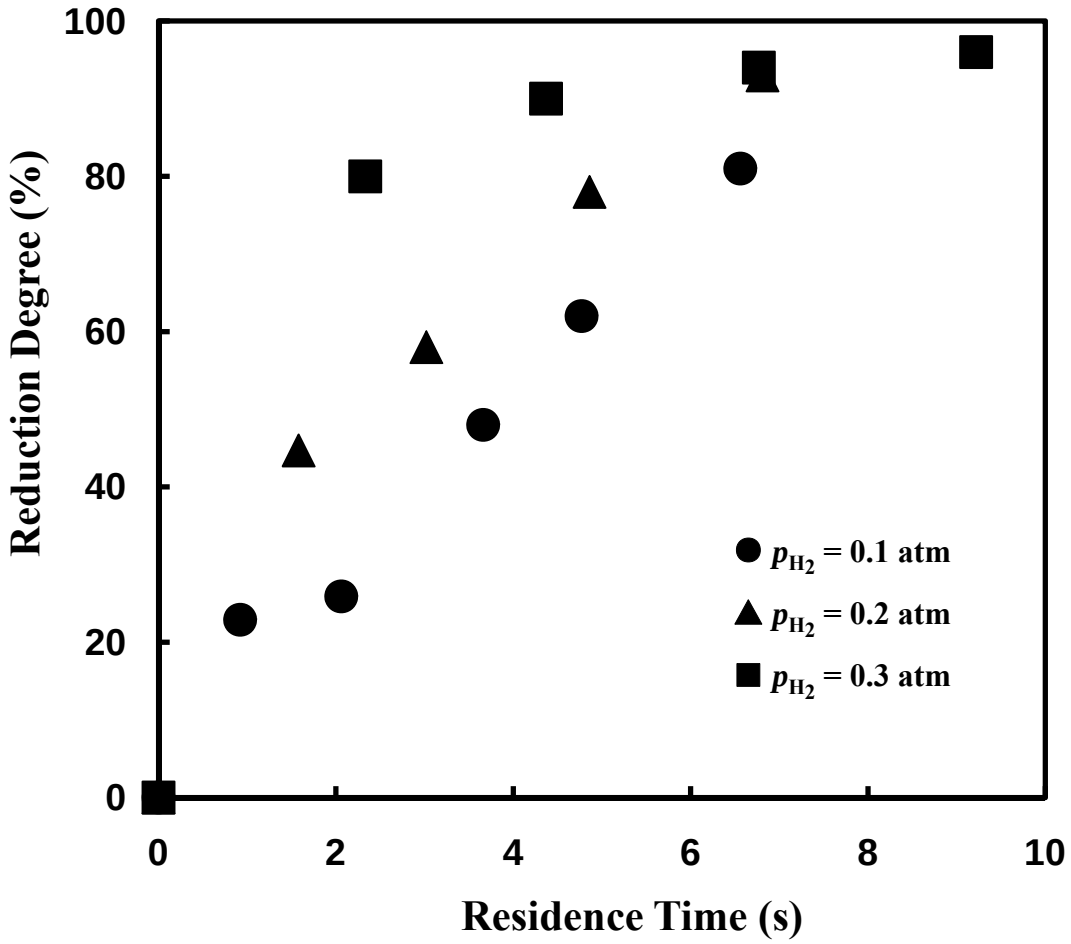

Figure 8. Effect of partial pressure of hydrogen on the reduction rate of the sample with 20 - 25 μm at 1300℃.

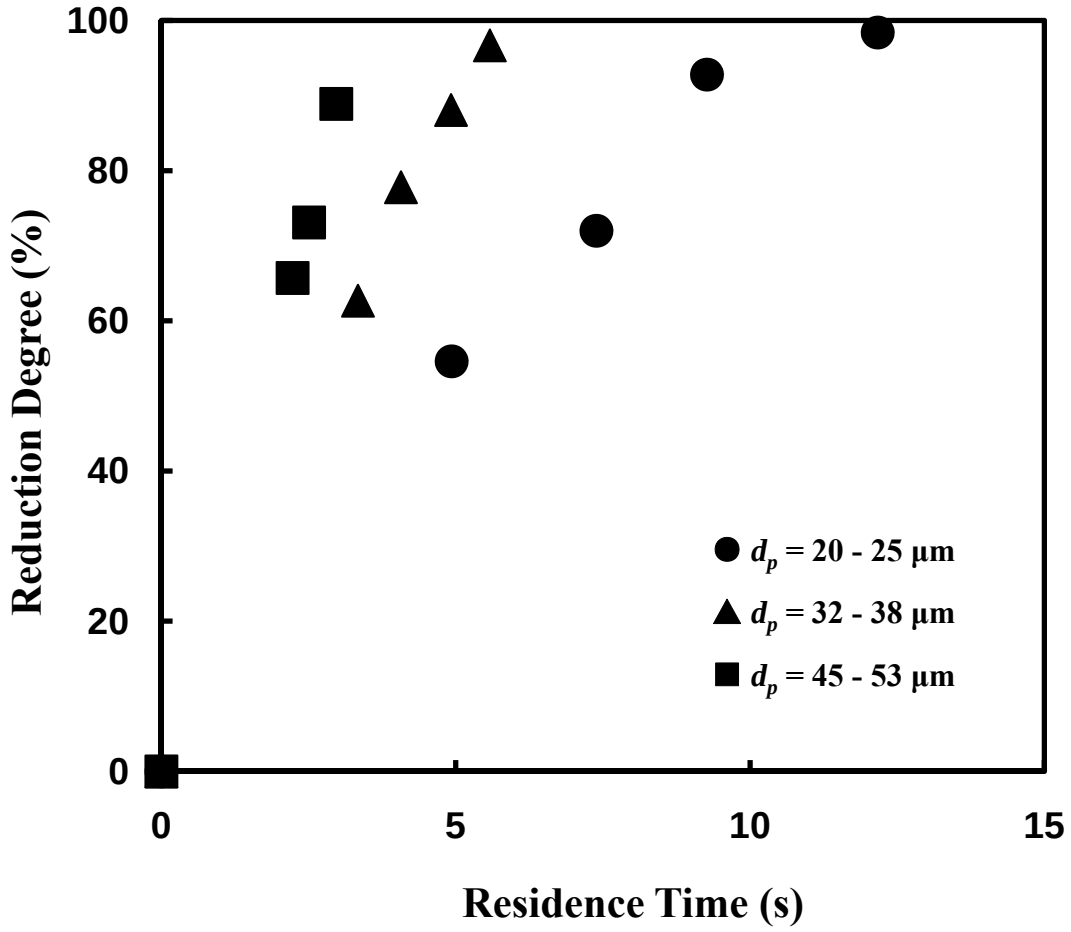

Figure 9. Effect of particle size on the reduction rate with 200% excess hydrogen at 1150℃ (p_{H2} = 0.85 atm).

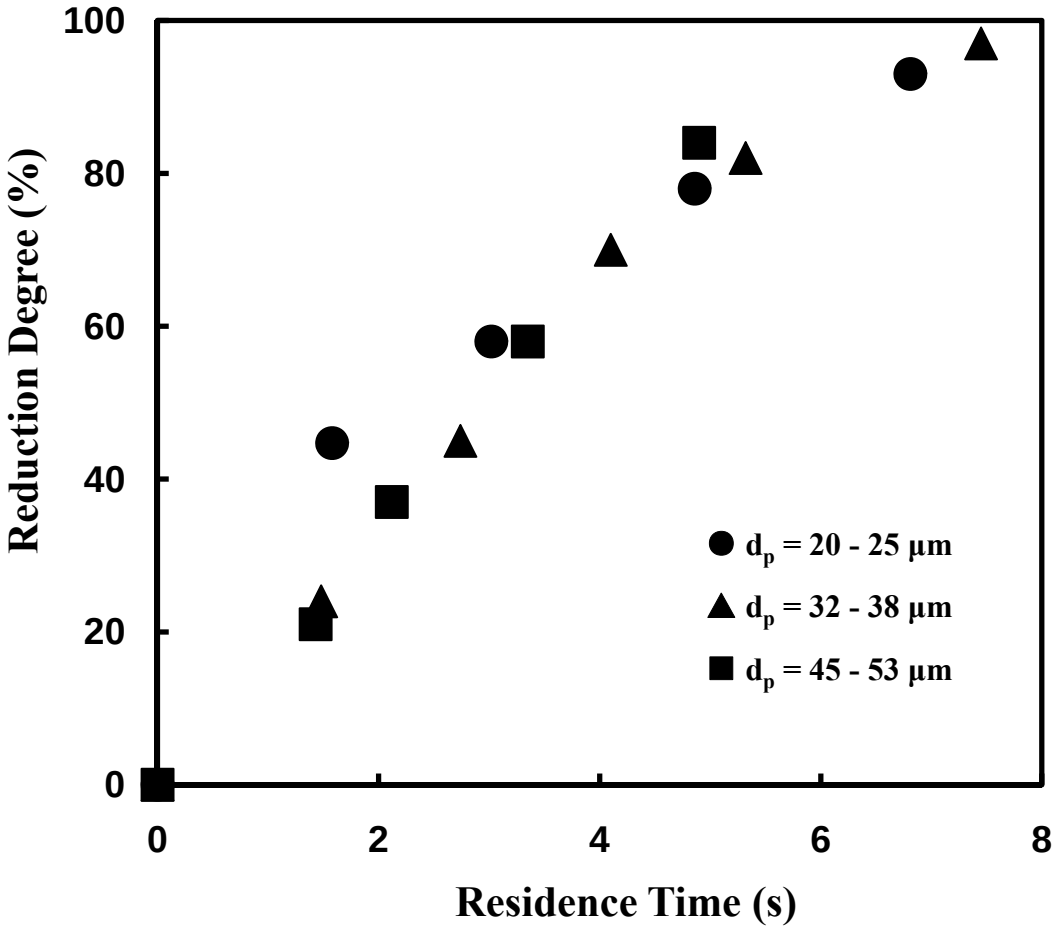

Figure 10. Effect of particle size on the reduction rate with 200% excess hydrogen at 1300℃ (p_{H2} = 0.2 atm).

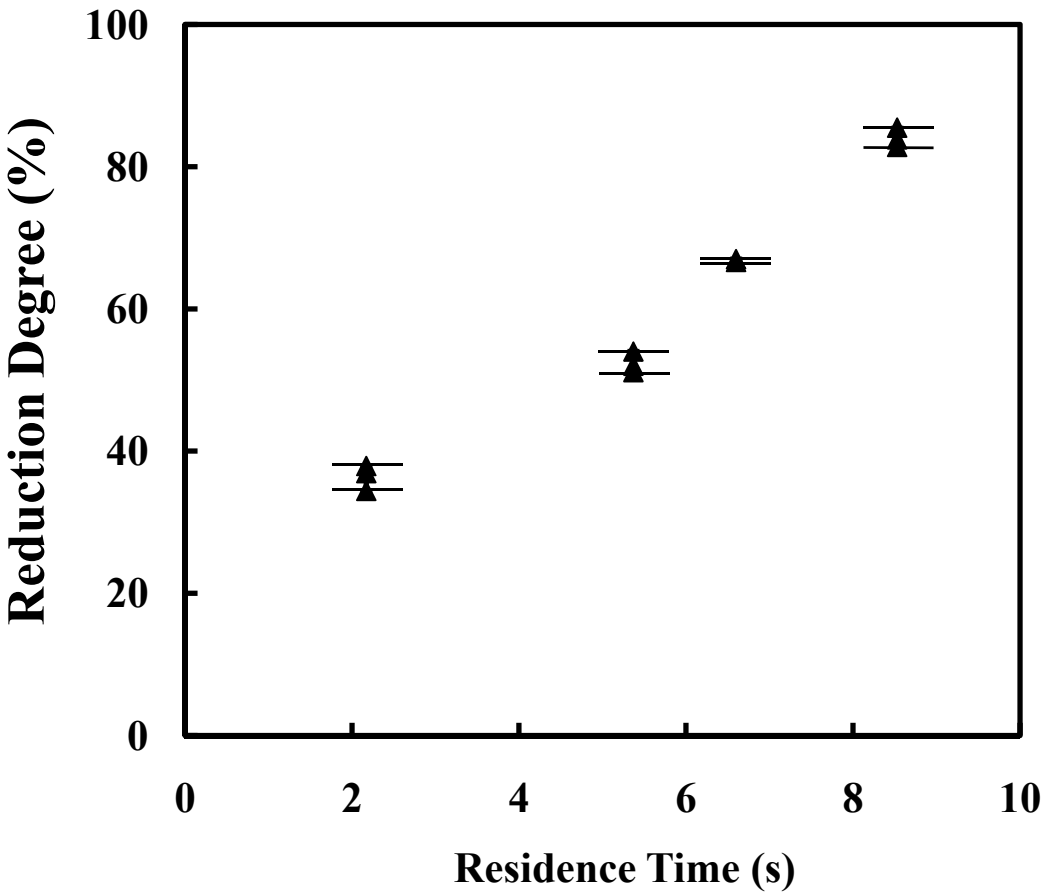

Figure 11. Reduction degree of sample with 32-38 μm vs. residence time at 1200℃

12. From the micrographs of polished sections, it was observed that at this temperature, the iron formation started from active sites at the initial stage of the reduction. And the growth of the solid product iron casued the product to be porous with reduction degree increase, which is supported by the micrographs at a higher reduction degree, 85%. These observed phenomena were further supported by the SEM micrographs of the reduced particles, as shown in Figure 12.

SEM micrographs of the reduced samples with similar reduction degree were obtained to examine the morphological changes with reduction temperature, as shown in Figure 13. At temperatures below 1400℃, the solid product iron formed a porous layer.

When temperature was increased to 1400℃, the reduced product tendered to be sphere, which is due to the fact that the melting point of wustite is 1376℃. Therefore, it was seen that the solid iron product coalesced in the center and was surrounded by unreduced wustite, as shown in Figure 14. Similar phenomenon was also reported in other investigations (Hayashi and Iguchi, 1994 and 1995).

4.3 Selection of Reaction Rate Model

It was reported (Rao, 1979) that the reduction of iron oxide starts at nuclei which are formed on the exposed surface of the particle. The reduction involves the formation of metallic iron nuclei and their subsequent growth at the expense of iron oxide phase. The nucleation and growth phenomena in the reduction of iron oxide were also mentioned in other investigations (Themelis and Gauvin, 1962; Hayes, 1979; El-Rahaiby and Rao, 1979).

"*Gas-solid reactions usually involve the adsorption of gaseous reactants at preferred sites on the solid surface and the formation of nuclei of the solid product. For*

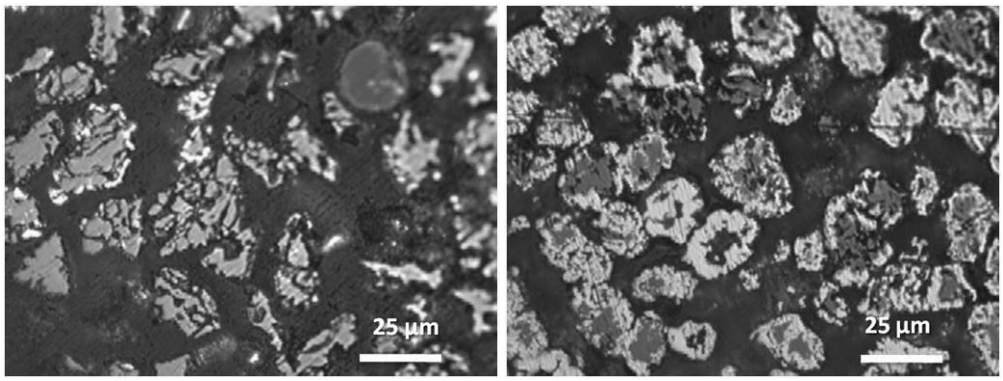

X = 24% X = 85%

A. Micrographs of polished sections

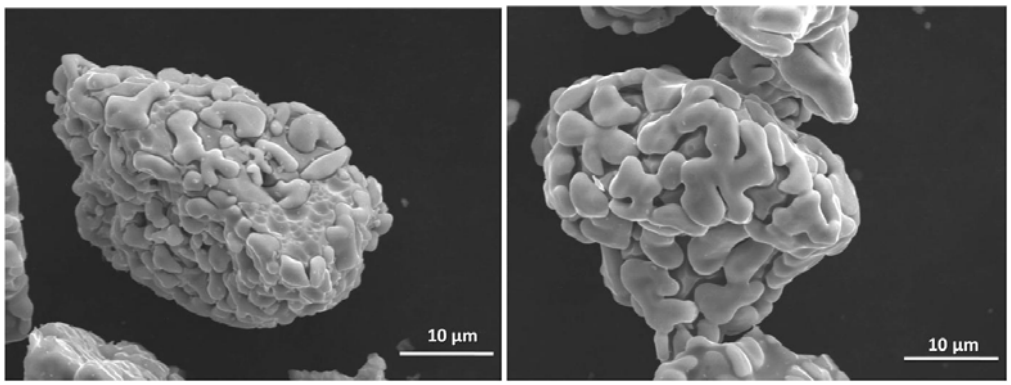

X = 24 % X = 85%

B. SEM Micrographs of reduced particles

Figure 12. Morphology examination of reduced samples with 32 - 38 µm at 1200℃.

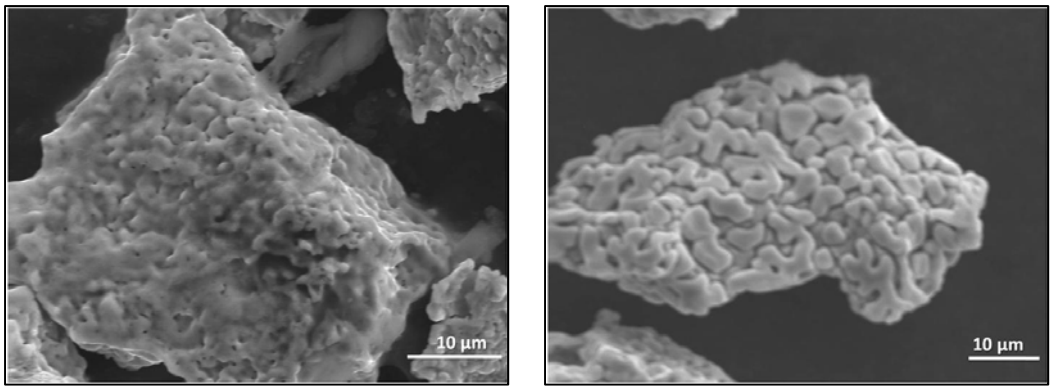

A. T = 1150℃ X = 98%

B. T = 1200℃ X = 99%

C. T = 1300℃ X = 97%

D. T = 1400℃ X = 98%

Figure 13. SEM micrographs of reduced sample with 32 - 38 µm at 1200 - 1400℃.

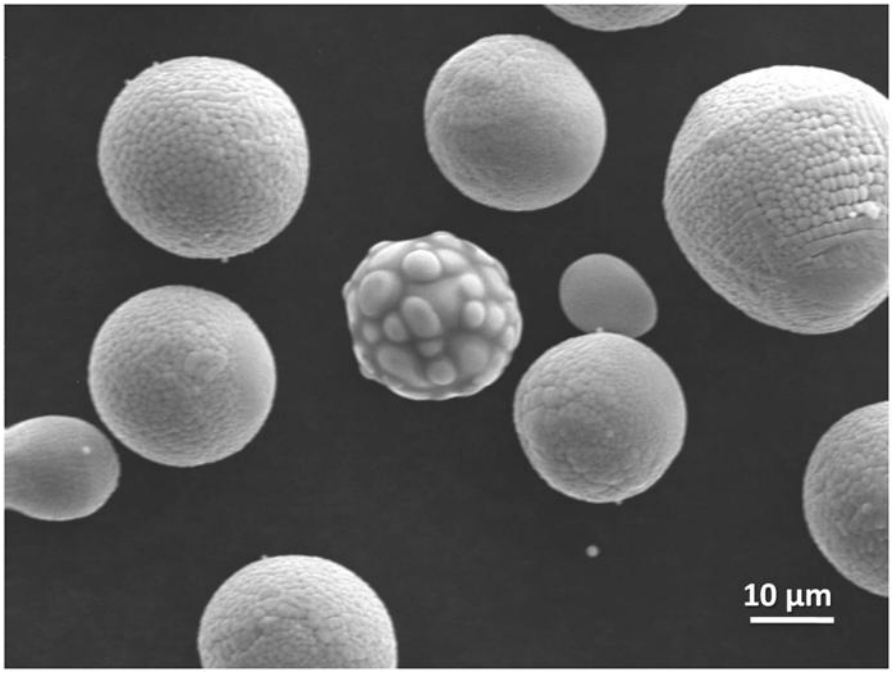

A. T = 1400℃ X = 69 %

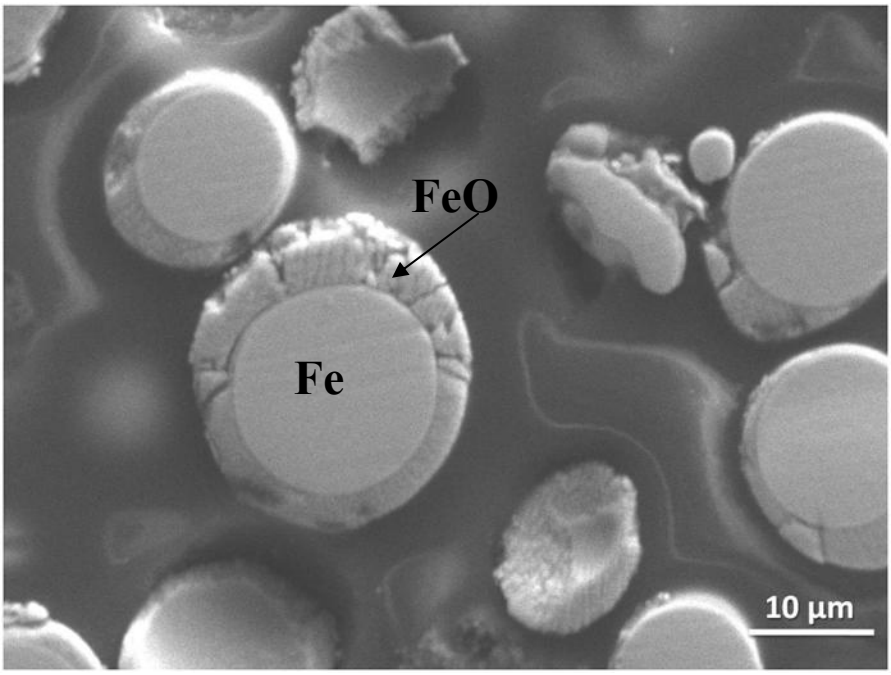

B. T = 1400℃ X = 69 %

Figure 14. Morphology of reduced sample with 32 - 38 µm at 1400℃.
A: SEM micrograph of reduced sample
B: SEM micrograph of polished sections

small particles the period of the formation and growth of nuclei occupies essentially the entire conversion range" (Seetharaman and Sohn, 2005, pp. 299 - 310).

Therefore, the nucleation and growth kinetics expression given by the following equation was found to describe the rates of reduction in this study:

$$[-Ln\ (1-X)]^{1/n} = \left[k \cdot f_p\left(p_{H_2}, p_{H_2O}\right) \cdot f_d\left(d_p\right)\right] \cdot t = k_{app} \cdot t \qquad (12)$$

where X = fractional reduction degree, t = reaction time, n = Avrami parameter, k = rate constant, d_p = particle size, $f_p\left(p_{H_2}, p_{H_2O}\right)$ = function of gas partial pressures, $f_d\,(d_p)$ = function of particle size, k_{app} = apparent rate constant.

It was obtained that the nucleation and growth rate equation represent the reduction reaction, and that n = 2 gives the best fit of the experimental data at different reduction temperatures and partial pressures, as shown in Figure 15.

Other functions of X applied in describing the reduction kinetics of the gas solid reactions limited by chemical reaction on the solid surface, such as shrinking-unreacted-core model, were also tried to plot the experimental data in this study. They did not represent the data as well. Meanwhile, the nucleation-and growth kinetics rate equation best represented the data, which is also justified from the viewpoint of reaction mechanism, as discussed above and also seen in micrographs like Figure 12 (A). The reduction of magnetite to iron proceeds through the formation of FeO with a change in reactivity. However, for small particles, it is extremely difficult to follow the irregular evolution of morphology involving FeO formation. Thus, equation (12) is used as a global rate equation involving the overall reduction steps.

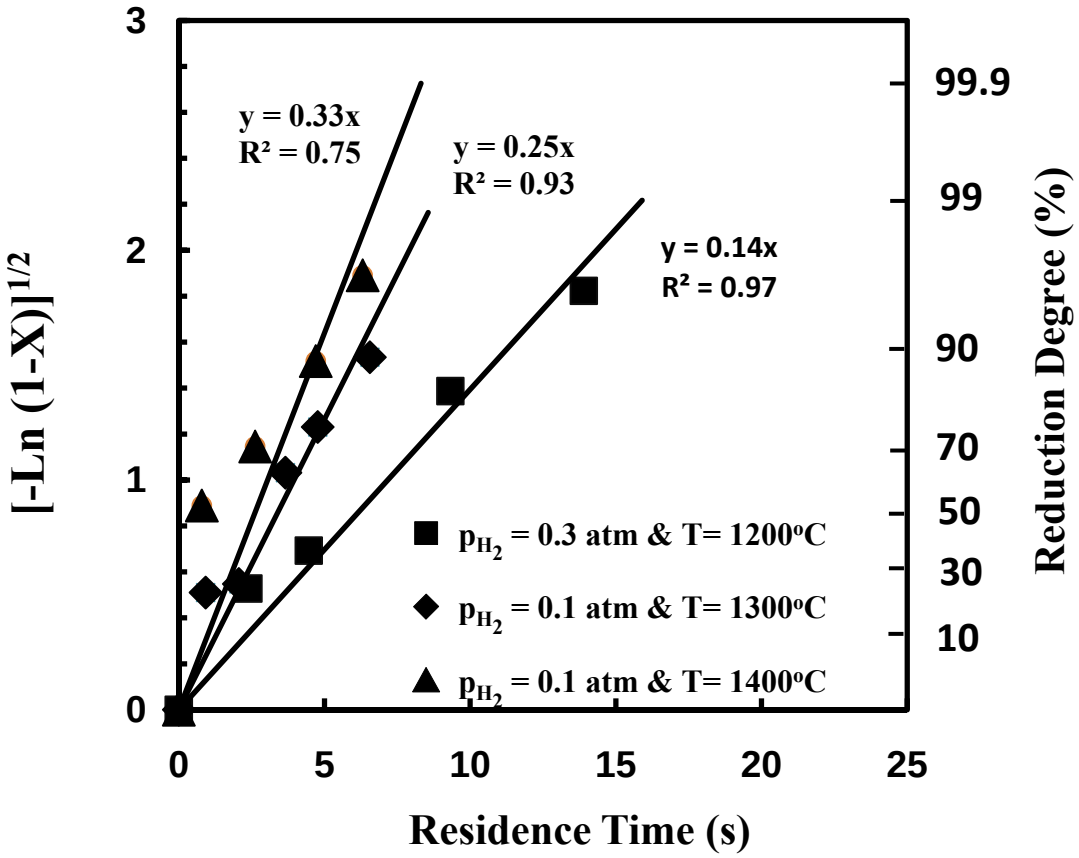

Figure 15. Determination of Avarami parameter, n. (particle size: 20 - 25 μm)

4.4 Determination of Reaction Order with Respect to H_2 Partial Pressure

In this study, mixtures of hydrogen and nitrogen were used, which formed water vapor as a result of the reduction. Its amount changes during the course of the reduction, which reduced the reduction potential of hydrogen. Although the experiments were performed with as much excess hydrogen as possible, the generation of small but nonnegligible amounts of water vapor is unavoidable in some runs. Thus, the presence of water vapor is treated as follows:

We let

$$k_{app} = k \cdot f_p\left(p_{H_2}, p_{H_2O}\right) \cdot f_d\left(d_p\right) \tag{13}$$

When the particle size and reduction temperature are fixed, the relationship between k_{app} and $f_p\left(p_{H_2}, p_{H_2O}\right)$ should be linear. The following expression for pressure dependence, which satisfies the equilibrium condition as a special case when the net rate is zero, is used for iron-oxide reduction, the last step ($FeO + H_2 = Fe + H_2O$) of which is equilibrium-limited:

$$f_p\left(p_{H_2},\, p_{H_2O}\right) = p_{H_2}^m - \left(p_{H_2O}/K\right)^m \tag{14}$$

where K is the equilibrium constant for the hydrogen reduction of FeO, and m is the reaction order with respect to partial pressure of hydrogen.

Due to the formation of water vapor during the reduction course, partial pressure of water vapor increased with reduction degree X, and partial pressure of hydrogen decreased because of consumption of reduction. Thus, the value of $f_p\left(p_{H_2},\, p_{H_2O}\right)$ varies with the reduction degree of X. Therefore, an average value of $f_p\left(p_{H_2},\, p_{H_2O}\right)$ was used.

Log mean average was adopted to be used as the instantaneous value of $f_p(p_{H_2}, p_{H_2O})$ at each X when reaction was assumed to be 1st-order with respect to partial pressure of H_2. Meanwhile, arithmetic mean average was used for 1/2-order reaction with respect to partial pressure of H_2 (see Appendix E).

At different initial partial pressures of H_2, a set of experiments were conducted with the sample of 45 - 53 μm at 1573 K. The k_{app} values obtained from straight lines at each X according to equation (12) with n = 2 are plotted against $f_p(p_{H_2}, p_{H_2O})$ in Figures 16 and 17.

The results in Figure 17 indicate that m = 1/2 gives the best fit of the experimental data. This is consistent with the reaction mechanism in which adsorbed H_2 molecules dissociate into H atoms before reacting with the oxide.

4.5 Determination of Particle Size Dependence

The effect of particle size on the reduction rate at different reduction temperatures was determined. The results are shown in Figures 18 - 21. In equations (12) and (14), it was observed that functional dependence of rate on partial pressure of H_2 varies with reduction degree along the change of residence time. For reduction of the samples with the same particle size at fixed temperature, the plot should be linear after we combined the terms containing X as one variable, which was plotted as Y axis in these figures.

The results show that reduction rate increased with the particle size at 1150 and 1200℃. However, the effect of particle size on reduction rate was negligible after temperature reached 1300℃. This could be explained by the following reasons:

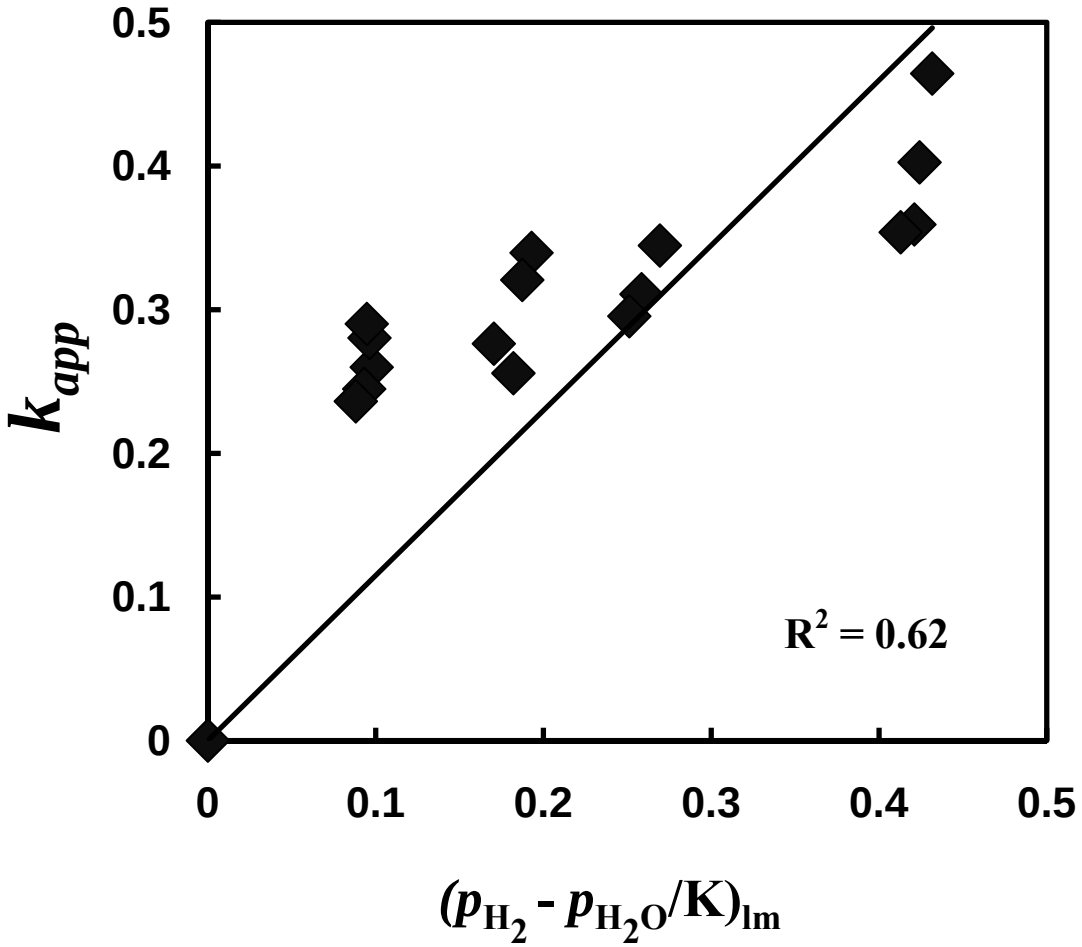

Figure 16. The relationship between $k \cdot f_p(p_{H_2}, p_{H_2O}) \cdot f_d(d_p)$ and $f_p(p_{H_2}, p_{H_2O})$ with 45 - 53 μm samples at 1573 K.

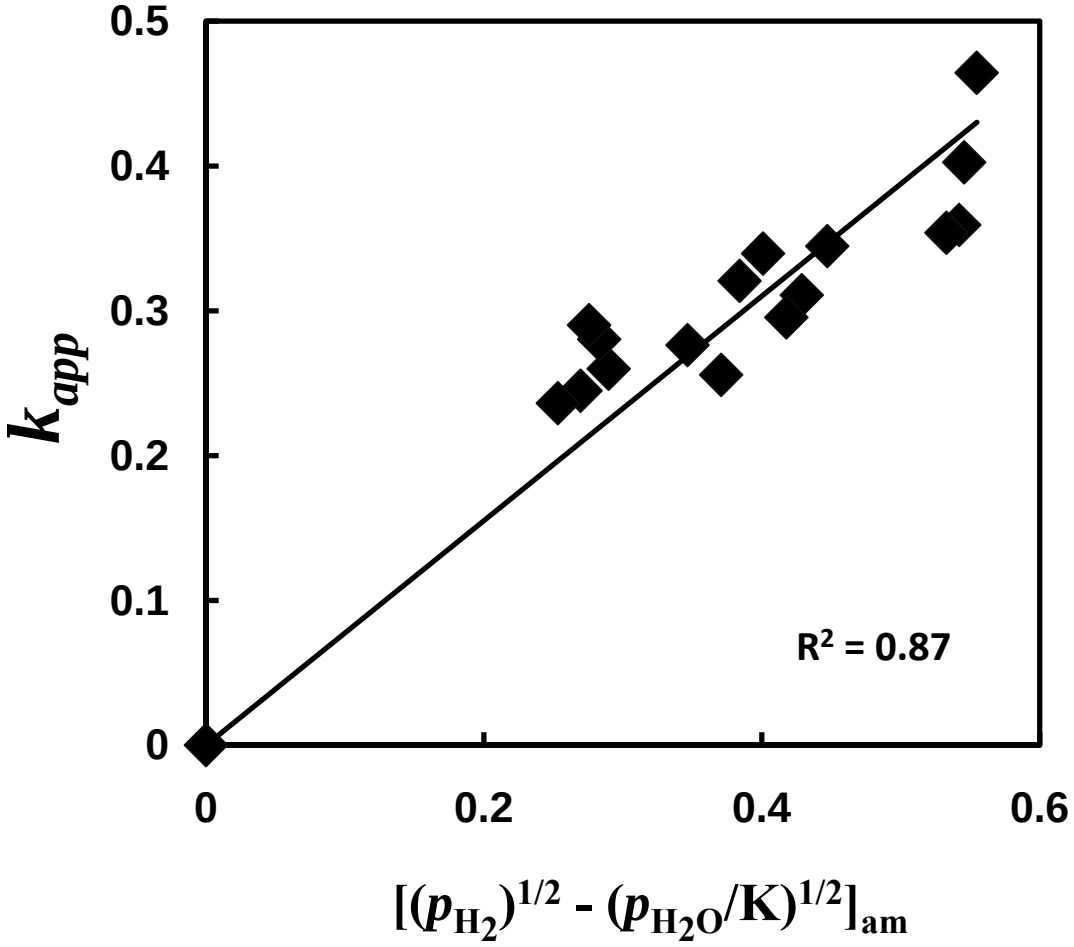

Figure 17. The relationship between $k \cdot f_p(p_{H_2}, p_{H_2O}) \cdot f_d(d_p)$ and $f_p(p_{H_2}, p_{H_2O})$ with 45 - 53 μm samples at 1573 K.

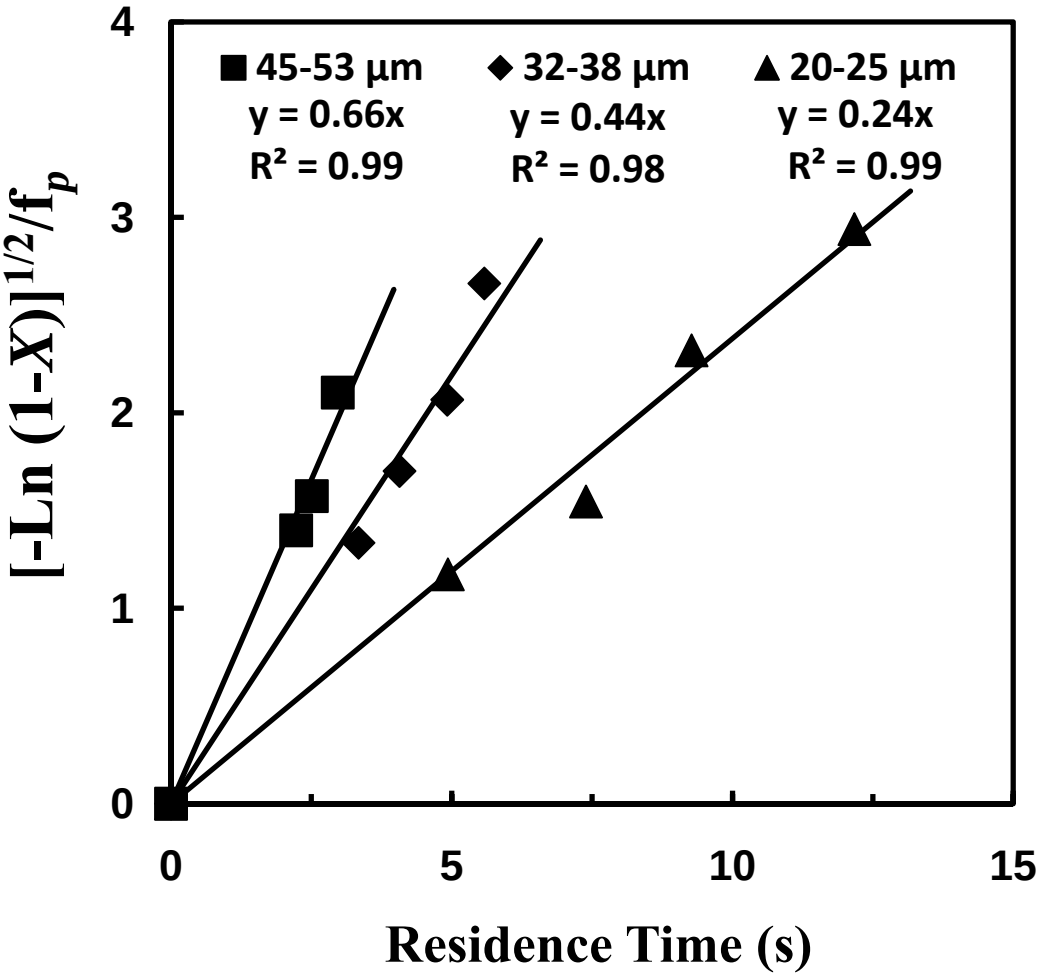

Figure 18. Relationship between $\left[-Ln\ (1-X)\right]^{1/2}/f_p\left(p_{H_2}, p_{H_2O}\right)$ and residence time with 200% excess hydrogen at 1150℃.

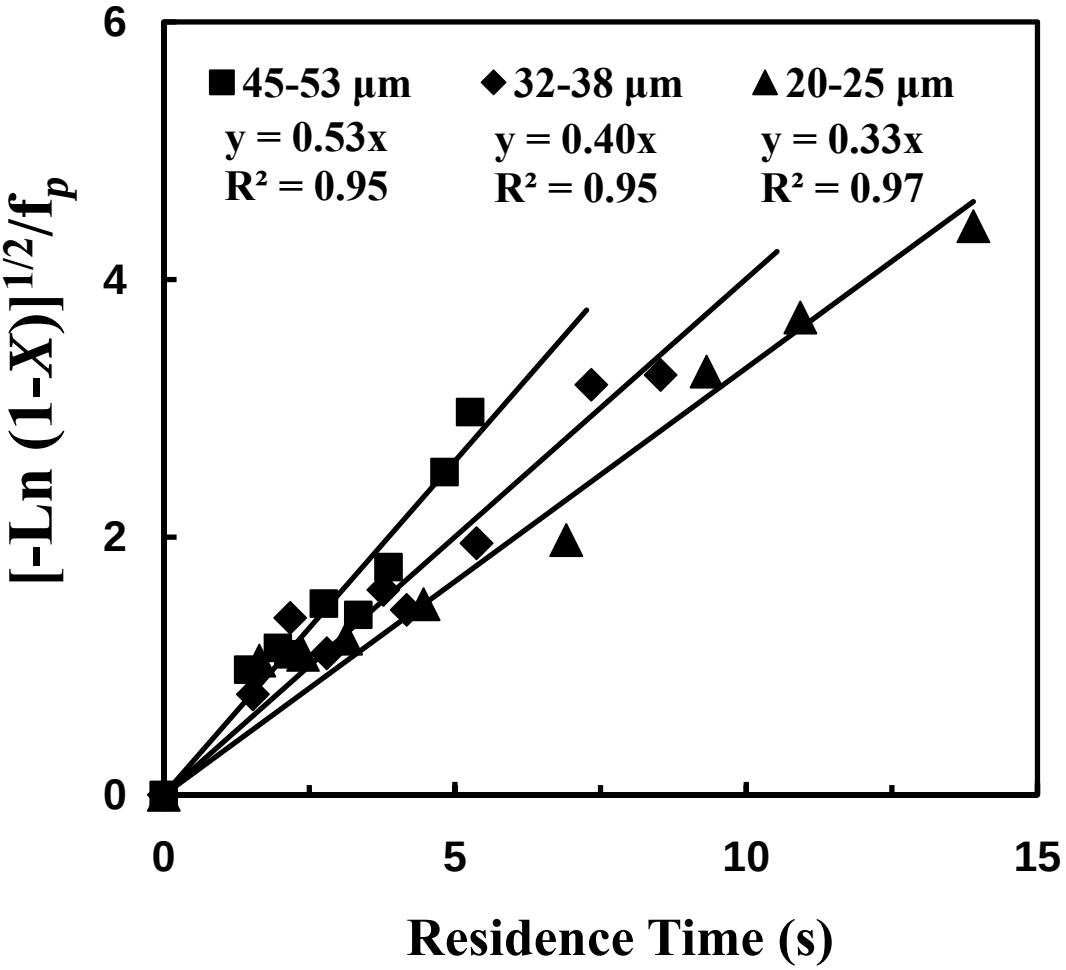

Figure 19. Relationship between $\left[-Ln\,(1-X)\right]^{1/2}/f_p\left(p_{H_2}, p_{H_2O}\right)$ and residence time with 200% excess hydrogen at 1200℃.

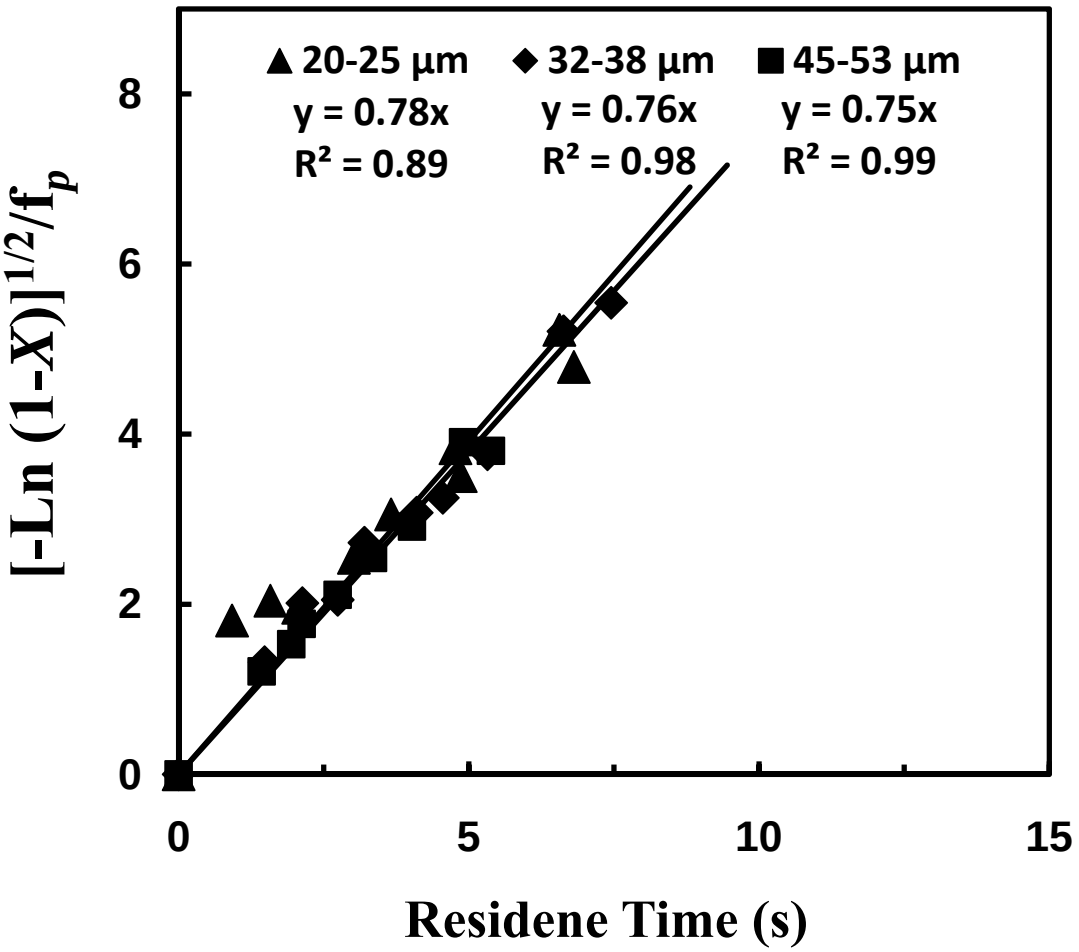

Figure 20. Relationship between $\left[-Ln\,(1-X)\right]^{1/2}/f_p\left(p_{H_2}, p_{H_2O}\right)$ and residence time with 200% excess hydrogen at 1300℃.

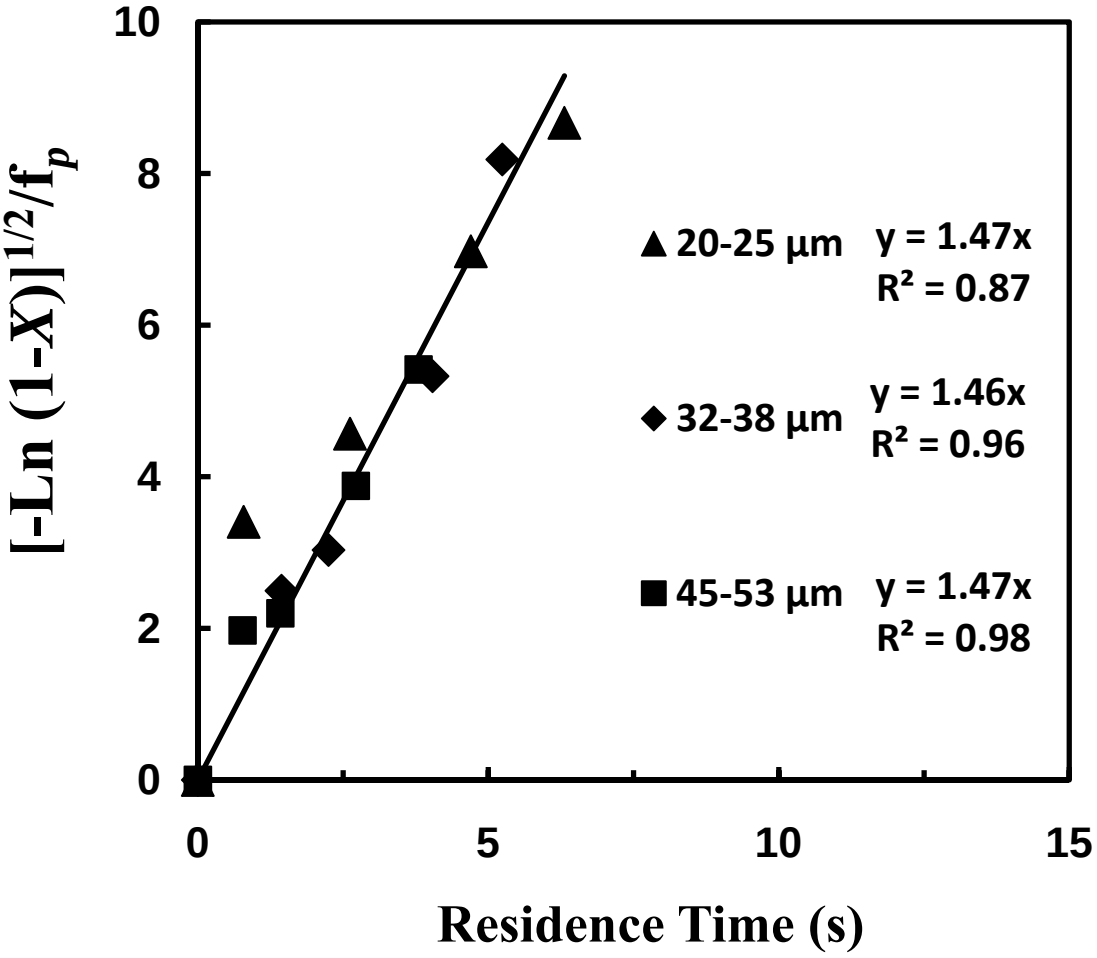

Figure 21. Relationship between $\left[-Ln\ (1-X)\right]^{1/2}/f_p\left(p_{H_2}, p_{H_2O}\right)$ and residence time with 200% excess hydrogen at 1400℃.

"*Gas-solid reactions usually involve the adsorption of gaseous reactants at preferred sites on the solid surface and the formation of nuclei of the solid product. For small particles the period of the formation and growth of nuclei occupies essentially the entire conversion range*" (Seetharaman and Sohn, 2005, pp. 299 - 310).

But the number of preferential nuclei forming sites per unit area of the surface depends on the properties of the exposed surface of the single particle including scratches, lattice defects, and the presence of the impurities (Rao, 1979). The iron oxide concentrates with different particle sizes were obtained by grinding before it was concentrated by various mineral processes, which could possibly make the particles have different surface properties. And also the gangue content is different among them. The contents of the main gangue materials (SiO_2, CaO and MgO) in iron oxide concentrate particles increase with particle size, as shown in Table 1 and Figures 22 - 24. Previous investigations have shown that the addition of CaO (Iguchi and Inouye, 1982; Shigematsu and Iwai, 1989) or MgO (McCune and Wynblatt, 1983; Tasker et al., 1985) promotes the gaseous reduction of wustite. What is more, the cracks tend to be formed in the big particles during the reduction more readily than in the samller particles, and the dimension of solid between cracks can be smaller than the size of the smaller particles. All of these are possible reasons why larger particles have higher reduction rate below 1300℃. This has also been observed previously by Tsukihashi et al. (1982).

As described above, at the same temperature, samples with different particle sizes reacted at different rates. The rate dependence on the particle size is correlated with a function of $(d_p)^s$. The s value is obtained from the slopes of the straight line in Figures 18 - 21 which represents $k \cdot f_d$:

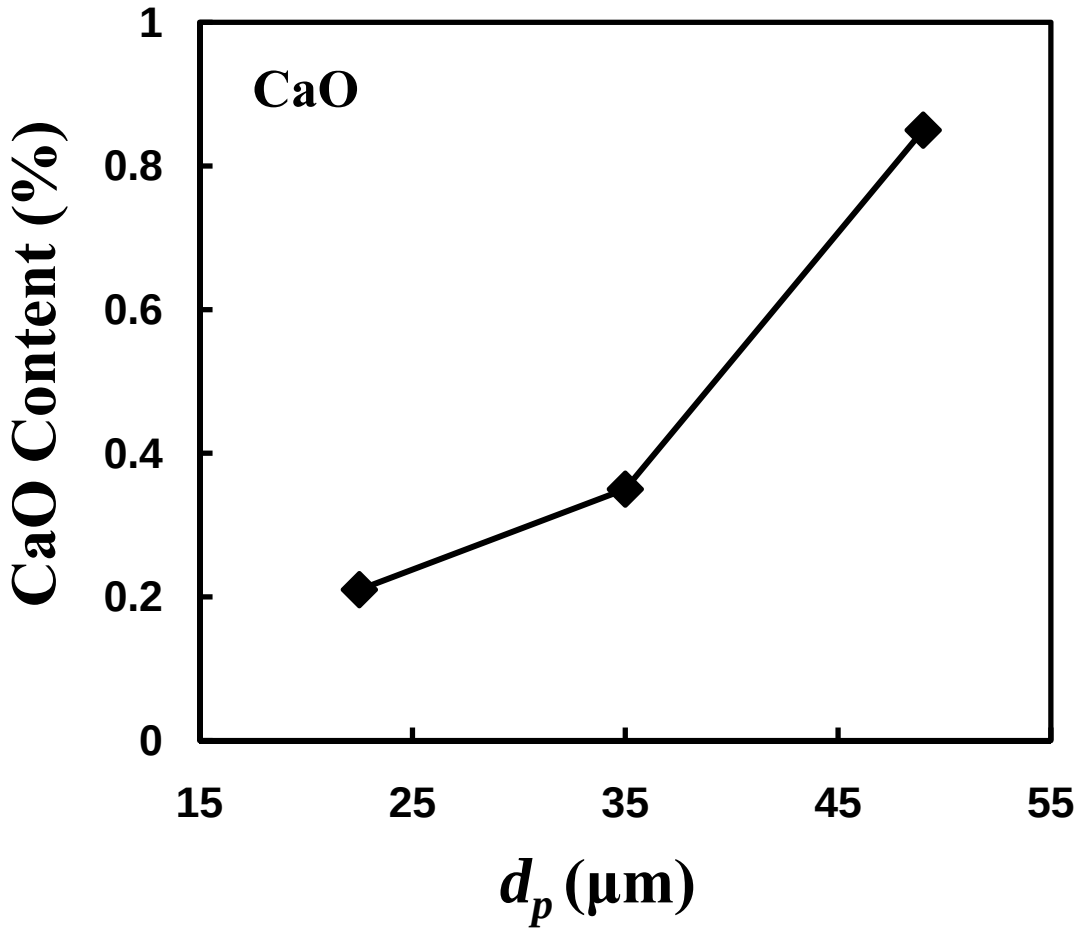

Figure 22. The relationship between CaO content and particle size of concentrate.

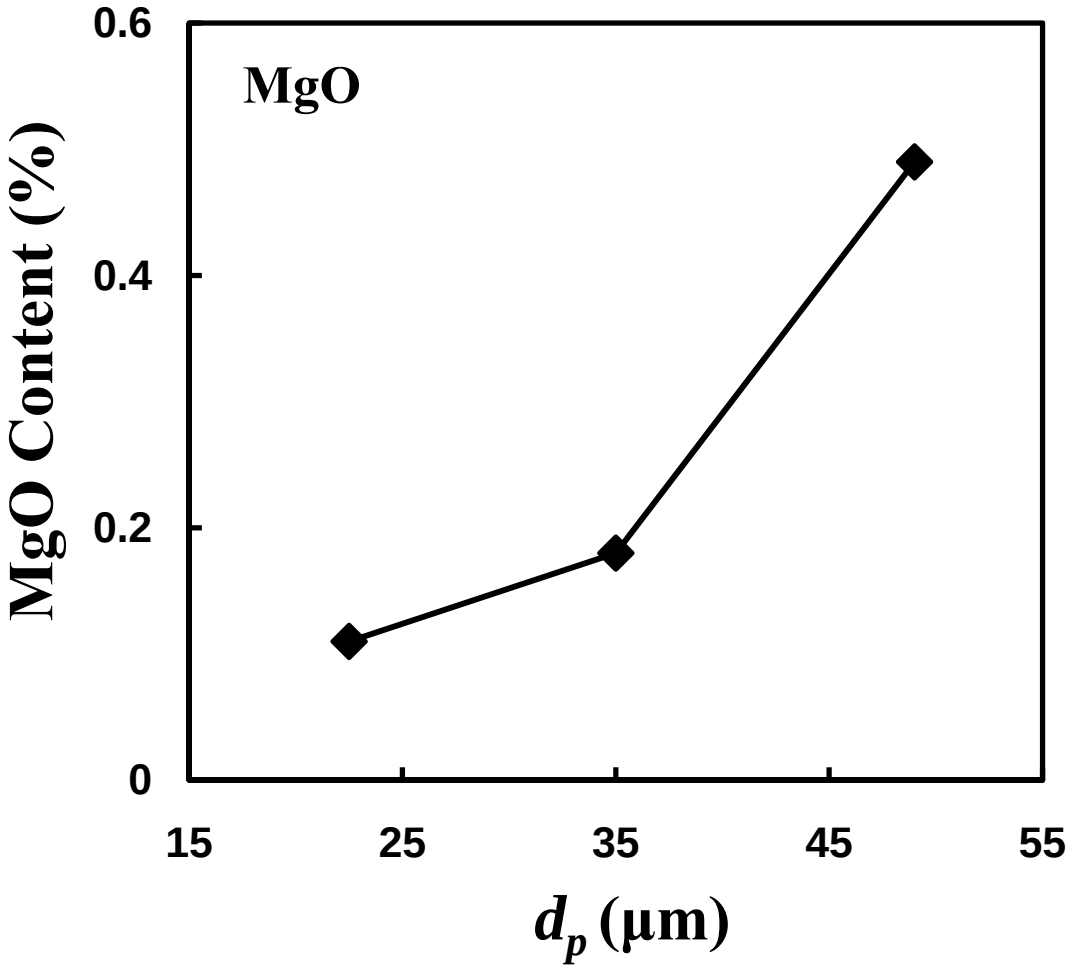

Figure 23. The relationship between MgO content and particle size of concentrate.

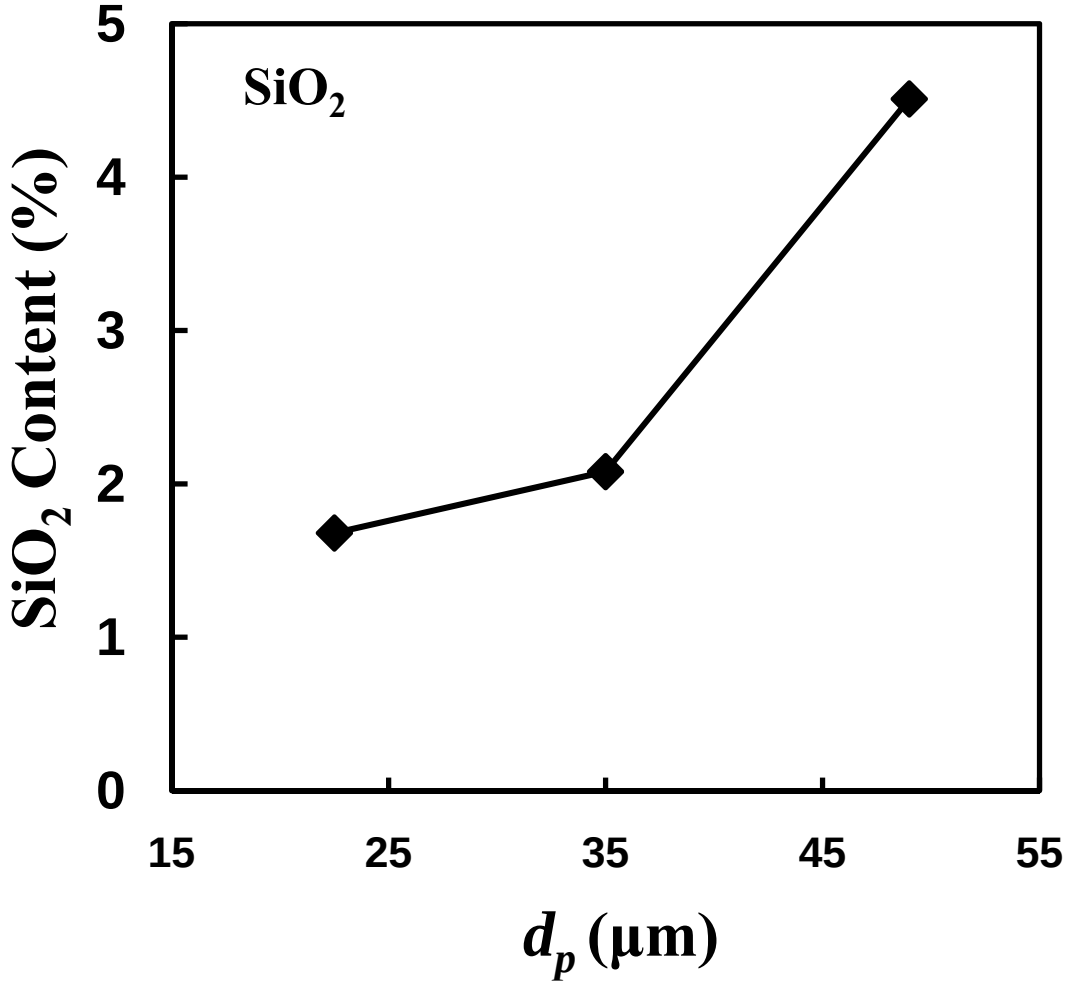

Figure 24. The relationship between SiO_2 content and particle size of concentrate.

$$\text{slope} = k \cdot f_d = k \cdot (d_p)^s \quad (15)$$

$$Ln\ (slope) = Ln\ k + s \cdot Ln\ (d_p) \quad (16)$$

The plots of equation (16) at different temperatures are shown in Figures 25 - 28, which indicate that the value of s varied with the temperature. The relationship is shown in Figure 29. The relationship between particle size factor and temperature is expressed in equation (17) - (18).

$$s = \frac{2.73 \times 10^8}{T^2} - \frac{345930}{T} + 109.5 \qquad T = 1423 \sim 1573\ \text{K} \quad (17)$$

$$s = 0 \qquad T \geq 1573 \quad (18)$$

4.6 Determination of Activation Energy

After the functional dependence of the rate on partial pressures of reducing gaseous species (f_p) and particle size (f_d) are determined, the reaction rate constant k is obtained by combining equations (12) and (13).

$$k = k_{app}/(f_p \cdot f_d) \quad (19)$$

$$k = k_0 \cdot exp\ (-E/RT) \quad (20)$$

$$Ln\ k = Ln\ k_0 - \frac{E}{R} \cdot \frac{1}{T} \quad (21)$$

Combining equations (19) - (21), activation energy is obtained from the slope of the plot of *Ln k* vs *1/T*.

The activation energy is obtained from the plot of $(Ln\ k_0 - E/RT)$ and $10^4/T$, as shown in Figure 30. The slope in Figure 30 leads to the value of E/R = 55790, which yields an activation energy value of 463 kJ/mol in the temperature range between 1423

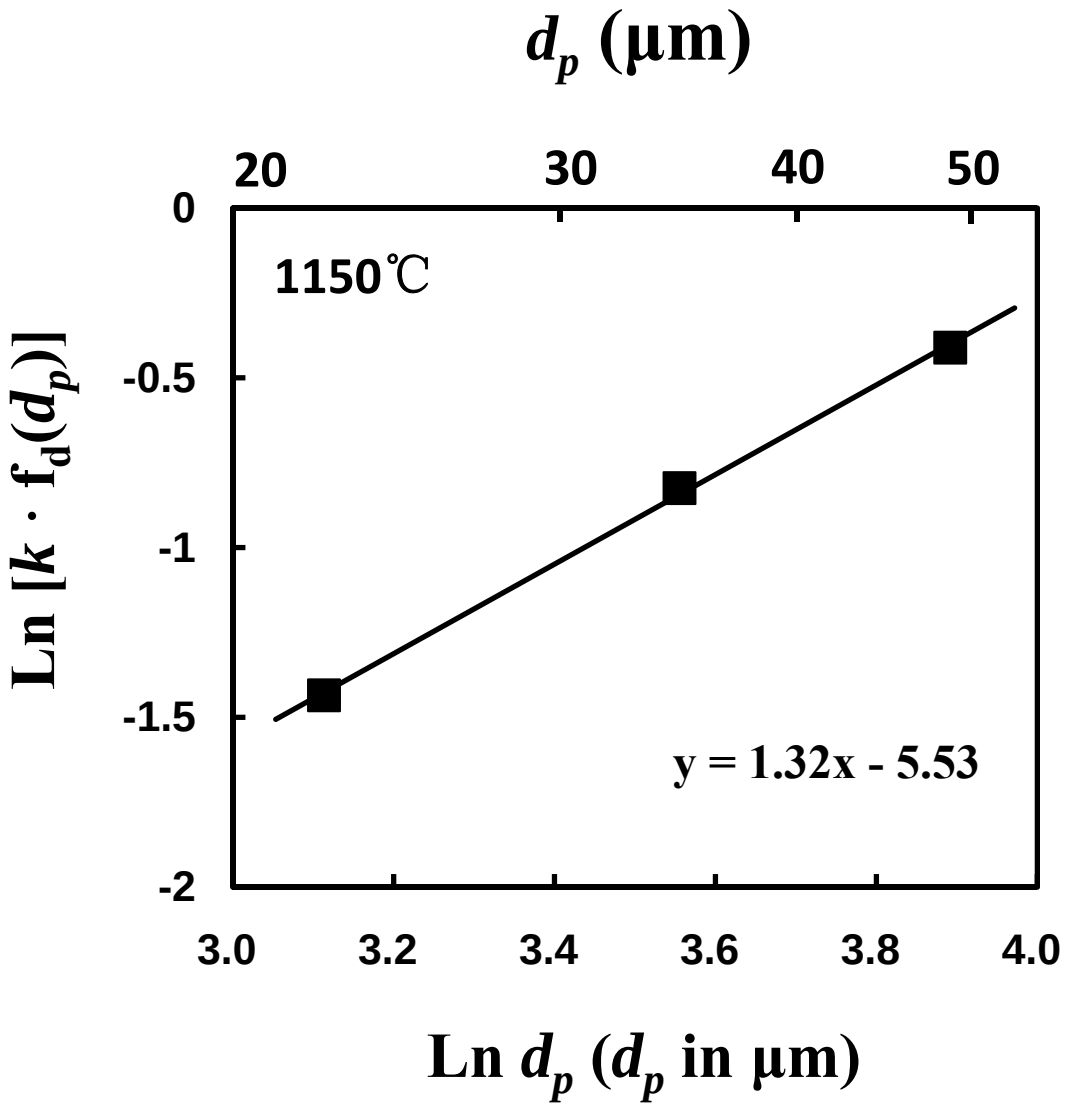

Figure 25. Relationship between particle size, d_p and $k \cdot f_d(d_p)$ at 1150℃.

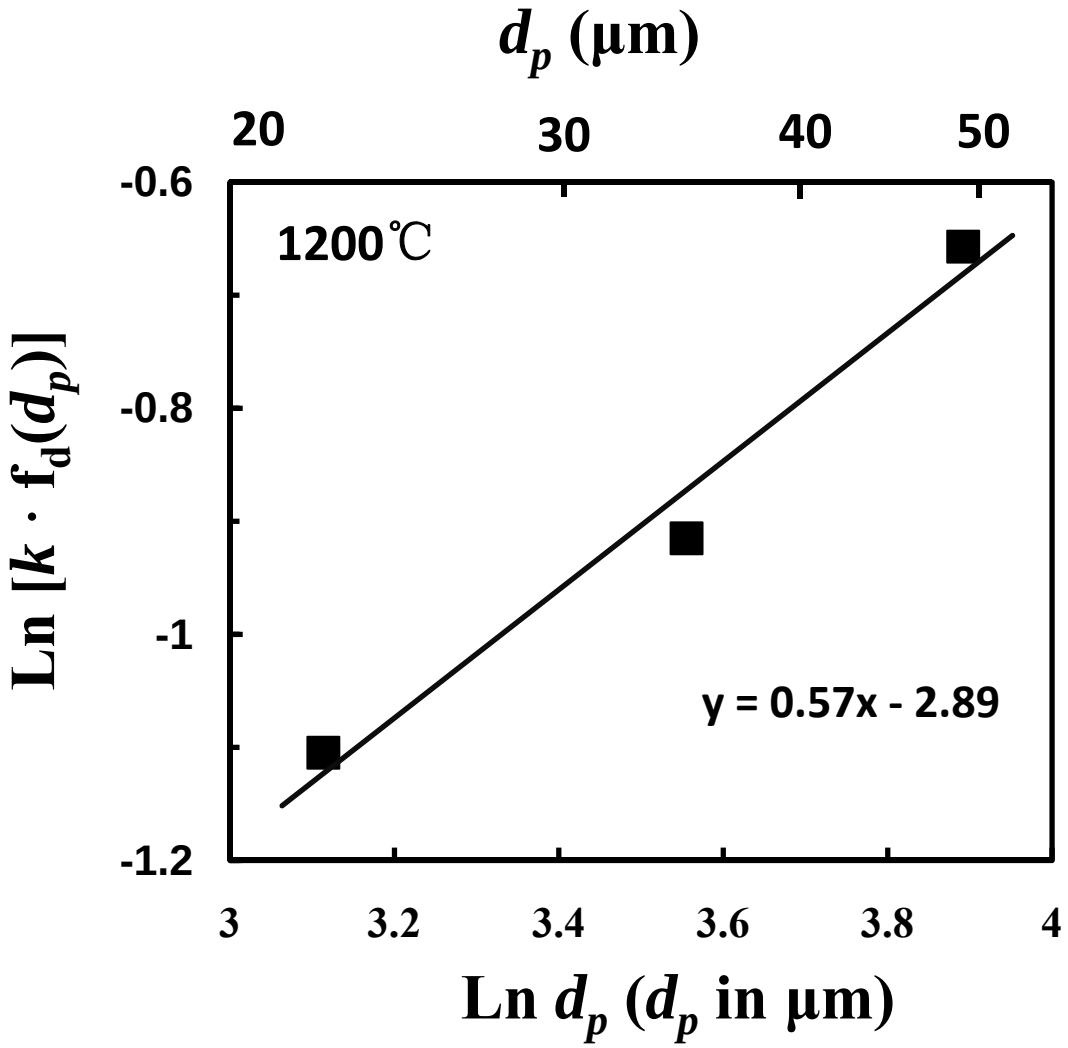

Figure 26. Relationship between particle size, d_p and $k \cdot f_d(d_p)$ at 1200℃.

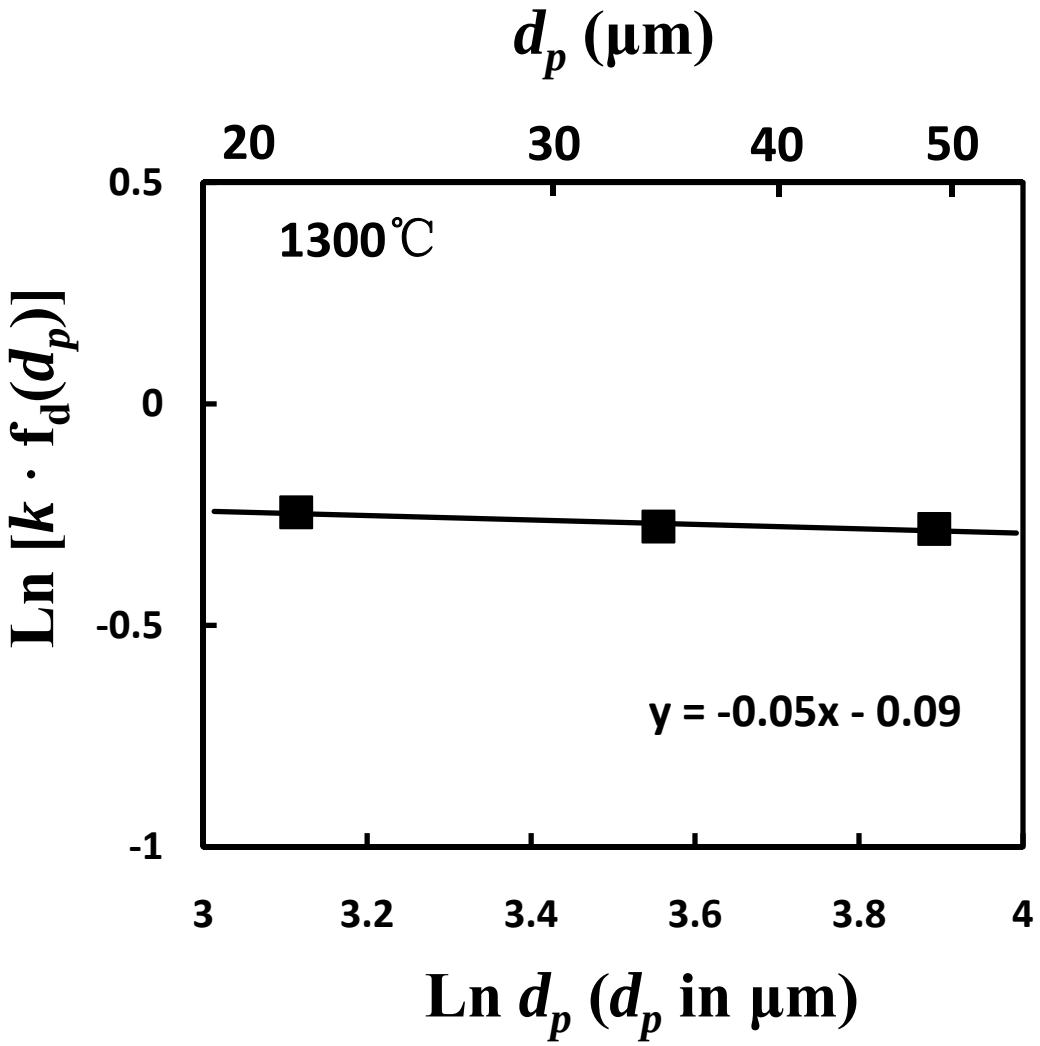

Figure 27. Relationship between particle size, d_p and $k \cdot f_a(d_p)$ at 1300℃

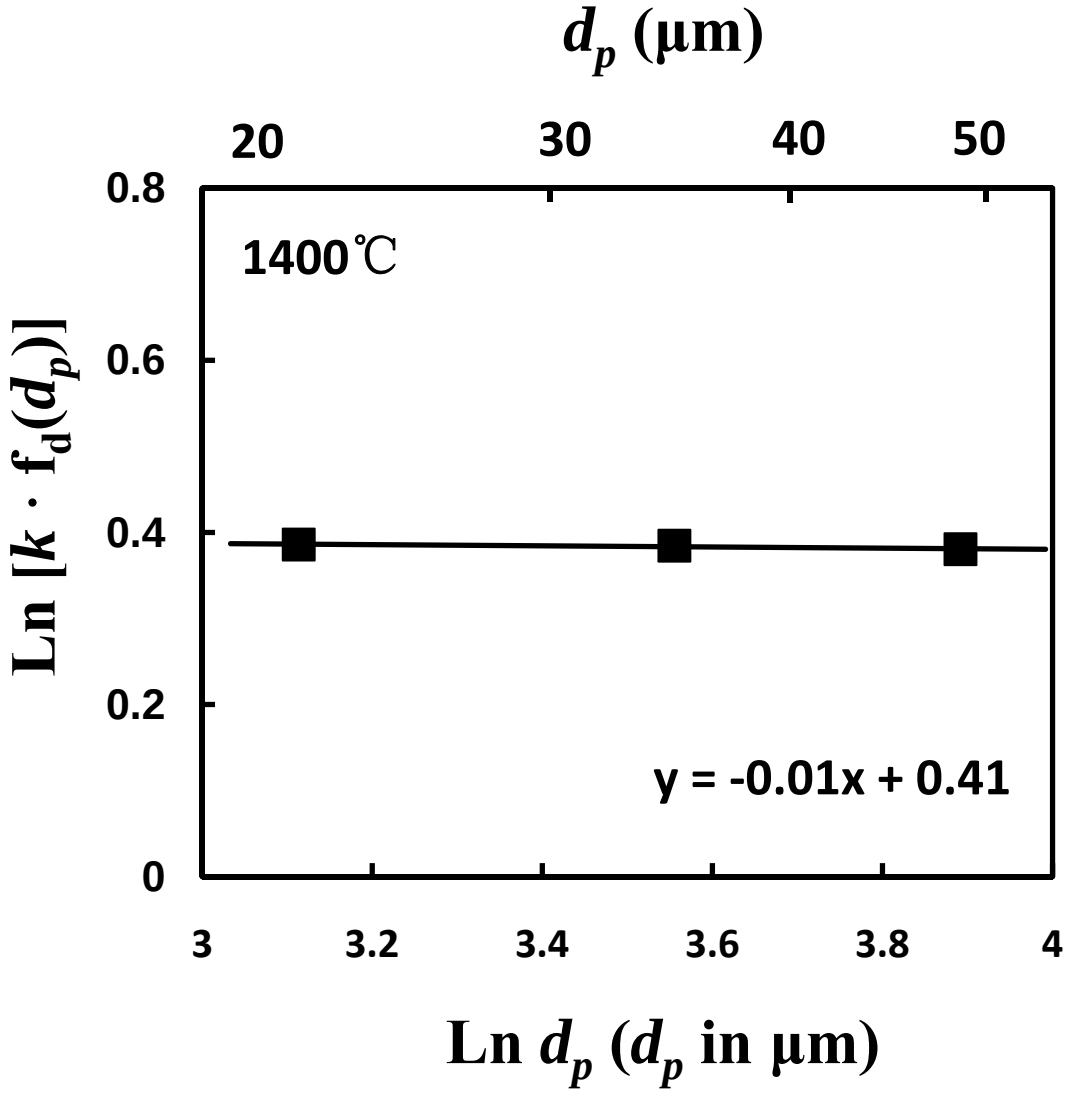

Figure 28. Relationship between particle size, d_p and $k \cdot f_d(d_p)$ at 1400℃

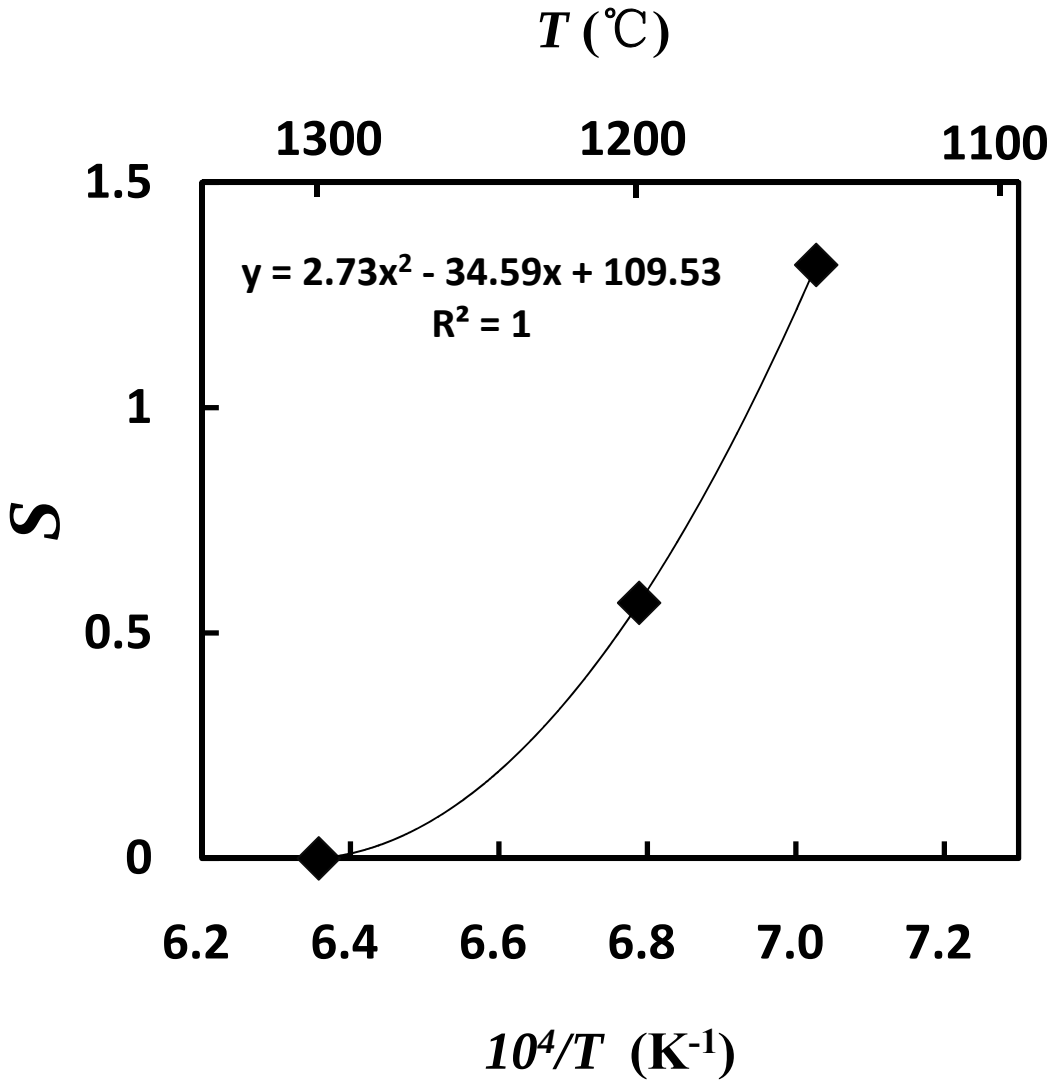

Figure 29. the relationship between s and temperature

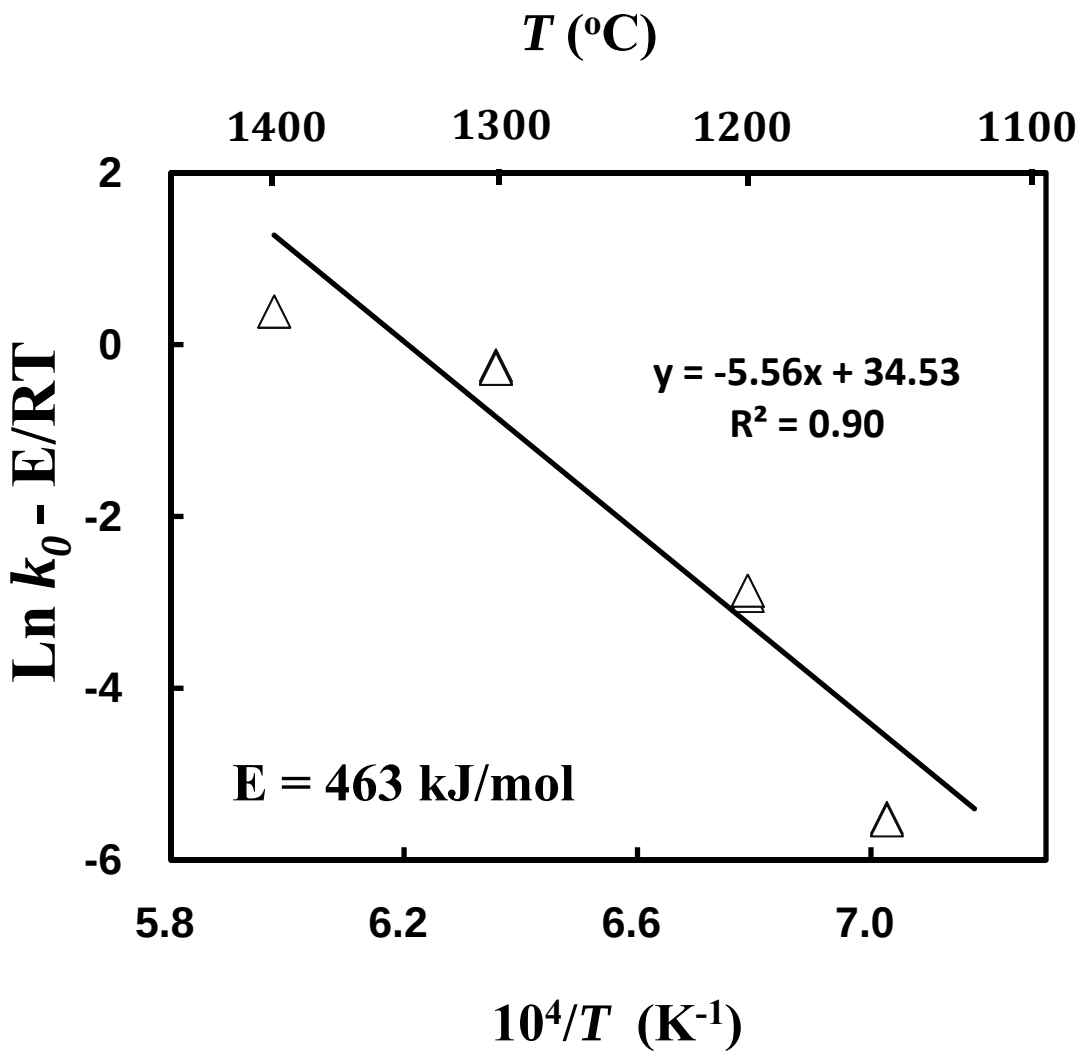

Figure 30. Arrhenium plot between Ln k_0 - E/RT and $10^4/T$.

and 1673 K. The complete rate equation is now expressed as follows:

$$\frac{dX}{dt} = 2\,k \cdot \left[p_{H_2}^{1/2} - (p_{H_2O}/K)^{1/2}\right]_{am} \cdot \left(d_p\right)^{s} \cdot (1-X) \cdot [-Ln\,(1-X)]^{1/2} \qquad (22)$$

Strictly speaking, the functional dependence of rate on partial pressure of hydrogen and water vapor, $p_{H_2}^{1/2} - (p_{H_2O}/K)^{1/2}$, should be integrated. But when its variation is small or when $p_{H_2}^{1/2} - (p_{H_2O}/K)^{1/2}$ is constant by using a large excess amount of H_2, it could be also expressed as follows:

$$[-Ln\ (1-X)]^{1/2} = (9.9 \times 10^{14}) \cdot e^{-\frac{463000}{RT}} \cdot \left[p_{H_2}^{1/2} - (p_{H_2O}/K)^{1/2}\right]_{am} \cdot (d_p)^{s} \cdot t \qquad (23)$$

where:

$$s = \frac{2.73 \times 10^{8}}{T^2} - \frac{345930}{T} + 109.5 \qquad T = 1423\sim1573\ \text{K}$$

$$s = 0 \qquad T \geq 1573 \qquad (24)$$

R is 8.314 J/mol/K, *T* is in K, *p* is in atm, d_p is in μm, and *t* is in seconds.

In Figure 30, there are three different values representing the values of Ln *k* with three different particle sizes listed at each temperature. When the value of $f_d(d_p)$, the functional dependence of rate on the particle size was obtained, different initial H_2 partial pressures were involved and the same value of the functional dependence of rate was achieved. Totally, the value of the vertical axis at every temperature represents at least six different experimental runs.

4.7 Comparison of Experimental and Calculated Results

Comparison was made between the experimental results and those calculated by the rate expression developed in this study. Figures 31 - 36 show the comparison for 32 - 38 μm particles at different temperatures. The plot of calculated results versus experimental results was made, as shown in Figure 37. The rest of the comparison is given in Appendix F. It is seen that the calculated results agreed well with the experimental results except for some points at low reduction degrees. As mentioned previously, the reduction of magnetite to iron proceeds through the formation of FeO with a change in reactivity after the removal of about 25 % of the initial oxygen content. This increased the difference at lower reduction degrees between the experimental results and those calculated by the global rate expression that mainly represents the kinetics of wustite reduction.

4.8 Effect of Addition of CO on the Reduction Rate

The previous sections described work on kinetics measurements conducted using H_2 or the mixture of H_2 and N_2. Syngas and reformed natural gas, which are mainly composed of CO and H_2, are also possible reducing reagents in this process. Experiments were done to determine the kinetics of concentrate reduction by the mixtures of CO and H_2.

At 1200℃, N_2 was replaced by CO while the partial pressure of H_2 was kept at 0.3 atm. The results showed that there was little effect of the addition of CO on the reduction degree, as shown in Figure 38. At 1300℃, N_2 was replaced by CO while the partial pressure of hydrogen was kept at 0.2 atm. The results in Figure 39 indicate that the replacement of N_2 by CO promoted the reduction rate. When temperature was further

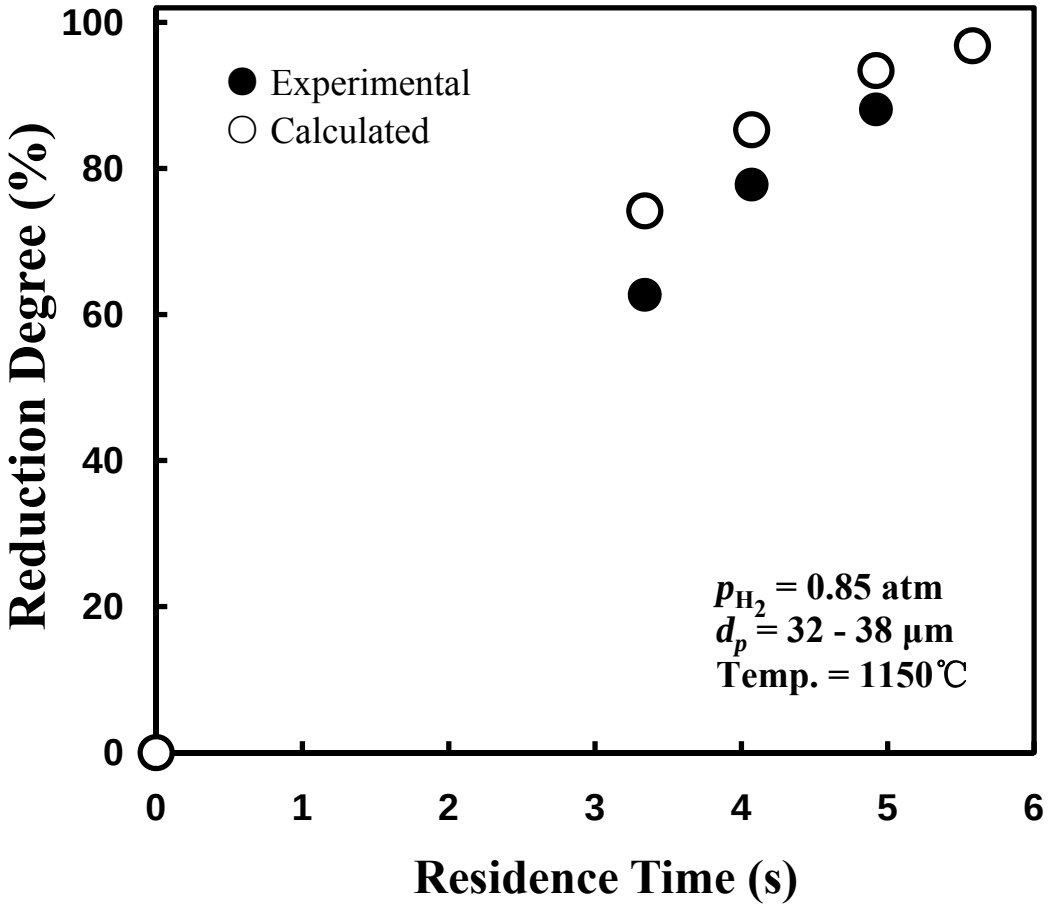

Figure 31. Comparison of experimental and calculated results

p_{H2} = 0.85 atm; d_p = 32 - 38 μm; Temp. = 1150℃

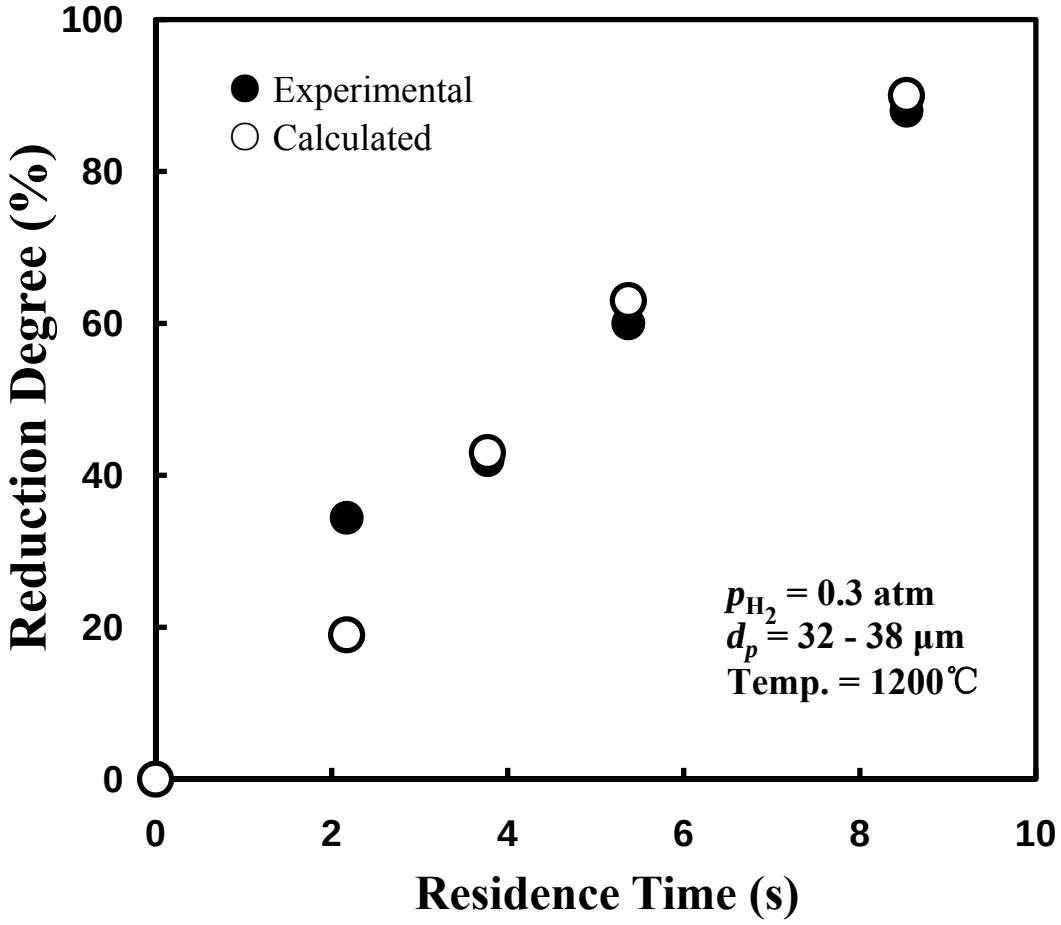

Figure 32. Comparison of experimental and calculated results

p_{H2} = 0.3 atm; d_p = 32 -38 μm; Temp. = 1200℃

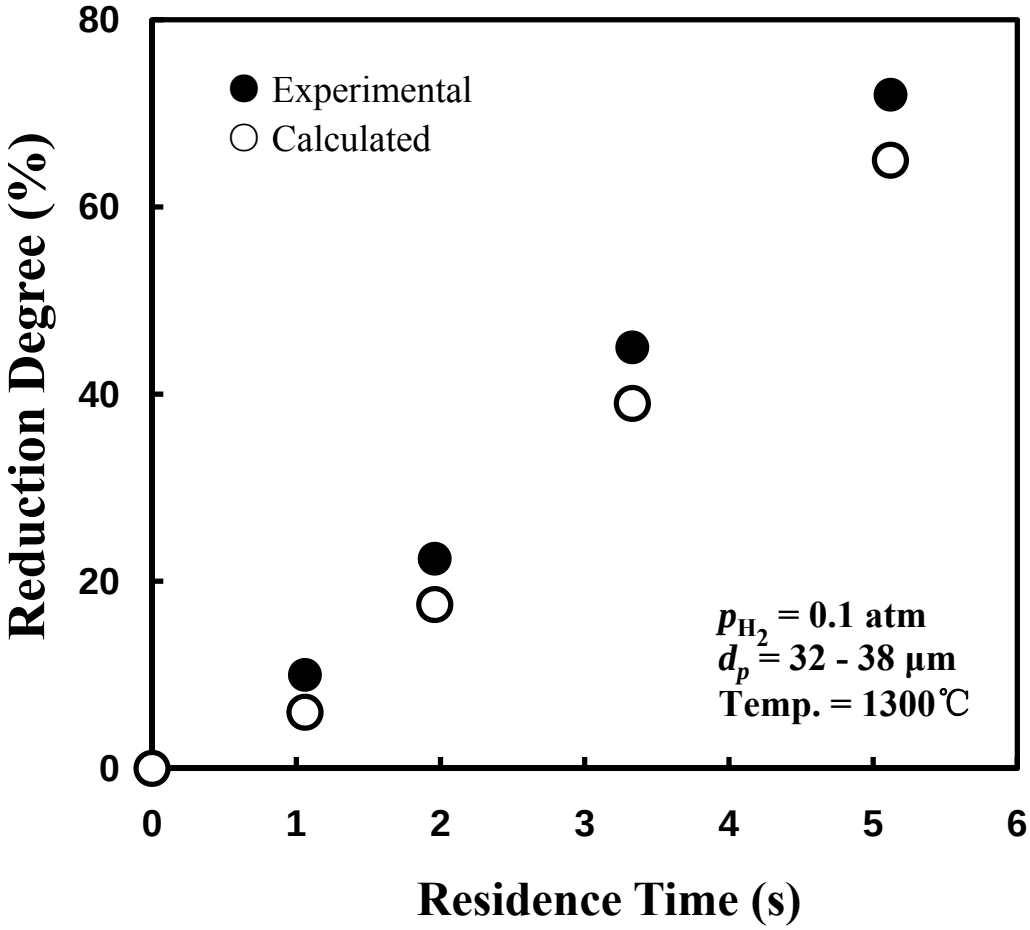

Figure 33. Comparison of experimental and calculated results

p_{H2} = 0.1 atm; d_p = 32 - 38 μm; Temp. = 1300℃

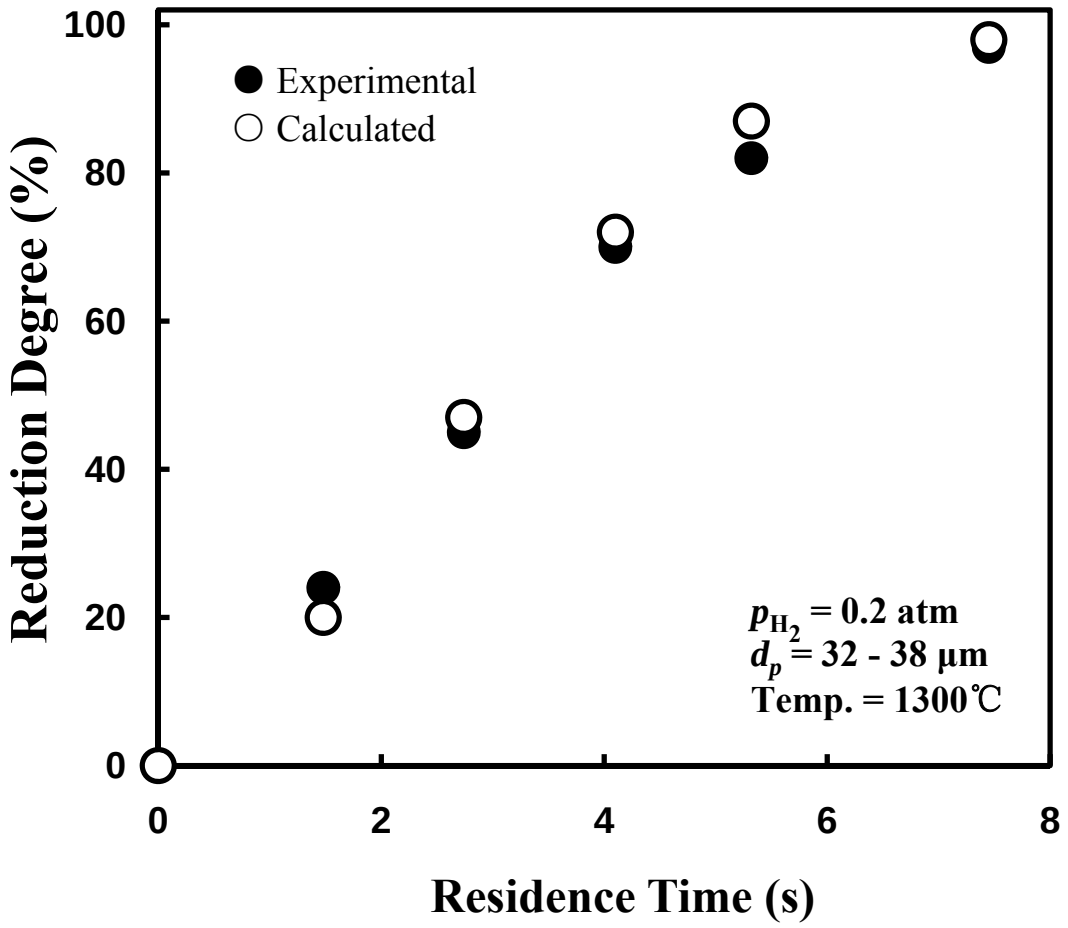

Figure 34. Comparison of experimental and calculated results

p_{H2} = 0.2 atm; d_p = 32 - 38 μm; Temp. = 1300℃

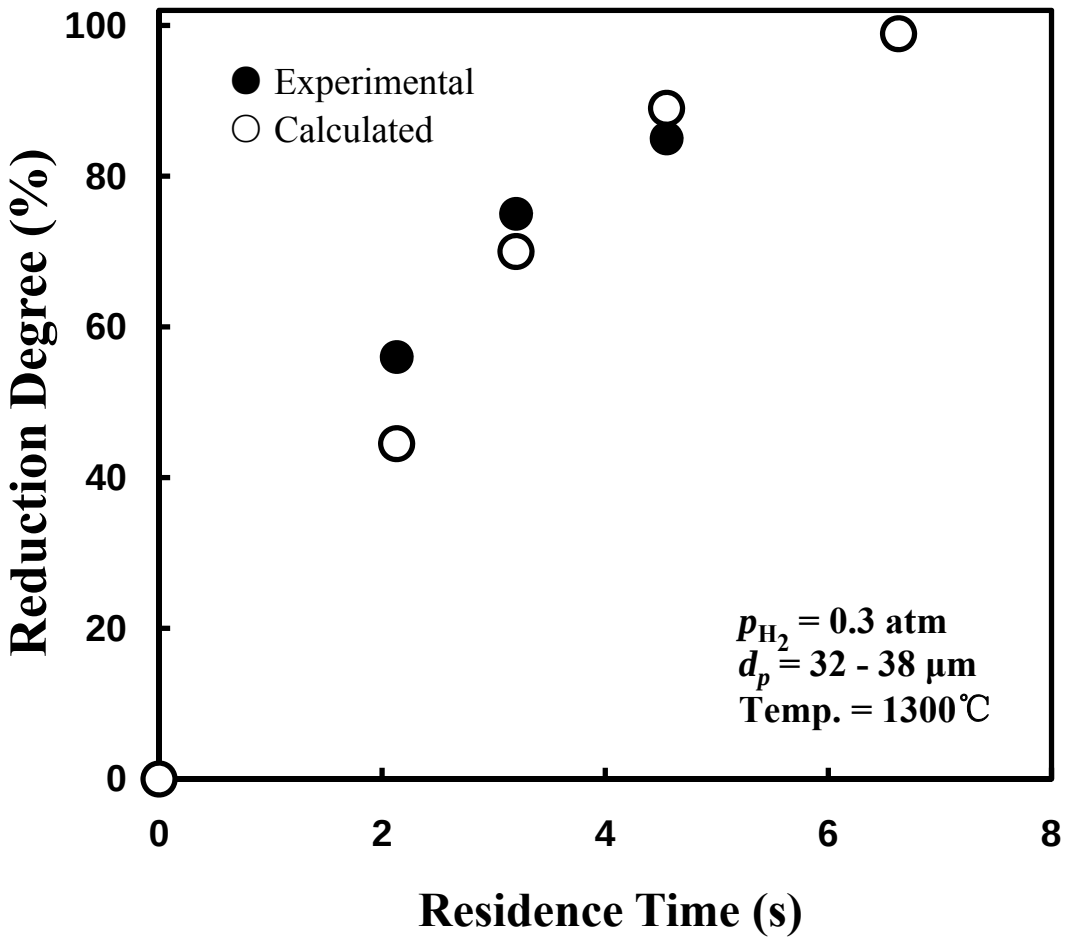

Figure 35. Comparison of experimental and calculated results

p_{H2} = 0.3 atm; d_p = 32 - 38 μm; Temp. = 1300℃

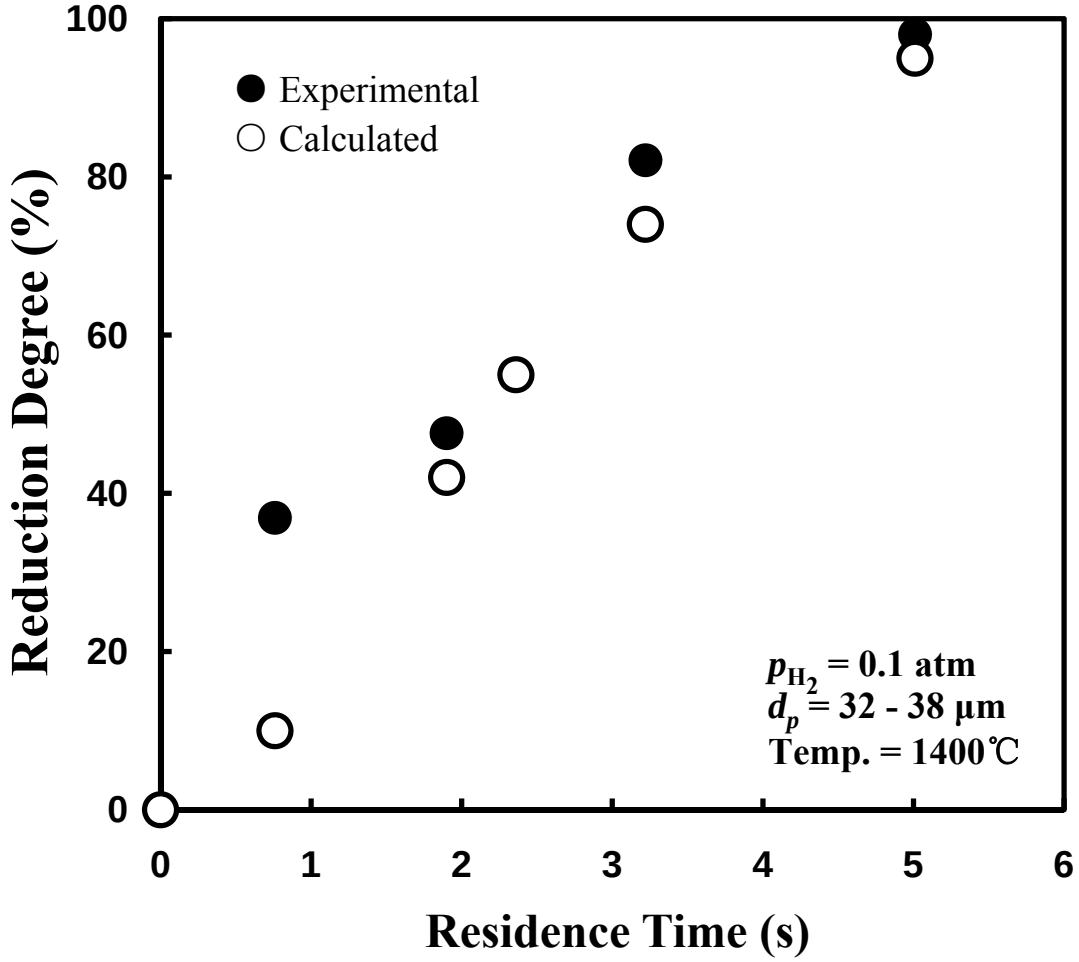

Figure 36. Comparison of experimental and calculated results

p_{H2} = 0.1 atm; d_p = 32 - 38 μm; Temp. = 1400℃

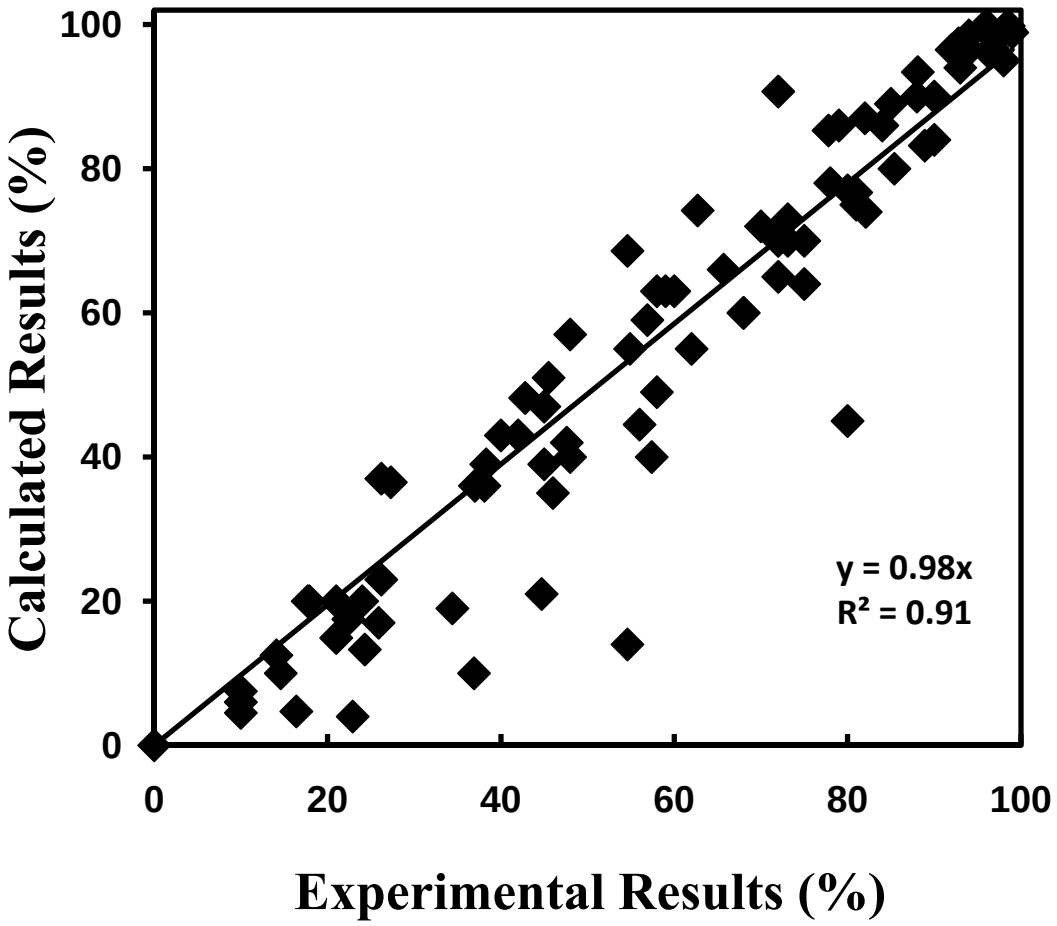

Figure 37. Comparison between calculated results and experimental results.

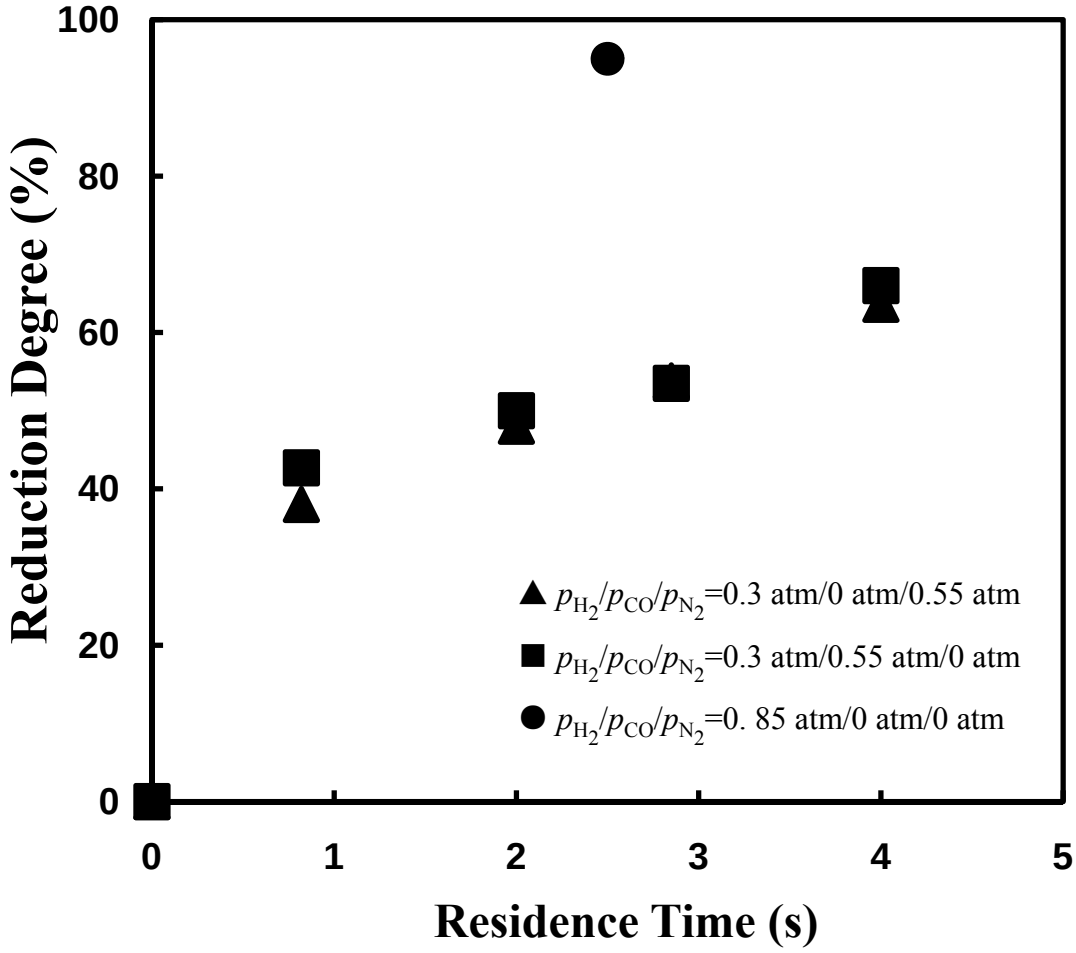

Figure 38. Effect of reducing gas type on the reduction rate of sample with 32 - 38 μm at 1200℃ with 800% excess H_2 for all mixtures.

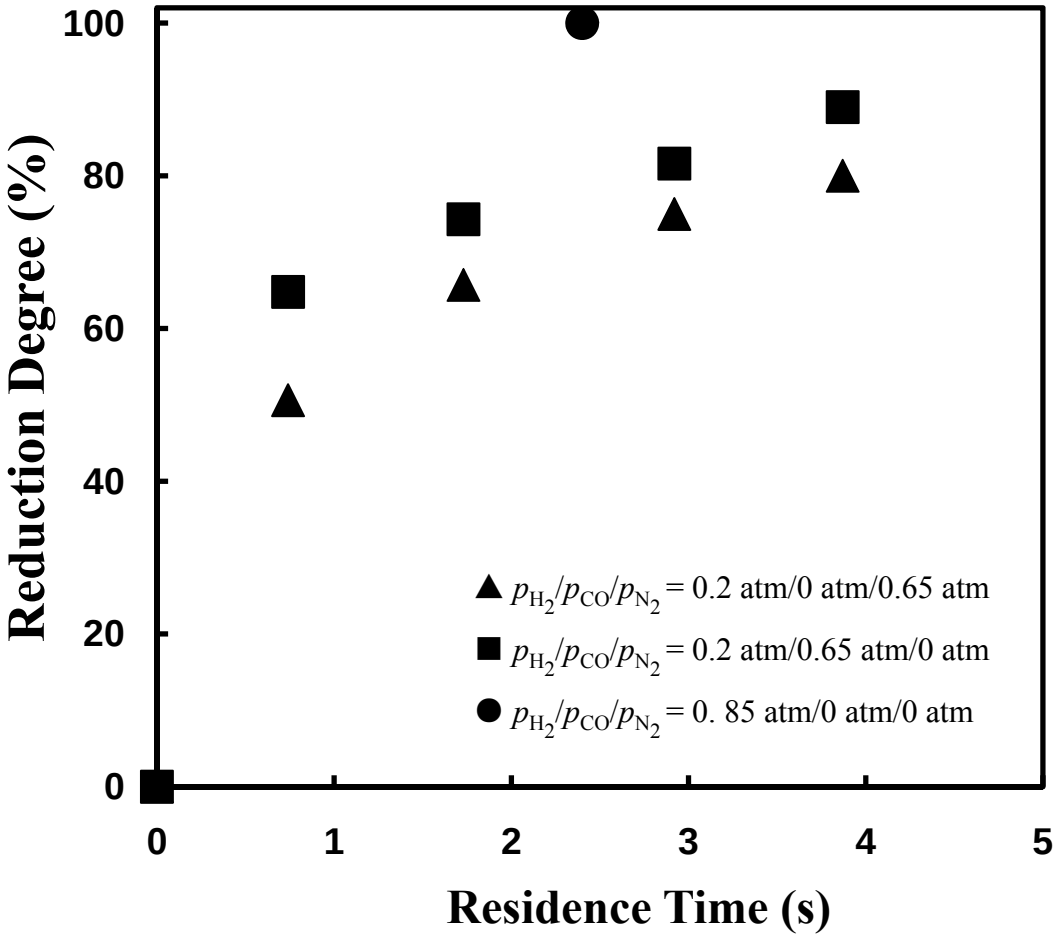

Figure 39. Effect of reducing gas type on the reduction rate of sample with 32 - 38 μm at 1300℃ with 800% excess H_2 for all mixtures.

increased to 1400℃, the reduction rate was significantly increased when N_2 was replaced by CO, as shown in Figure 40. All these runs were in the presence of excess hydrogen.

The reduction of iron oxide by a mixture of H_2 and CO is complicated due to the simultaneous reduction by the two reductants as well as the water-gas shift reaction involving CO and H_2 with the production gases H_2O and CO_2. More detailed determination of the kinetics of reduction by CO/H_2 mixture was beyond the scope of this work. However, the results showed that the reduction rate was decreased significantly when pure hydrogen was replaced by syngas with different composition of H_2 and CO when experiments were conducted at 1200 - 1400℃.

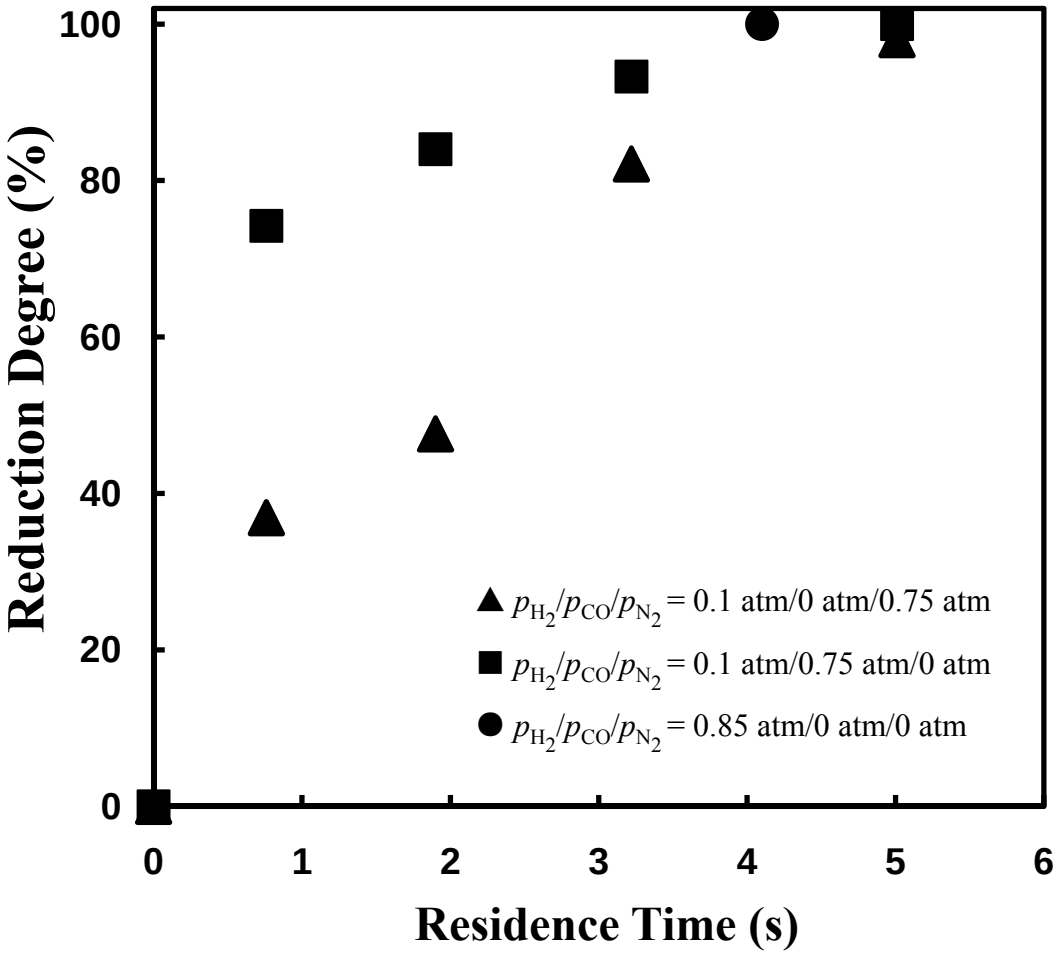

Figure 40. Effect of reducing gas type on the reduction rate of sample with 32 - 38 μm at 1400℃ with 200% excess H_2 for all mixtures.

CHAPTER 5

CONCLUSIONS

The kinetics feasibility tests showed that 90 - 99% reduction of iron ore concentrate by hydrogen was obtained within 1 - 7 seconds at 1200 - 1400℃, depending on the amount of excess hydrogen supplied with iron oxide. This reduction rate is fast enough for a flash reduction process.

The nucleation and growth kinetics expression was found to describe the kinetics after detailed calculation and morphological examination of the reduced sample, and it gave the best fit of the experimental data. The dependences of rate on partial pressure of hydrogen, partical size, and temperature were determined. The following conclusions were reached:

1. Results at different temperatures indicated that Avarami parameter of n = 2 gave the best fit of the experimental data.
2. The reduction rate has 1/2-order dependence on the partial pressure of hydrogen, which suggests that an increase in partial pressure of reducing gas has a more moderate effect on reduction rate than a typical 1st-order reaction.
3. The reduction rate increased with the particle size when reduction temperature is lower than 1300℃. The effect of particle size is negligible at temperatures

higher than 1300℃. The temperature dependence of particle size effect was determined quantitatively.

4. The activation energy of hydrogen reduction of iron ore concentrate was determined to be 463 kJ/mol, which demonstrats that this process has greater temperature effect on the reducion rate than most reactions.
5. A complete rate equation was obtained.

Although hydrogen is best as a reductant and/or fuel from the environmental and reduction kinetics points of view, it is currently expensive. Then, syngas which is mainly composed of H_2 and CO from the reforming of natural gas or the coal gasification, is used as a reducing gas mixture for the majority of direct reduction processes. The results at different temperatures showed that the replacement of N_2 by CO significantly increases the reduction rate above 1400℃. On the other hand, the rate was much slower when a part of H_2 was replaced by CO.

APPENDIX A

MODIFIED TITRATION METHOD OF DETERMINATION OF

TOTAL IRON CONTENT IN IRON OXIDE CONCENTRATE

SAMPLE GRAVIMETRIC ANALYSIS OF IRON

1. Preparation of Potassium Dichromate solution

- Pulverize 2 grams of potassium dichromate in an agate mortar.
- Add the pulverized content to a clean 50-ml beaker.
- (Weigh the beaker and its contents before drying). Using a watch glass and 50-ml beaker and its contents, dry the solid in an oven @ 110℃ for 1 hour.
- After drying, put the arrangement of beaker and watch glass into a sealed desiccator, let cool for 10-20 min.
- Remove the beaker from the desiccator.

NOTE: The intial and final weights of the beaker should be weighed to be subtracted later on.

- Transfer 0.4800-0.4900 gram of dried potassium dichromate into a clean 50-ml beaker, and reweigh the empty beaker to the nearest milligram in order to determine the weight of the potassium dichromate by difference.
- Dissolve the potassium dichromate by adding 10 ml distilled water to the beaker.
- Transfer the solution quantitatively, with the aid of a glass funnel, to a clean volumetric flask.

NOTE: To ensure that the potassium dichromate solution is transferred quantitatively, let the solution drain as completely as possible from the beaker into the funnel. Then place a small volume of distilled water into the beaker, rinse all the inside surface that had contacted the solution, and add the rinse solution to the volumetric flask. Two or three repetitions should be sufficient if each drainage has been as complete as possible and the solution has not beaded on the surface of the funnel due to improper cleaning.

- Add distilled water to the volumetric flask, to bring the solution up to the calibration mark.
- Put a stopper (lid) on the flask, and shake thoroughly.
- From the weight of potassium dichromate used, calculate the concentration of the solution. Be sure to label the volumetric flask containing your standard solution.
- Transfer the concentrated potassium dichromate to a burette with stop-cock.
- Open the stop-cock for 2-3 sec. so that the solution comes out from the end tip to rid any bubbles stuck inside and close.
- Record your initial volume.

2. Preparation of the iron sample

- Transfer approximately 0.1800-0.1900 gram of the iron sample into a clean dry 250-ml Erlenmeyer flask.
- Weigh by difference, reweigh an empty 250-ml conical Erlenmeyer flask.

3. Dissolving the iron sample

- Add 30 ml HCl acid to 250-ml Erlenmeyer flask containing iron sample.
- Add a small magnet to flask(s).
- Heat and magnetically stir @ 6 corning scale for 40-50 min.

- Turn off ‘heat’ and magnetically stir for 10-20 min.

NOTE: If the iron is not dissolved thoroughly in the solution, add 10 ml of HCl to your sample(s), heat and magnetically stir @ 6 corning scale for 40-50 min.

- When the iron sample(s) have dissolved thoroughly
- Let the sample(s) continue to cool 10-15 min.

NOTE: A residue of white or gray-white silica can be ignored.

4. Preparation of special reagents

Concentrated Tin (II) Chloride: Dissolve 7.5-7.6 grams of Tin (II) Chloride Dihydrate ($SnCl_2*2H_2O$), successively in small amounts, with 50 ml hydrochloric acid by warming. Cool, transfer the liquid to a volumetric flask (250 ml) and dilute to the calibrated mark.

Concentrated sulfuric-phosphoric acid mixture: Add cautiously, while stirring, 50 ml of sulfuric acid (>1,84 g/ml) and 50 ml phosphoric acid (>1.7 g/ml) to 200 ml of water. Cool, transfer the liquid to a volumetric flask (500 ml) and dilute to the calibrated mark.

Concentrated Mercury (II) Chloride: Dissolve 0.6500-0.6600 gram of Mercury (II) Chloride ($HgCl_2$), in 50 ml of hot water. Cool, transfer the liquid to a volumetric flask (250 ml) and dilute to the calibrated mark.

NOTE: Calculate the concentration of each special reagent and label.

Adding special reagents to flask(s) containing sample + HCl acid

NOTE: Have the correct volume of reagents ready before adding them to the sample(s), it has to be quick and smooth for the reactions to take place.

- Heat the sample solution up to boiling point.
- Now quickly add 0.1580-0.1600 M $SnCl_2$ solution drop by drop, while swirling the flask, until the yellow color of iron (III) just disappears.

- Add one more drop of $SnCl_2$ solution.
- Rapidly cool the solution below 25℃ and add *all* at once 10 ml of 0.0090 M Mercuric Chloride solution.

NOTE: A silky white precipitate should form, if the precipitate is grey or black, the sample must be discarded. An incorrect amount of $SnCl_2$ as added to the solution.

- After 2 or 3 minutes, add 10 ml sulfuric-phosphoric acid mixture and 50 ml distilled water and proceed to the addition of special reagents and the titration.

5. Addition of special reagents:

- Add 8 drops of Sodium Diphenylamine Sulfonate indicator solution before titration.

6. Titration

- Titrate the solution with your standard potassium dichromate solution to an endpoint marked by the sudden appearance of a deep violet color throughout the solution.
- Record the amount of the volume of potassium dichromate solution used in every set of titration.

APPENDIX B

FIGURES OF EFFECT OF TEMPERATURE ON REDUCTION RATE OF MAGNETITE CONCENTRATE PARTICLES

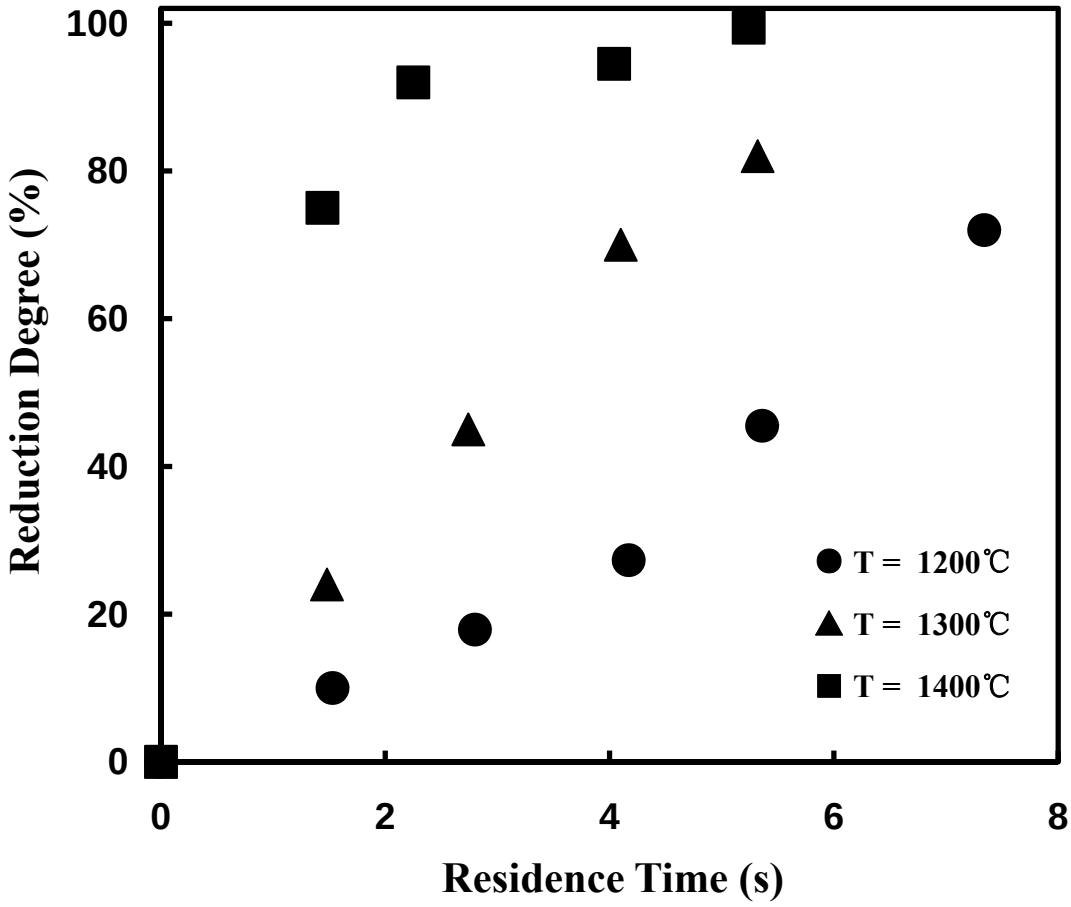

Figure 41. Effect of temperature on the reduction rate of the sample with 32 - 38 μm with 200% excess hydrogen (p_{H2} = 0.2 atm)

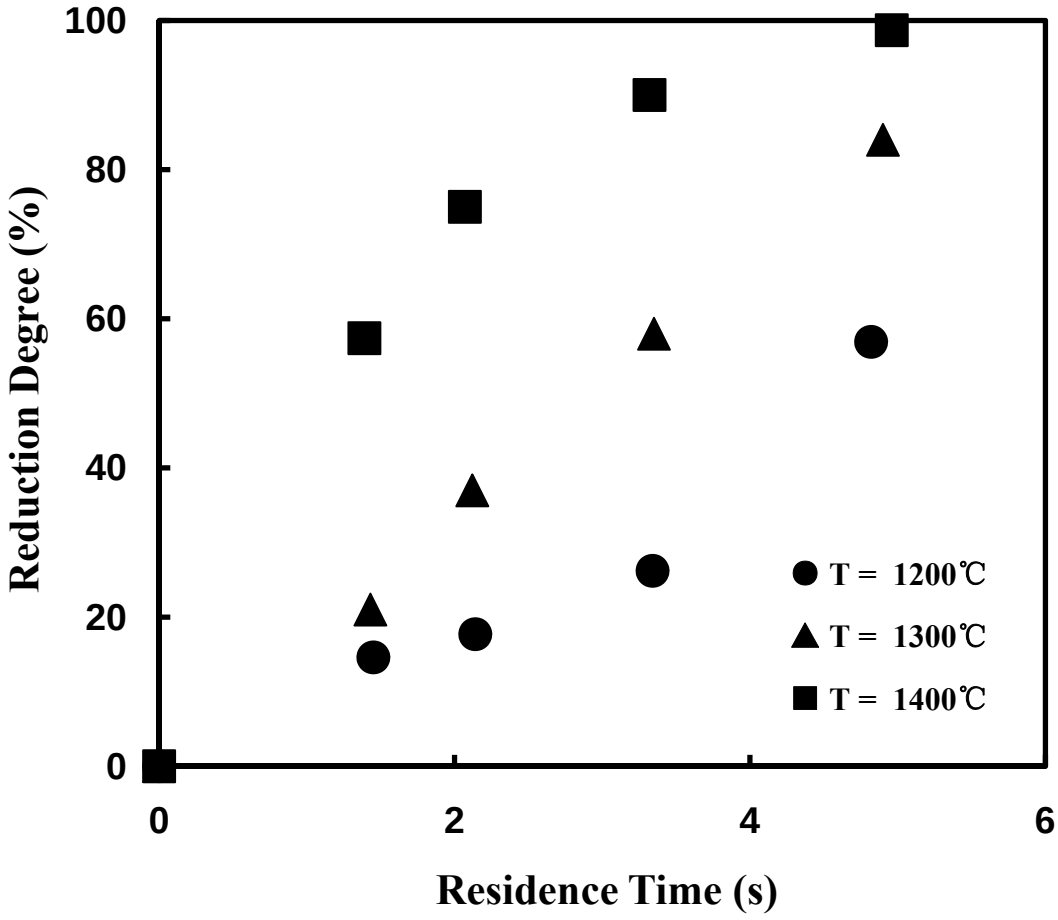

Figure 42. Effect of temperature on the reduction rate of the sample with 45 - 53 μm with 200% excess hydrogen (p_{H2} = 0.2 atm)

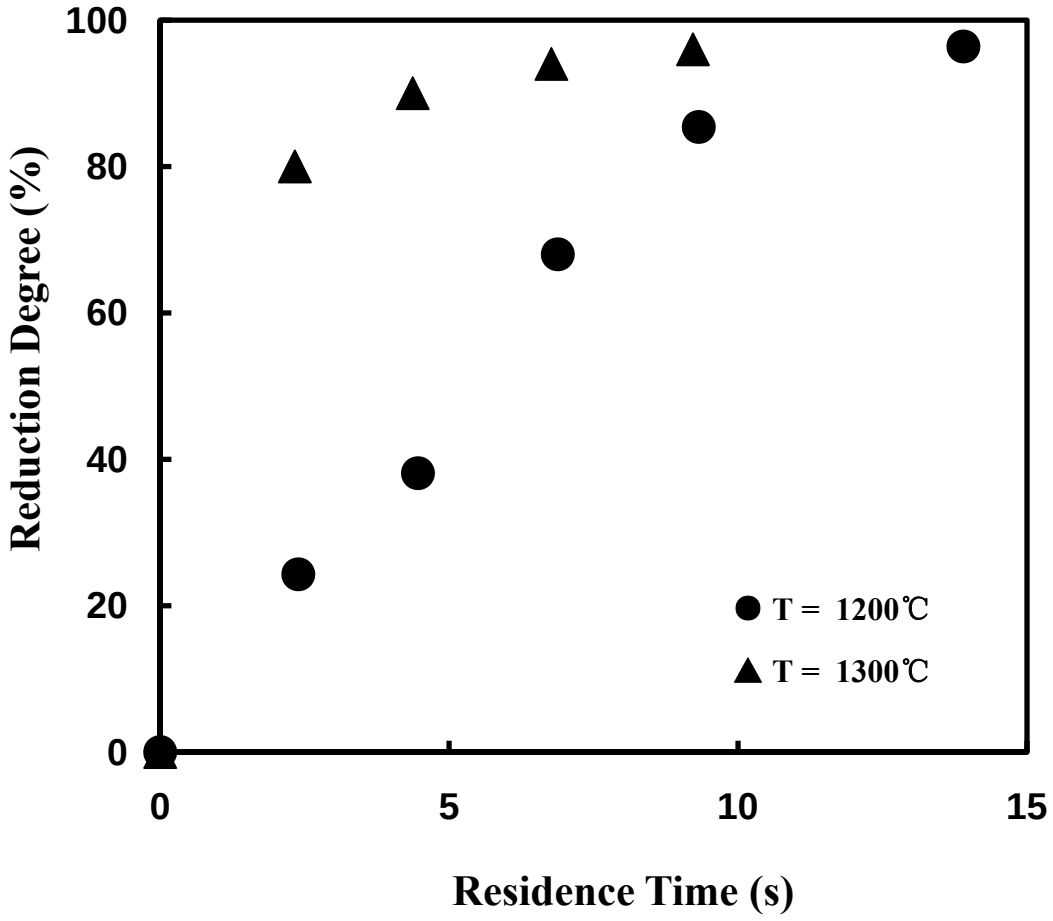

Figure 43. Effect of temperature on the reduction rate of the sample with 20 - 25 μm with 200% excess hydrogen (p_{H2} = 0.3 atm)

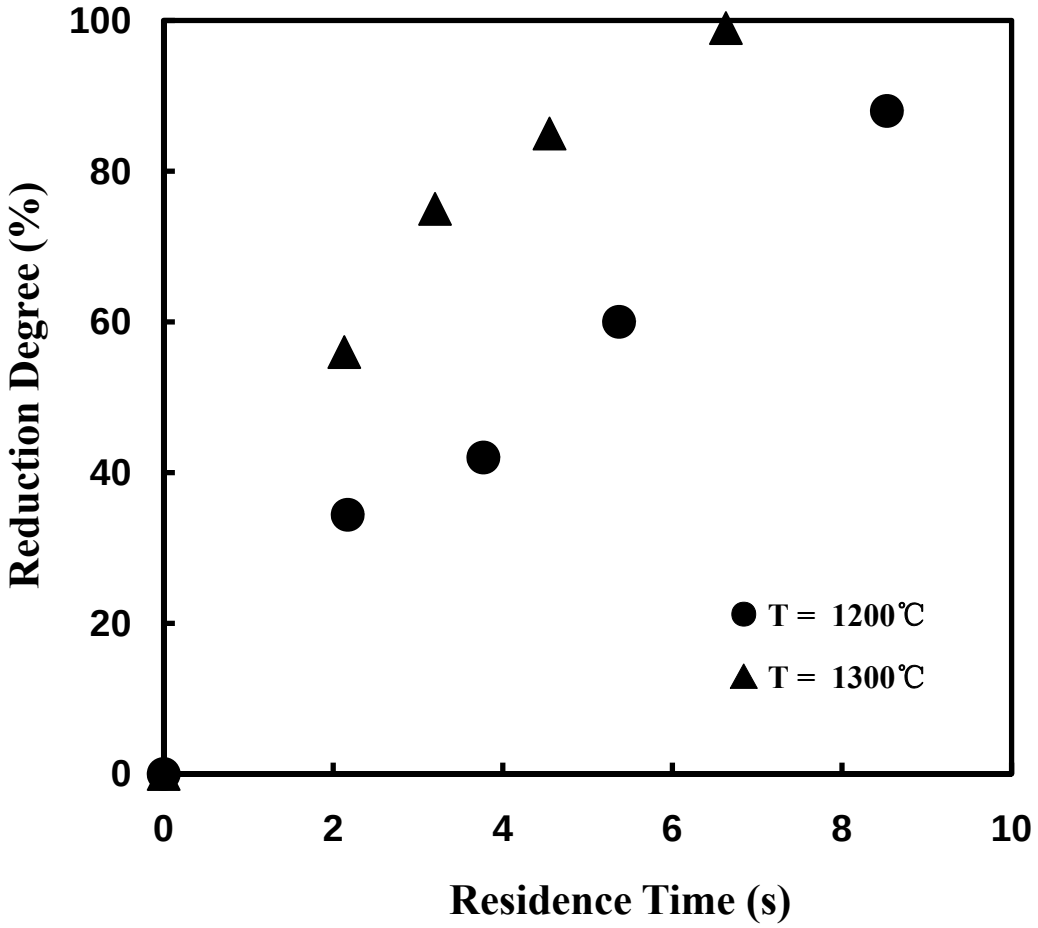

Figure 44. Effect of temperature on the reduction rate of the sample with 32 - 38 μm with 200% excess hydrogen (p_{H2} = 0.3 atm)

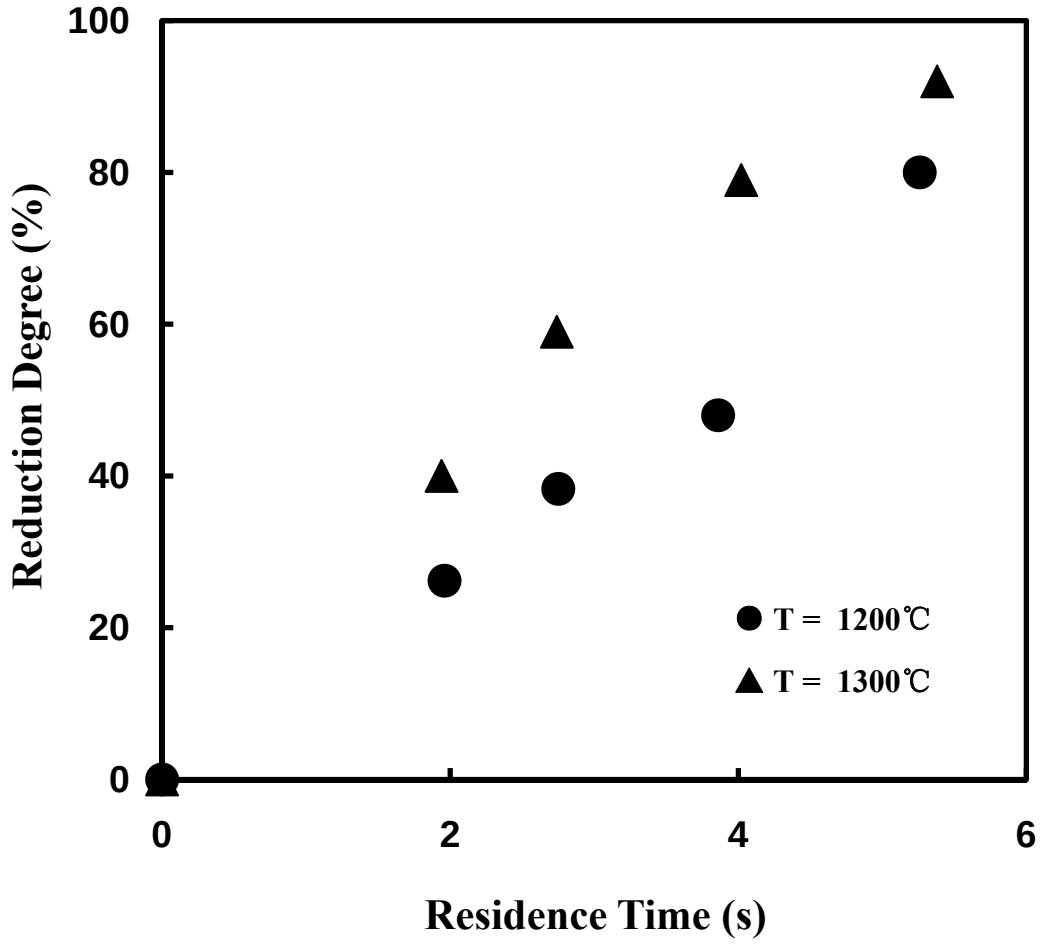

Figure 45. Effect of temperature on the reduction rate of the sample with 45 - 53 μm with 200% excess hydrogen (p_{H2} = 0.3 atm)

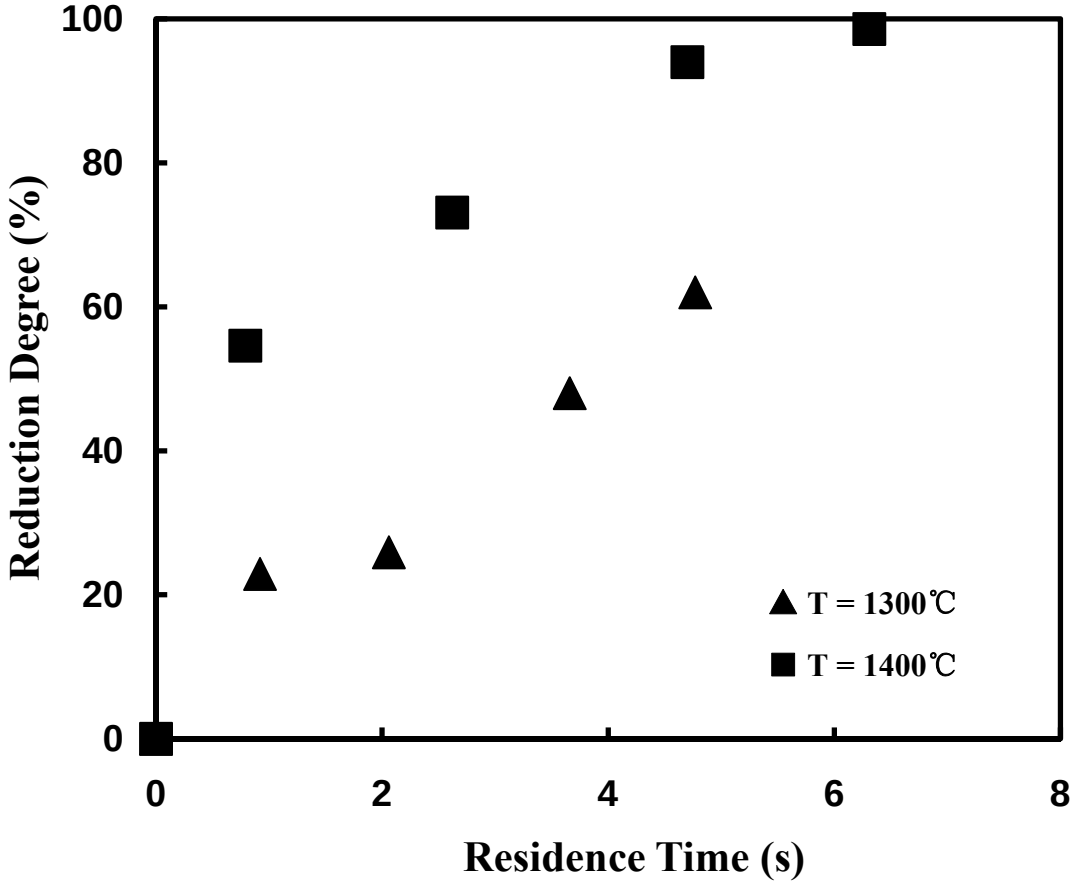

Figure 46. Effect of temperature on the reduction rate of the sample with 20 - 25 μm with 200% excess hydrogen(p_{H2} = 0.1 atm)

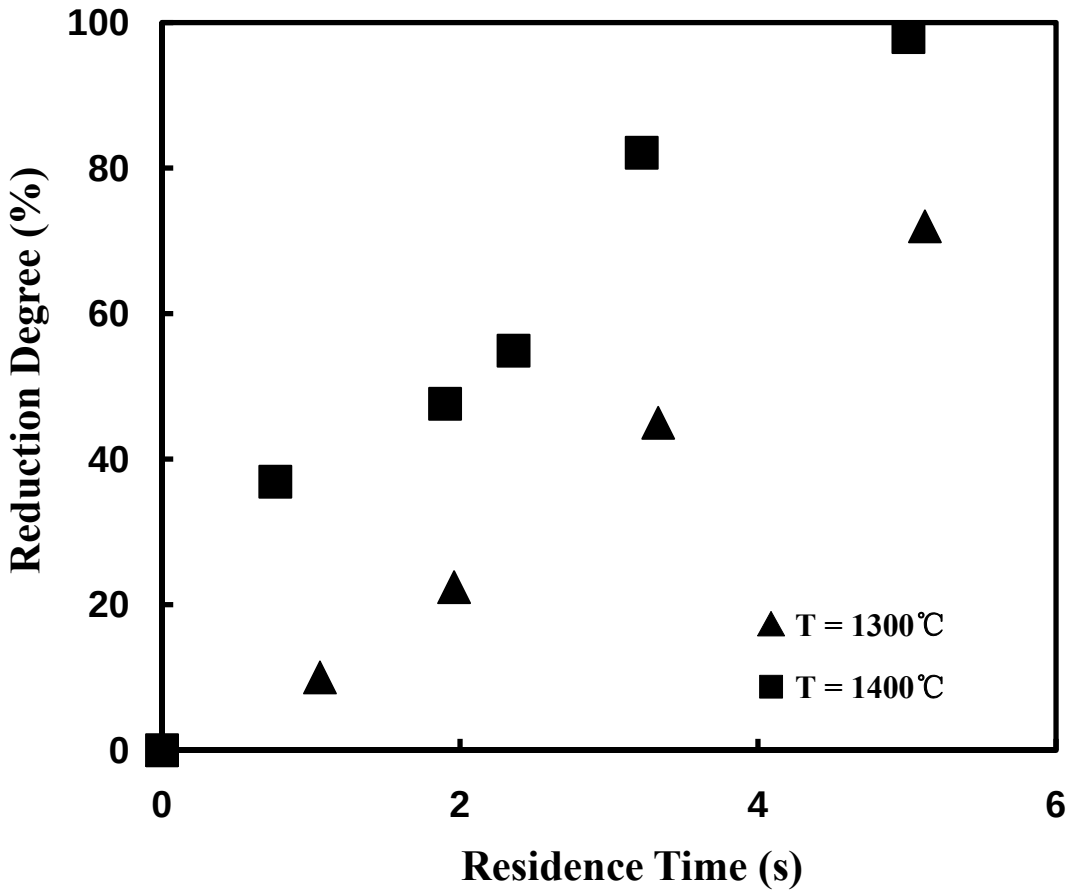

Figure 47. Effect of temperature on the reduction rate of the sample with 32 - 38 μm with 200% excess hydrogen (p_{H2} = 0.1 atm)

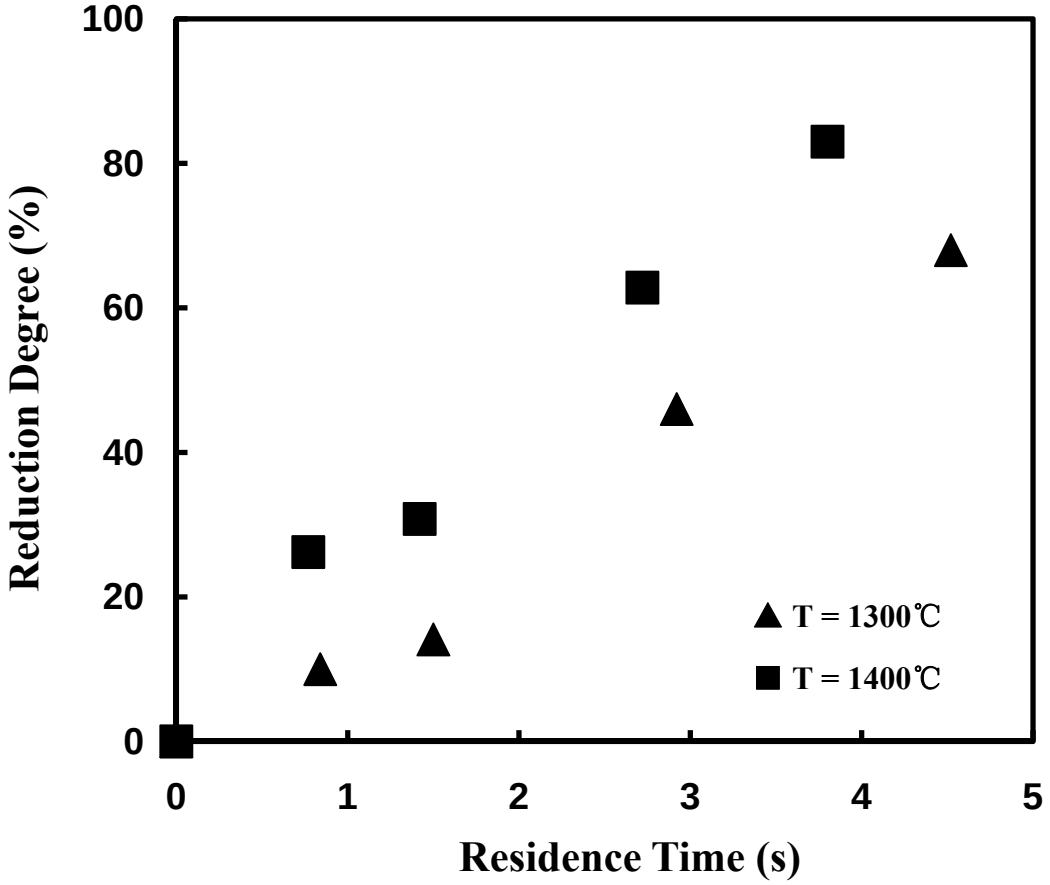

Figure 48. Effect of temperature on the reduction rate of the sample with 45 - 53 μm with 200% excess hydrogen (p_{H2} = 0.1 atm)

APPENDIX C

FIGURES OF EFFECT OF HYDROGEN PARTIAL PRESSURE ON REDUCTION RATE OF MAGNETITE CONCENTRATE PARTICLES

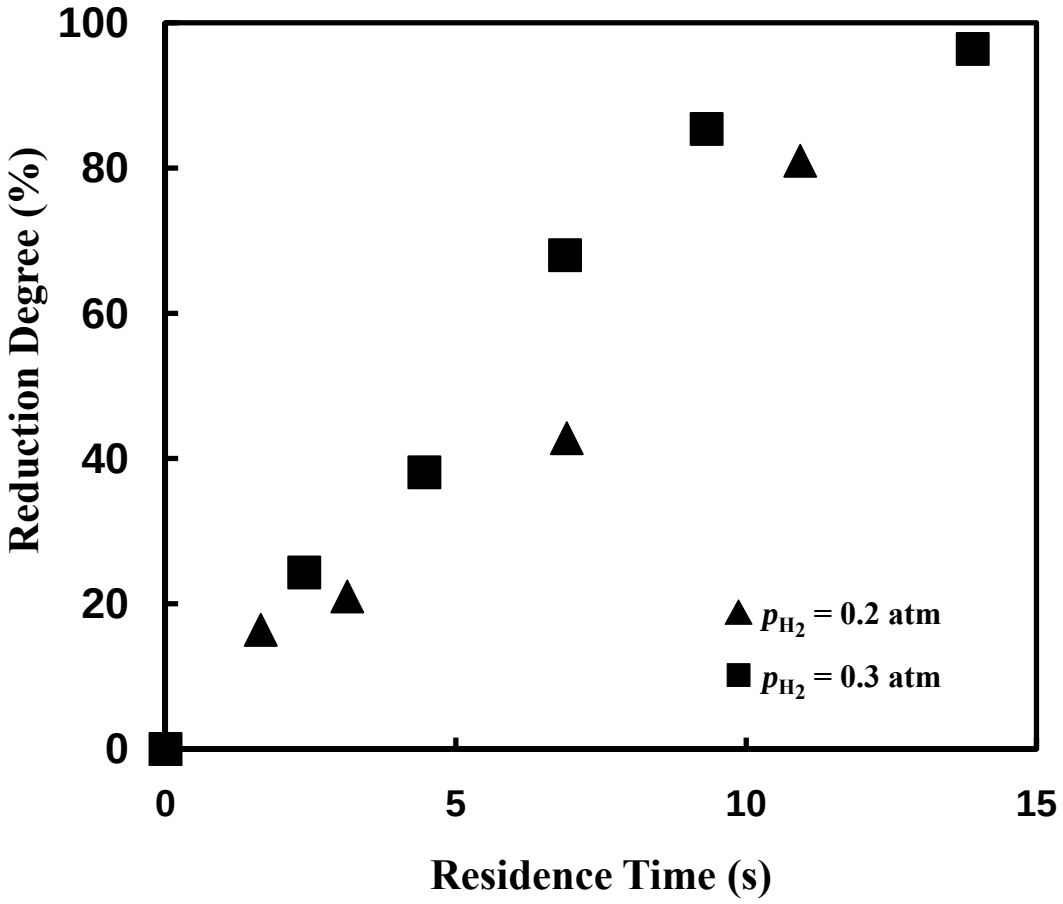

Figure 49. Effect of partial pressure of hydrogen on the reduction rate of the sample with 20 - 25 μm at 1200℃.

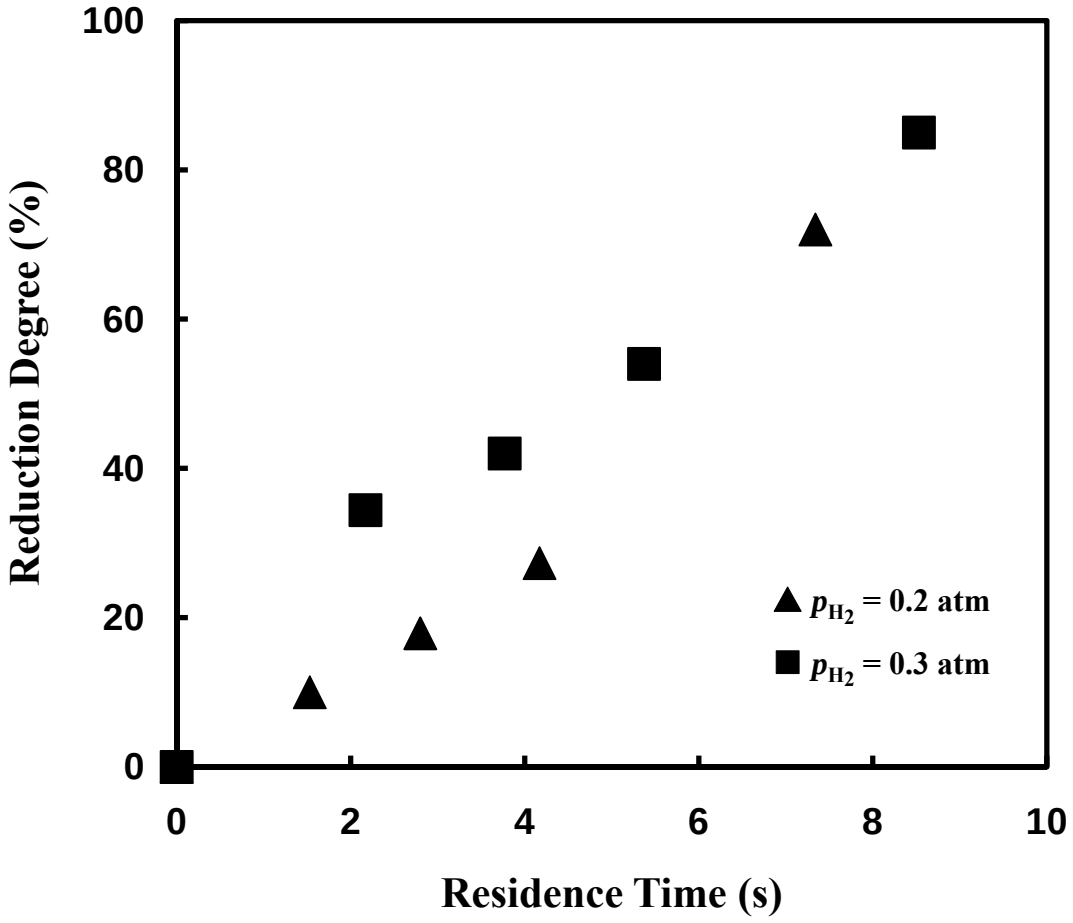

Figure 50. Effect of partial pressure of hydrogen on the reduction rate of the sample with 32 - 38 μm at 1200℃.

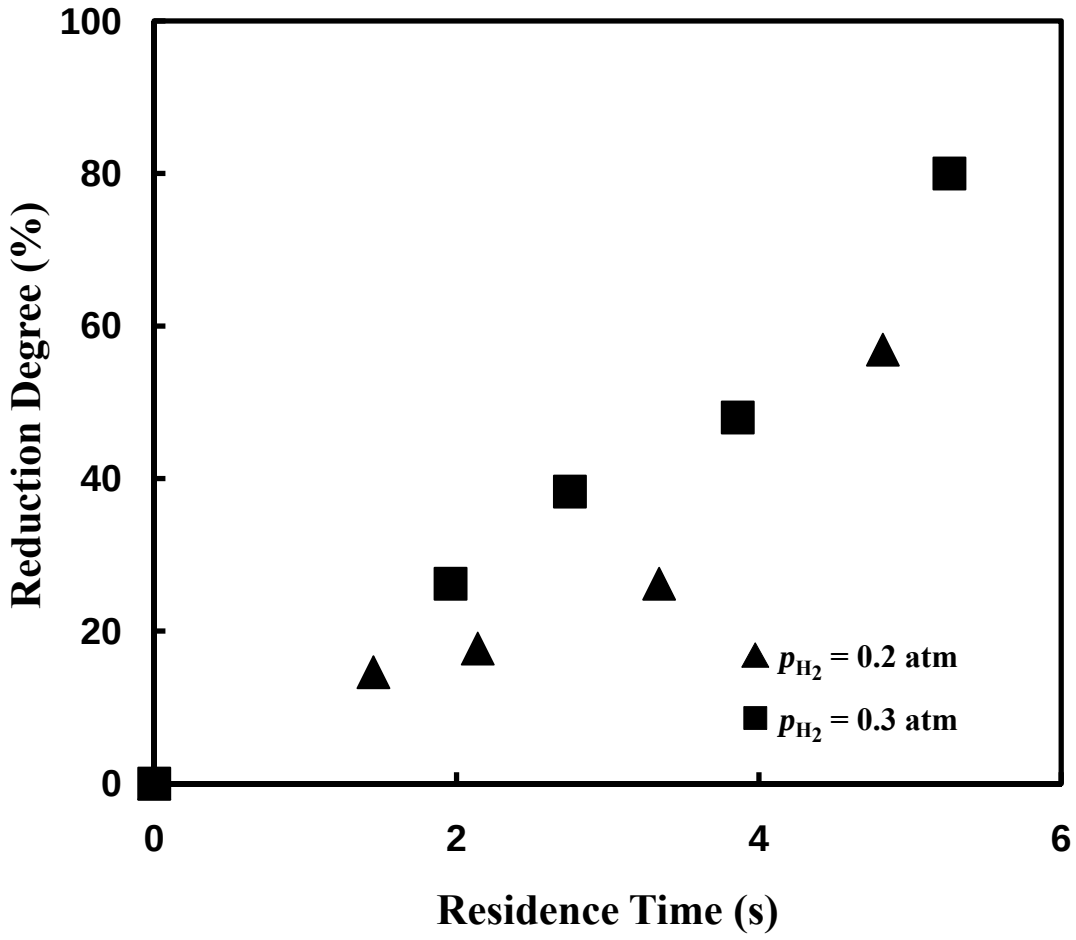

Figure 51. Effect of partial pressure of hydrogen on the reduction rate of the sample with 45 - 53 μm at 1200℃.

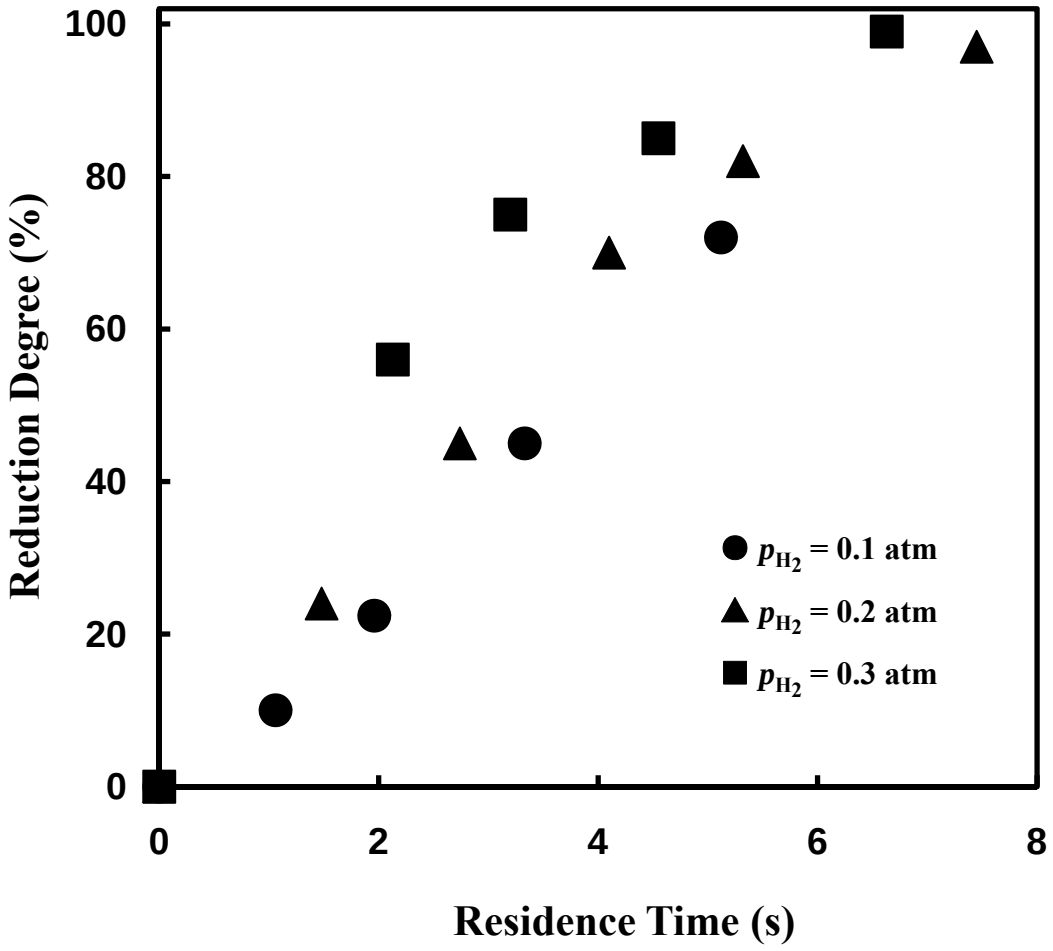

Figure 52. Effect of partial pressure of hydrogen on the reduction rate of the sample with 32 - 38 μm at 1300℃.

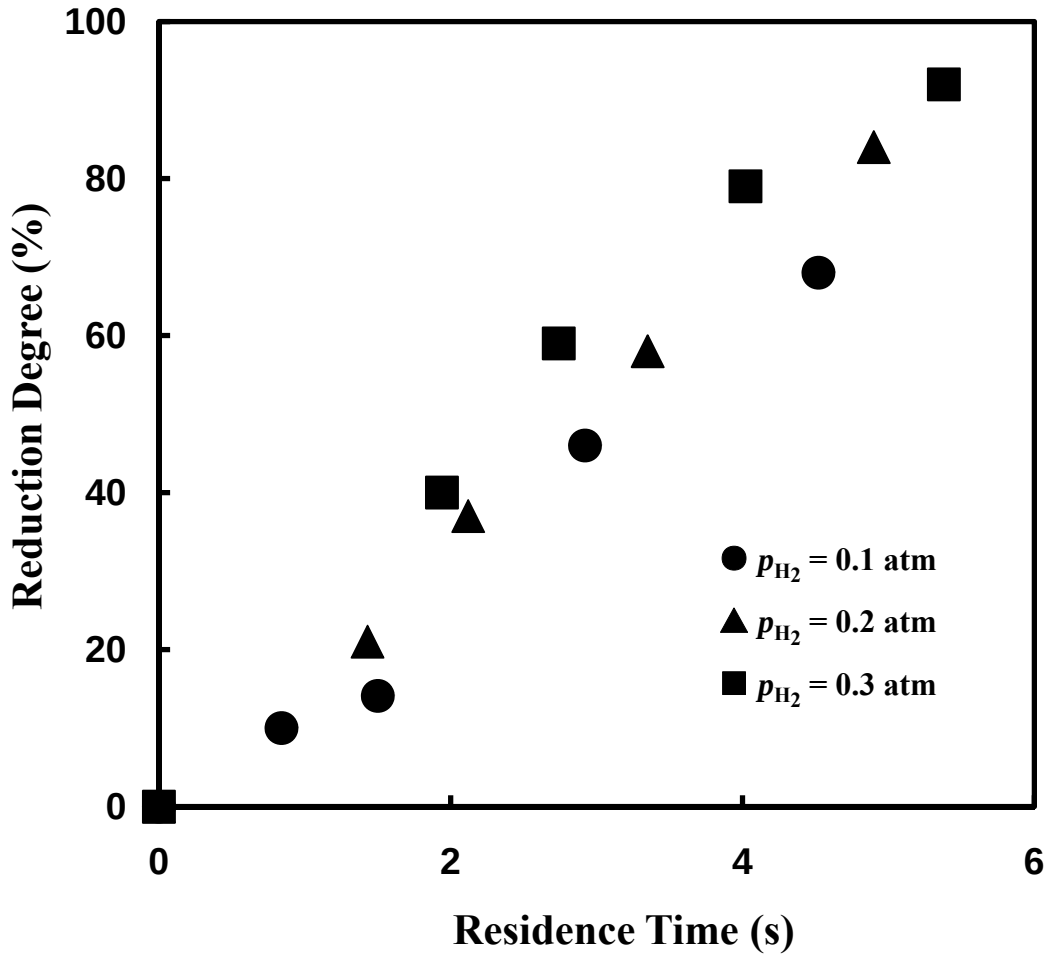

Figure 53. Effect of partial pressure of hydrogen on the reduction rate of the sample with 45 - 53 μm at 1300℃.

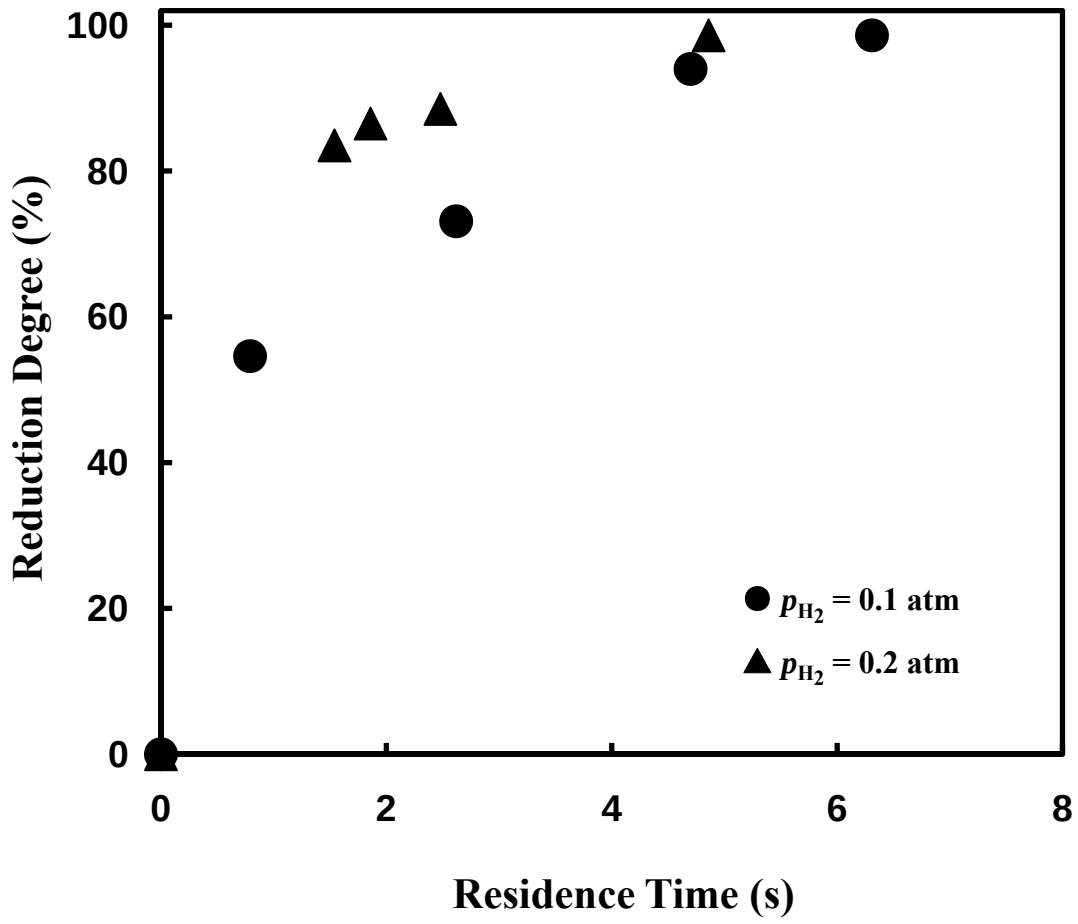

Figure 54. Effect of partial pressure of hydrogen on the reduction rate of the sample with 20 - 25 μm at 1400℃.

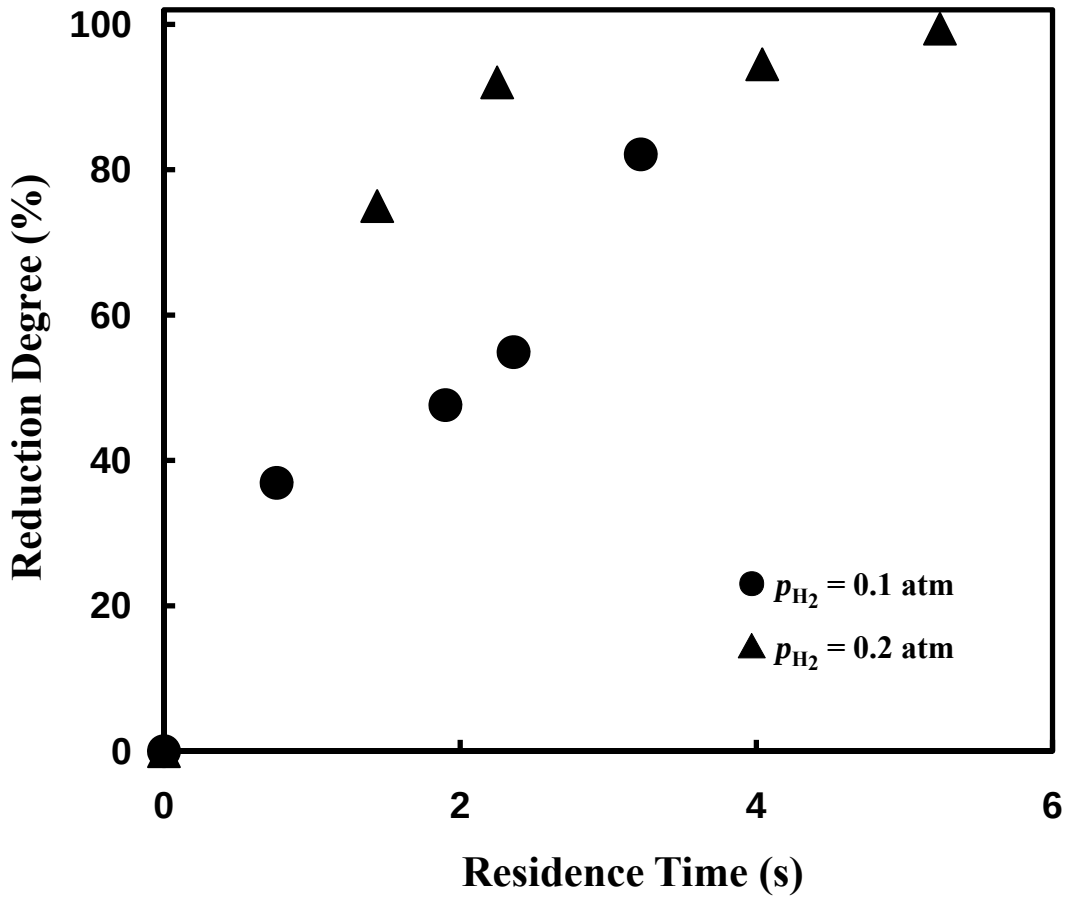

Figure 55. Effect of partial pressure of hydrogen on the reduction rate of the sample with 32 - 38 μm at 1400℃.

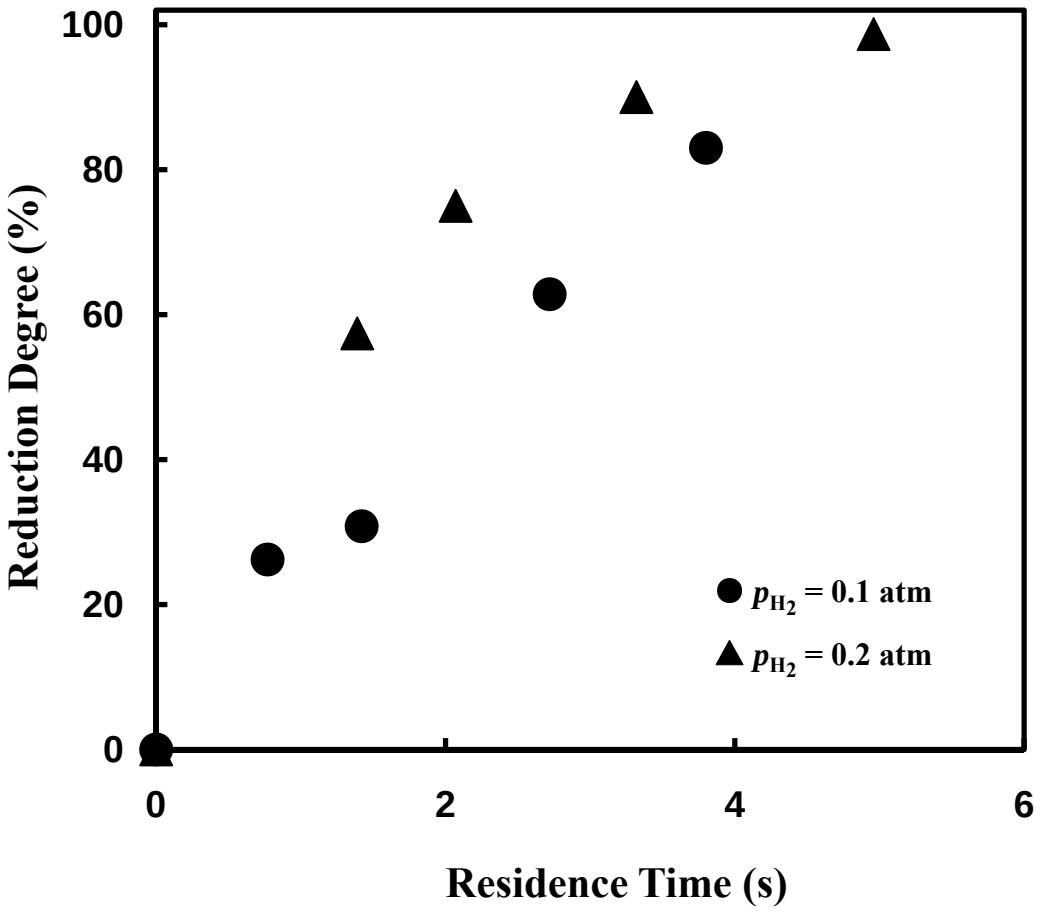

Figure 56. Effect of partial pressure of hydrogen on the reduction rate of the sample with 45 - 53 μm at 1400℃.

APPENDIX D

FIGURES OF EFFECT OF PARTICLE SIZE ON REDUCTION RATE OF MAGNETITE CONCENTRATE PARTICLES

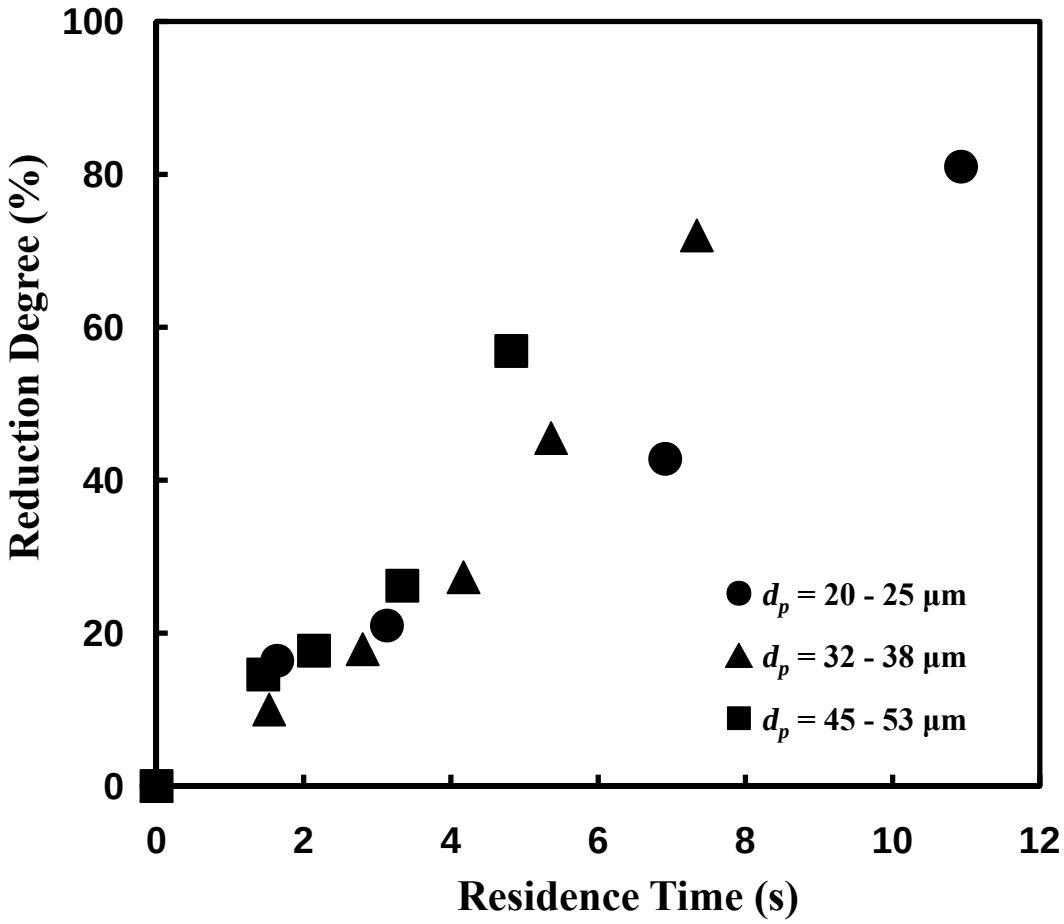

Figure 57. Effect of particle size on the reduction rate with 200% excess hydrogen at 1200℃ (p_{H2} = 0.2 atm).

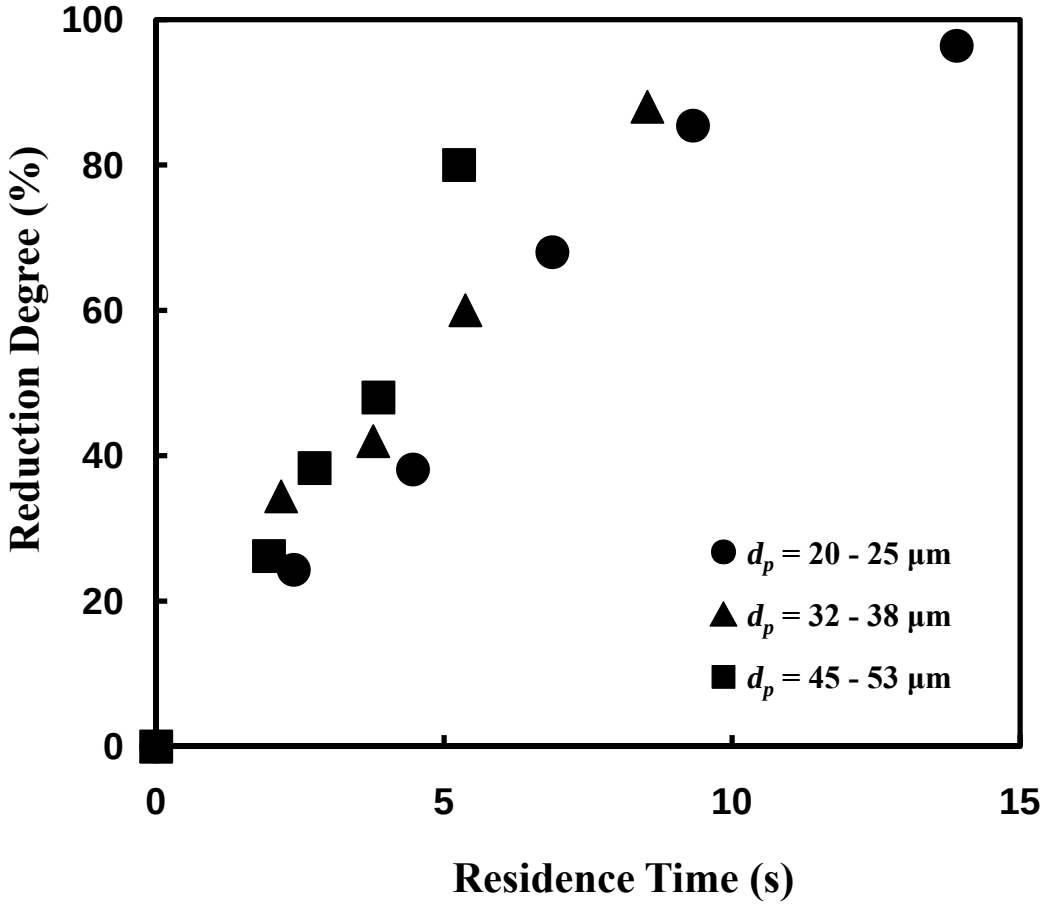

Figure 58. Effect of particle size on the reduction rate with 200% excess hydrogen at 1200℃ (p_{H2} = 0.3 atm).

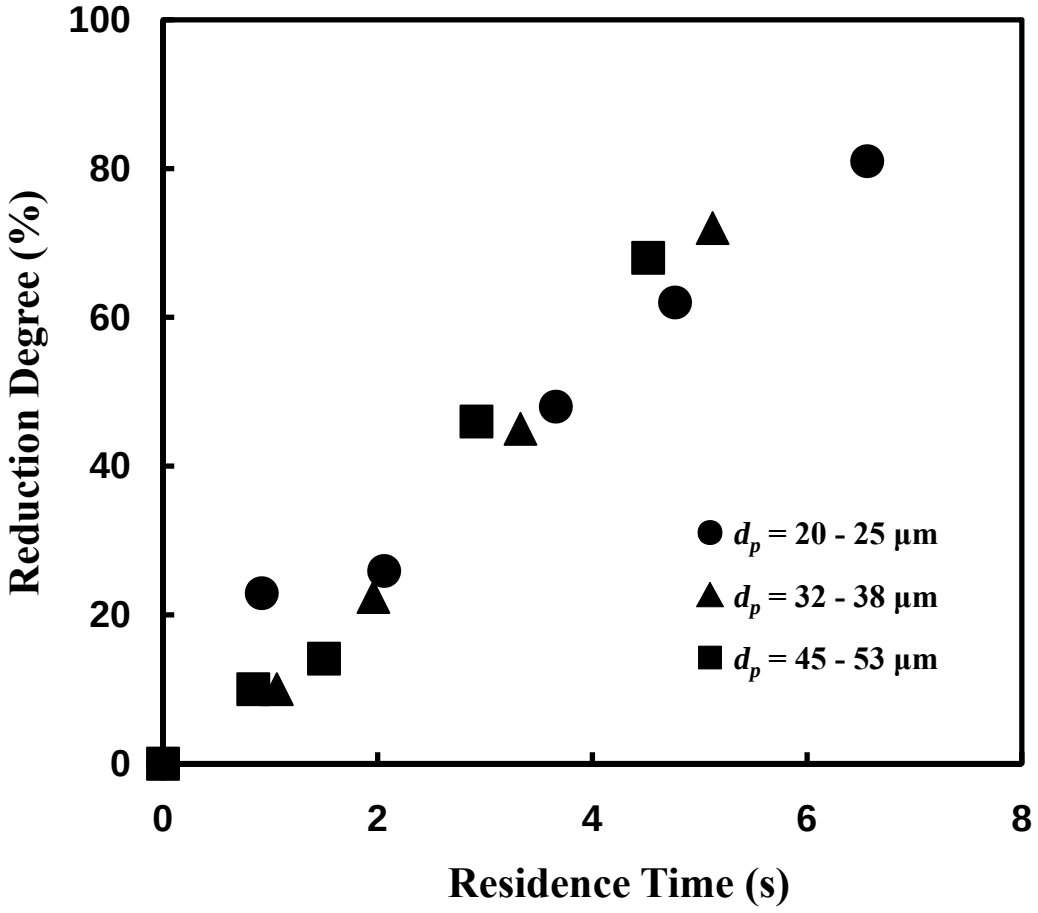

Figure 59. Effect of particle size on the reduction rate with 200% excess hydrogen at 1300℃ (p_{H2} = 0.1 atm).

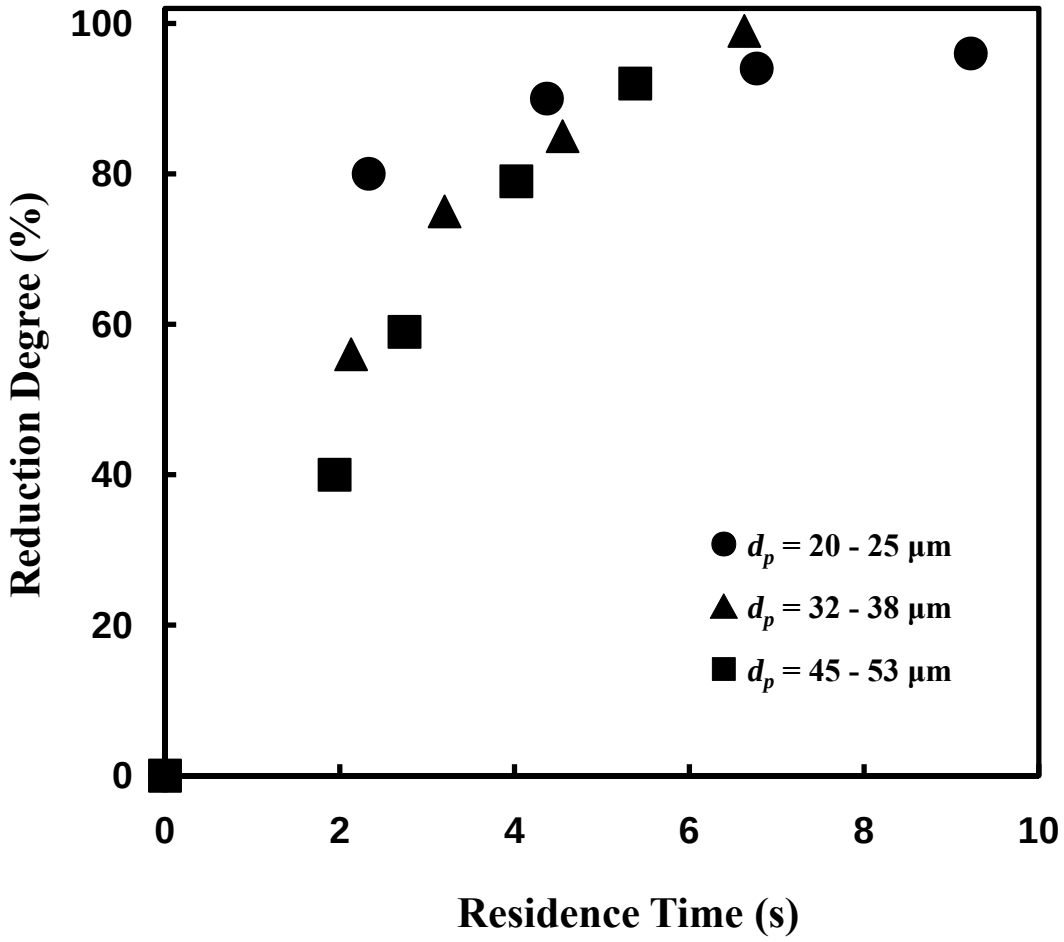

Figure 60. Effect of particle size on the reduction rate with 200% excess hydrogen at 1300℃ (p_{H2} = 0.3 atm).

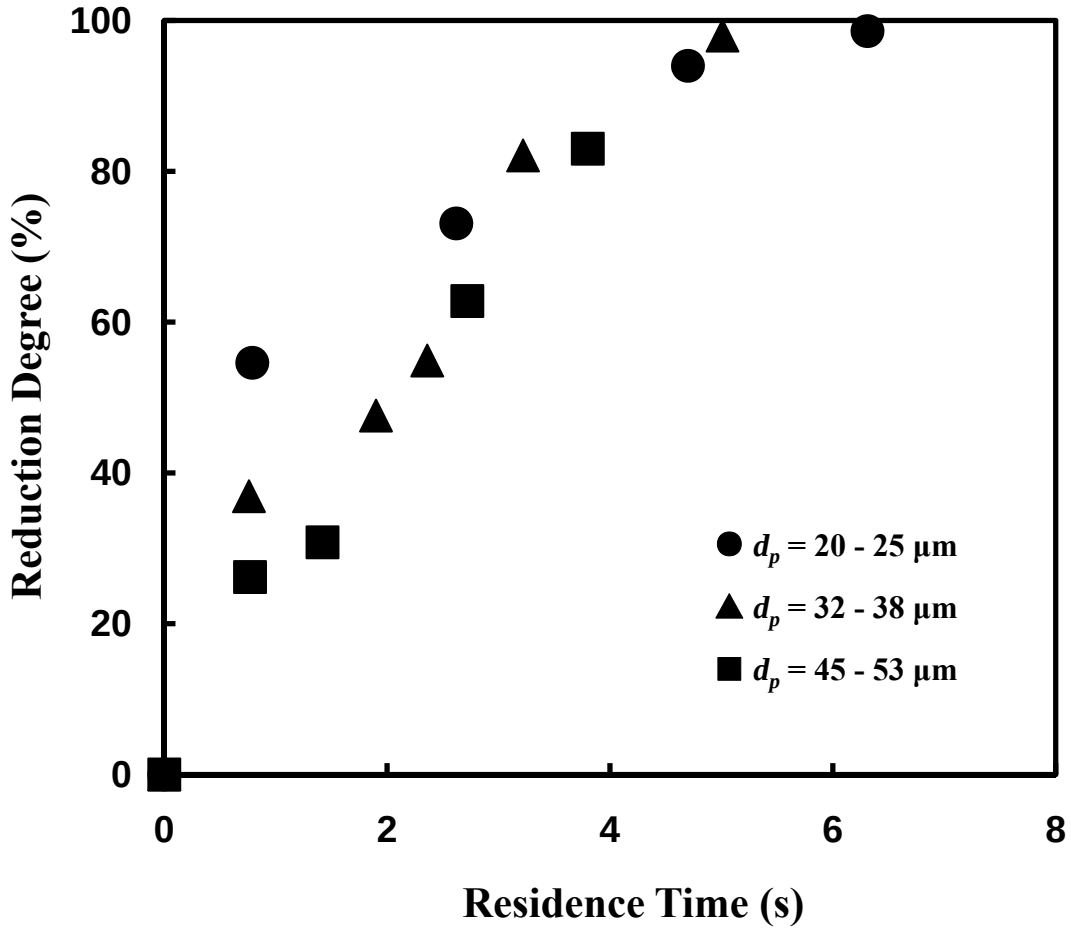

Figure 61. Effect of particle size on the reduction rate with 200% excess hydrogen at 1400℃ (p_{H2} = 0.1atm).

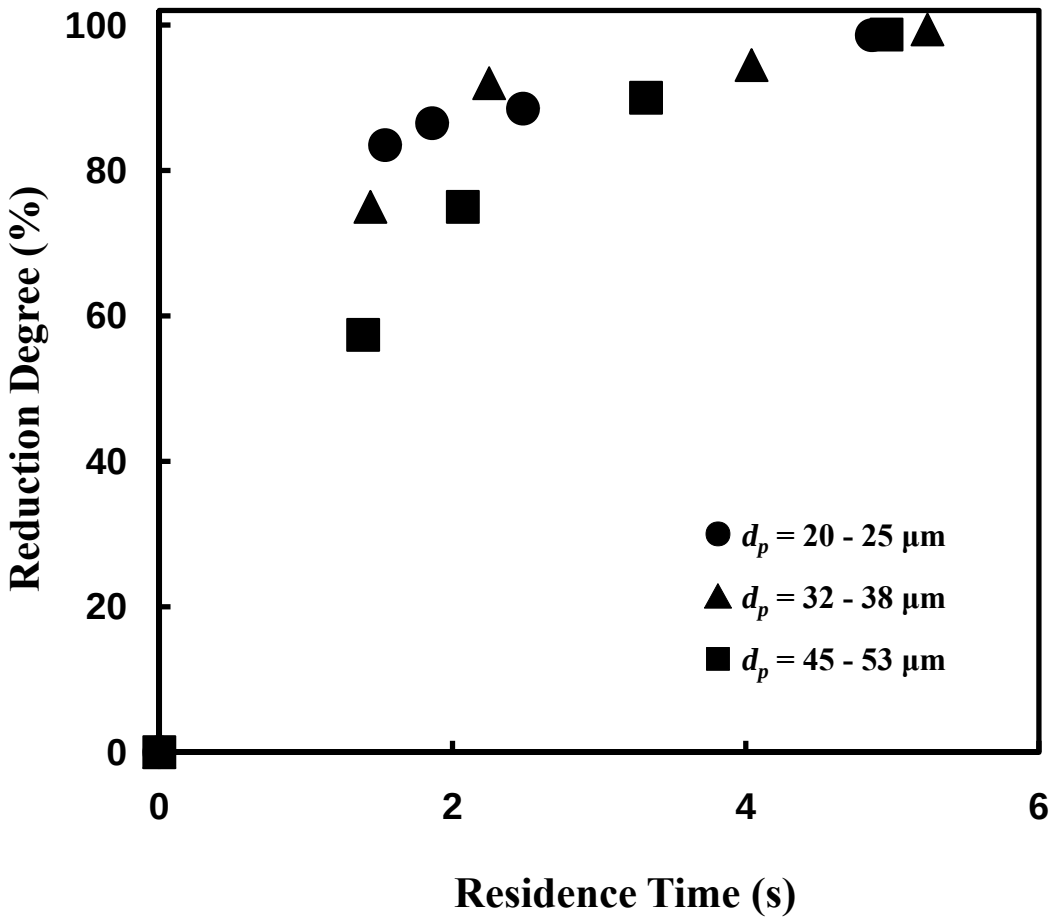

Figure 62. Effect of particle size on the reduction rate with 200% excess hydrogen at 1400℃ (p_{H2} = 0.2atm)

APPENDIX E

DERIVATION OF MEAN AVERAGE OF FUNCTIONAL DEPENDENCE OF RATE ON PARTIAL PRESSURE OF HYDROGEN

<u>Case 1:</u> Assume that the reaction is 1st-order with respect to H_2 partial pressure

$$\frac{d(p_{H_2})}{dt} = A(p_{H_2} - \frac{p_{H_2O}}{K_E}) \tag{E-1}$$

Here $p_{H_2} + p_{H_2O} = p^o$ (E-2)

$$\frac{d(p_{H_2})}{dt} = A\left(p_{H_2} - \frac{p^o - p_{H_2}}{K_E}\right) \tag{E-3}$$

After rearrangement,

$$\frac{d(p_{H_2})}{dt} = A\frac{1+K_E}{K_E}\left(p_{H_2} - \frac{p^o}{1+K_E}\right) \tag{E-4}$$

$$Ln\left(p_{H_2} - \frac{p^o}{1+K_E}\right) = A\frac{1+K_E}{K_E}\cdot t + Constant \tag{E-5}$$

$$Ln\left(p_{H_2} - \frac{p^o}{1+K_E}\right)_2 - Ln\left(p_{H_2} - \frac{p^o}{1+K_E}\right)_1 = A\frac{1+K_E}{K_E}\cdot(t_2 - t_1) \tag{E-6}$$

$$(t_2 - t_1) = \frac{1}{A}\frac{K_E}{1+K_E}\cdot\left[Ln\left(p_{H_2} - \frac{p^o}{1+K_E}\right)_2 - Ln\left(p_{H_2} - \frac{p^o}{1+K_E}\right)_1\right] \tag{E-7}$$

If the term $(p_{H_2} - \frac{p_{H_2O}}{K_E})$ in equation (E-1) is replaced with $(p_{H_2} - \frac{p_{H_2O}}{K_E})_{avg}$, then we get the following expression:

$$\frac{dp_{H_2}}{dt} = A(p_{H_2} - \frac{p_{H_2O}}{K_E})_{avg} \tag{E-8}$$

$$(p_{H_2} - \frac{p_{H_2O}}{K_E})_{avg} = \frac{1}{A} \cdot \frac{(p_{H_2})_2 - (p_{H_2})_1}{t_2 - t_1} \tag{E-9}$$

Substitute equations (E-7) into (E-9)

$$(p_{H_2} - \frac{p_{H_2O}}{K_E})_{avg} = \frac{1+K_E}{K_E} \cdot \frac{(p_{H_2})_2 - (p_{H_2})_1}{Ln\left(p_{H_2} - \frac{p^o}{1+K_E}\right)_2 - Ln\left(p_{H_2} - \frac{p^o}{1+K_E}\right)_1} \tag{E-10}$$

The log mean average of $p_{H_2} - \frac{p_{H_2O}}{K_E}$ is:

$$(p_{H_2} - \frac{p_{H_2O}}{K_E})_{lm} = \frac{\left(p_{H_2} - \frac{p_{H_2O}}{K_E}\right)_2 - \left(p_{H_2} - \frac{p_{H_2O}}{K_E}\right)_1}{Ln\frac{\left(p_{H_2} - \frac{p_{H_2O}}{K_E}\right)_2}{\left(p_{H_2} - \frac{p_{H_2O}}{K_E}\right)_1}} \tag{E-11}$$

Substitute equations (E-2) into equations (E-11) and rearrange it:

$$(p_{H_2} - \frac{p_{H_2O}}{K_E})_{lm} = \frac{1+K_E}{K_E} \cdot \frac{(p_{H_2})_2 - (p_{H_2})_1}{Ln\left(p_{H_2} - \frac{p^o}{1+K_E}\right)_2 - Ln\left(p_{H_2} - \frac{p^o}{1+K_E}\right)_1} \tag{E-12}$$

Compare equations (E-10) and (E-12),

$$(p_{H_2} - \frac{p_{H_2O}}{K_E})_{avg} = (p_{H_2} - \frac{p_{H_2O}}{K_E})_{lm} = \frac{1+K_E}{K_E} \cdot \frac{(p_{H_2})_2 - (p_{H_2})_1}{Ln\left(p_{H_2} - \frac{p^o}{1+K_E}\right)_2 - Ln\left(p_{H_2} - \frac{p^o}{1+K_E}\right)_1} \tag{E-13}$$

<u>Case 2:</u> Assume that the reaction is 1/2-order with respect to H_2 partial pressure

$$\frac{\mathrm{d}(p_{H_2})}{\mathrm{d}t} = \mathrm{B}\left[\left(p_{\mathrm{H_2}}\right)^{1/2} - \left(p_{\mathrm{H_2O}}/K_E\right)^{1/2}\right] \tag{E-14}$$

$$\text{Here } p_{\mathrm{H_2}} + p_{\mathrm{H_2O}} = p^{\mathrm{o}} \tag{E-15}$$

$$\frac{\mathrm{d}(p_{\mathrm{H_2}})}{\mathrm{d}t} = \mathrm{B}\left[\left(p_{\mathrm{H_2}}\right)^{1/2} - \left(\frac{p^{\mathrm{o}} - p_{\mathrm{H_2}}}{K_E}\right)^{1/2}\right] \tag{E-16}$$

When $\left(p_{\mathrm{H_2O}}/K_E\right)^{1/2}$ is relatively small, we get:

$$\frac{\mathrm{d}(p_{\mathrm{H_2}})}{\mathrm{d}t} = \mathrm{B}\left(p_{\mathrm{H_2}}\right)^{1/2} \tag{E-17}$$

$$2\left(p_{\mathrm{H_2}}\right)^{1/2} = \mathrm{B}\cdot\mathrm{t} + \mathrm{Constant} \tag{E-18}$$

$$2\cdot\left[\left(p_{\mathrm{H_2}}\right)_2^{1/2} - \left(p_{\mathrm{H_2}}\right)_1^{1/2}\right] = \mathrm{B}\cdot(t_2 - t_1) \tag{E-19}$$

If the term $\left(p_{\mathrm{H_2}}\right)^{1/2}$ in equations (E-17) is replaced with $(p_{H_2})_{avg}$, then we get the following expression:

$$\frac{\mathrm{d}(p_{\mathrm{H_2}})}{\mathrm{d}t} = \mathrm{B}\cdot\left[\left(p_{\mathrm{H_2}}\right)^{1/2}\right]_{\mathrm{avg}} \tag{E-20}$$

$$\left[\left(p_{\mathrm{H_2}}\right)^{1/2}\right]_{\mathrm{avg}} = \frac{1}{\mathrm{B}}\frac{(p_{\mathrm{H_2}})_2 - (p_{\mathrm{H_2}})_1}{t_2 - t_1} \tag{E-21}$$

Substitute equations (E-19) into equations (E-21):

$$\left[\left(p_{\mathrm{H_2}}\right)^{1/2}\right]_{\mathrm{avg}} = \frac{1}{\mathrm{B}}\cdot\frac{(p_{\mathrm{H_2}})_2 - (p_{\mathrm{H_2}})_1}{\frac{2}{\mathrm{B}}\cdot\left[\left(p_{\mathrm{H_2}}\right)_2^{1/2} - \left(p_{\mathrm{H_2}}\right)_1^{1/2}\right]} = \frac{\left(p_{\mathrm{H_2}}\right)_2^{1/2} + \left(p_{\mathrm{H_2}}\right)_1^{1/2}}{2} \tag{E-22}$$

The arithmatic mean average of $\left(p_{H_2}\right)^{1/2}$ is:

$$\left[\left(p_{H_2}\right)^{1/2}\right]_{am} = \frac{\left(p_{H_2}\right)_2^{1/2} + \left(p_{H_2}\right)_1^{1/2}}{2} \tag{E-23}$$

Combine equations (E-22) and (E-23),

$$\left[\left(p_{H_2}\right)^{1/2}\right]_{avg} = \left[\left(p_{H_2}\right)^{1/2}\right]_{am} = \frac{\left(p_{H_2}\right)_2^{1/2} + \left(p_{H_2}\right)_1^{1/2}}{2} \tag{E-24}$$

APPENDIX F

COMPARISON OF EXPERIMENTAL AND CALCULATED RESULTS

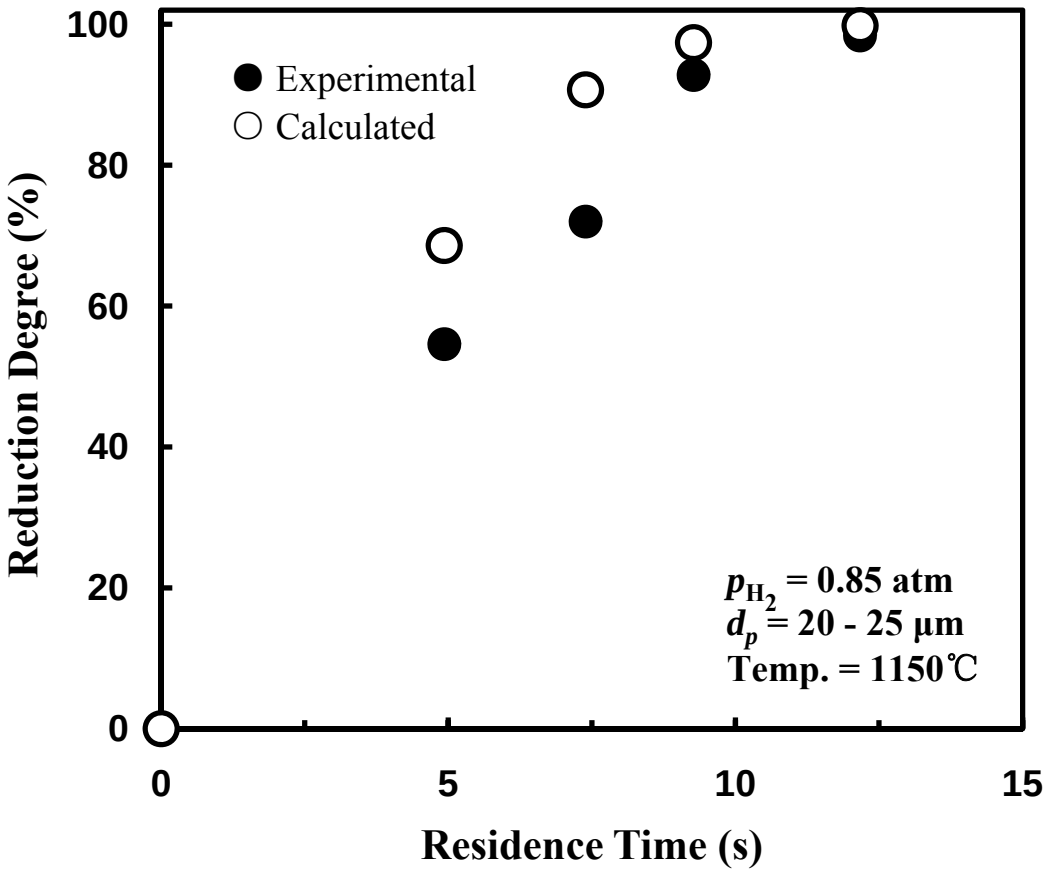

Figure 63. Comparison of experimental and calculated results

p_{H2} = 0.85 atm; d_p = 20 - 25 μm; Temp. = 1150℃

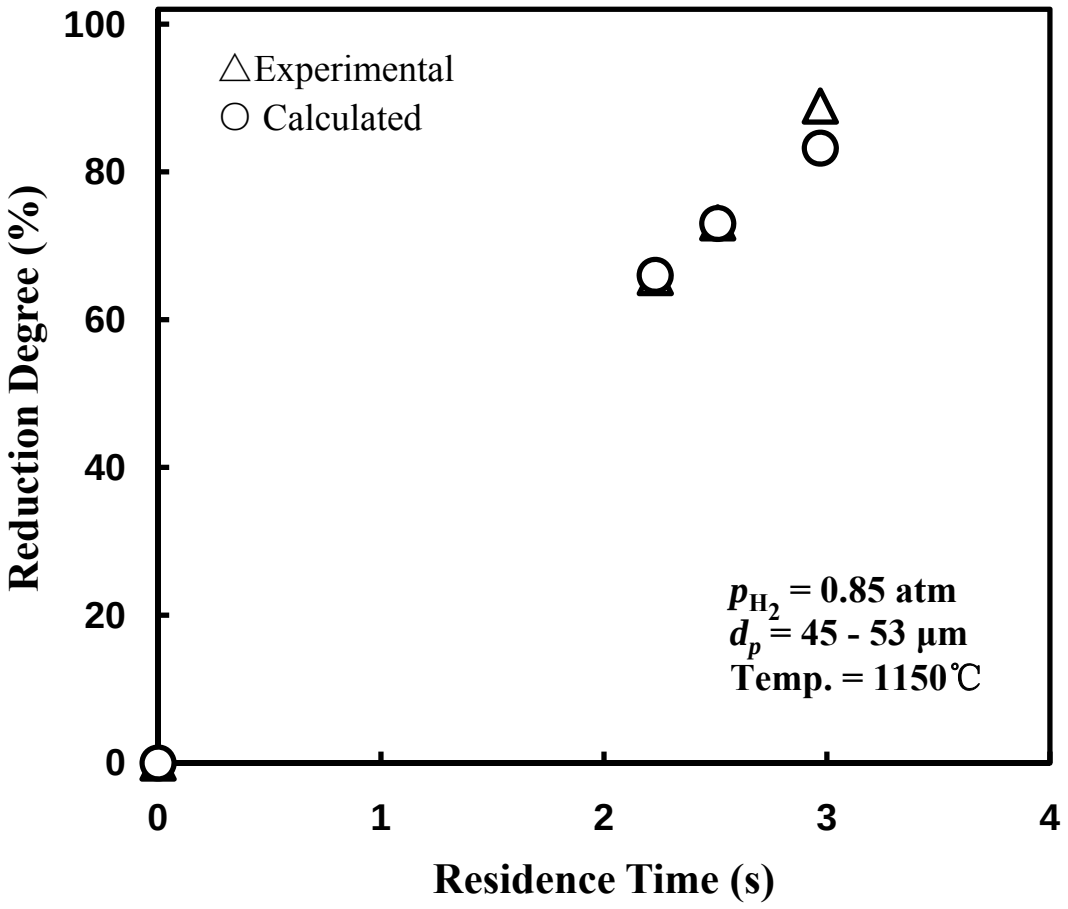

Figure 64. Comparison of experimental and calculated results

p_{H2} = 0.85 atm; d_p = 45 - 53 μm; Temp. = 1150℃

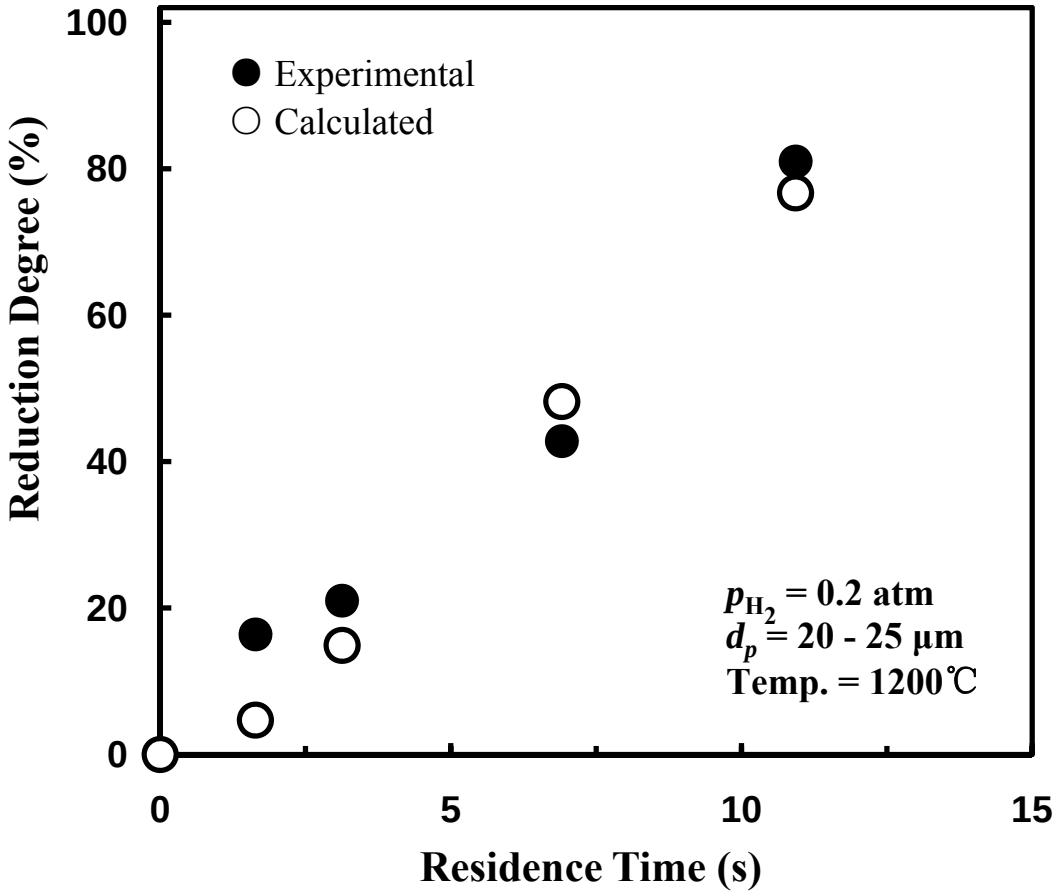

Figure 65. Comparison of experimental and calculated results

p_{H2} = 0.2 atm; d_p = 20 - 25 μm; Temp. = 1200℃

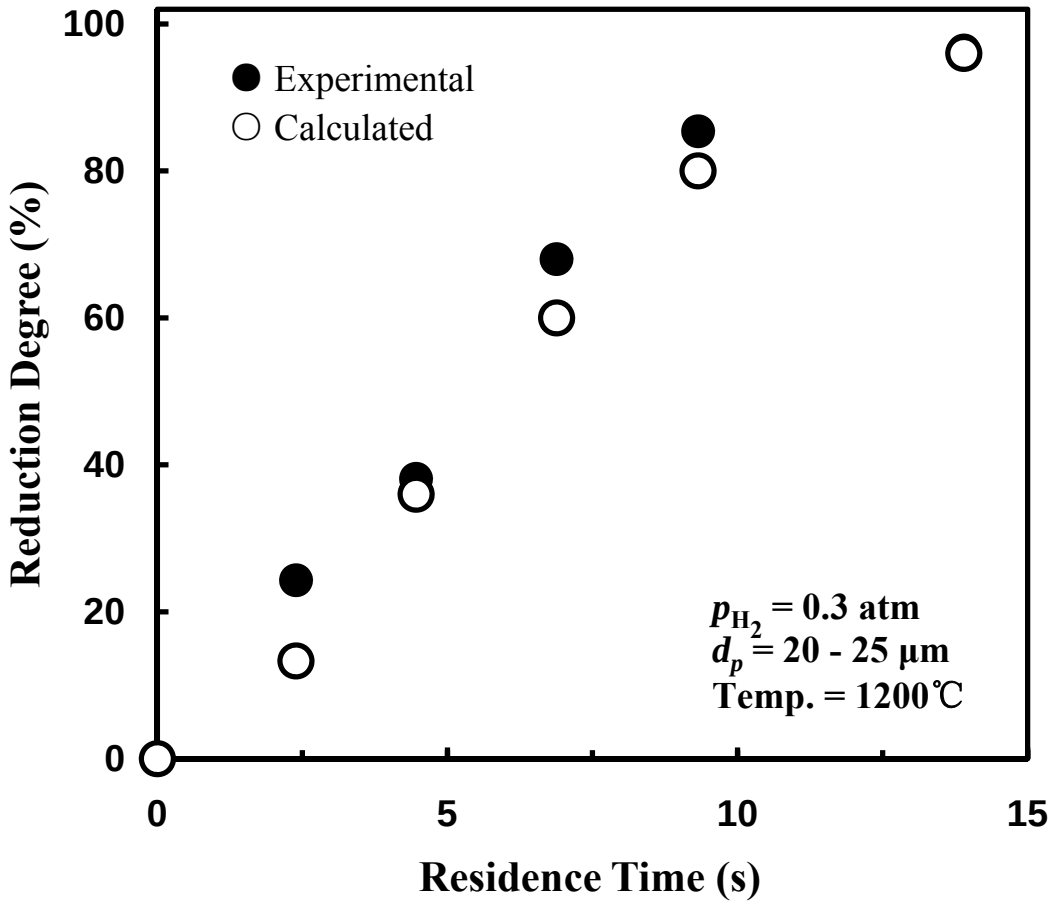

Figure 66. Comparison of experimental and calculated results

p_{H2} = 0.3 atm; d_p = 20 - 25 μm; Temp. = 1200℃

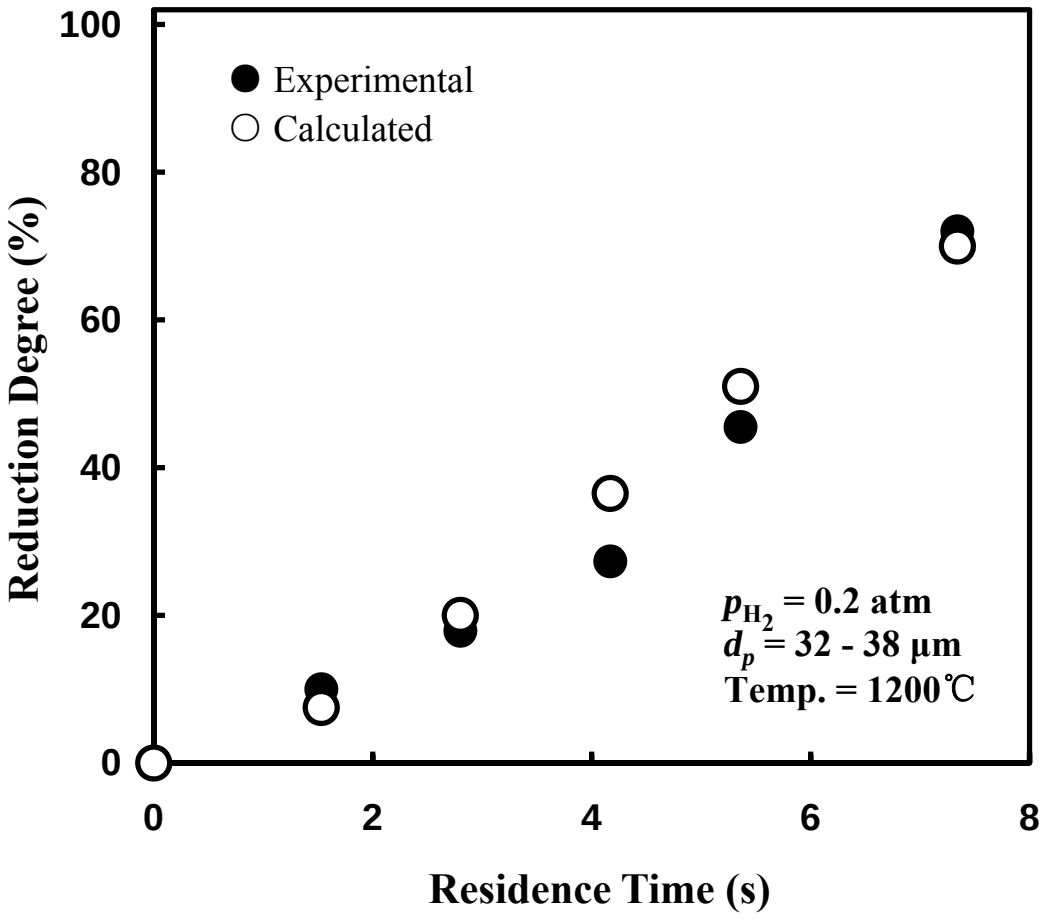

Figure 67. Comparison of experimental and calculated results

p_{H2} = 0.2 atm; d_p = 32 - 38 μm; Temp. = 1200℃

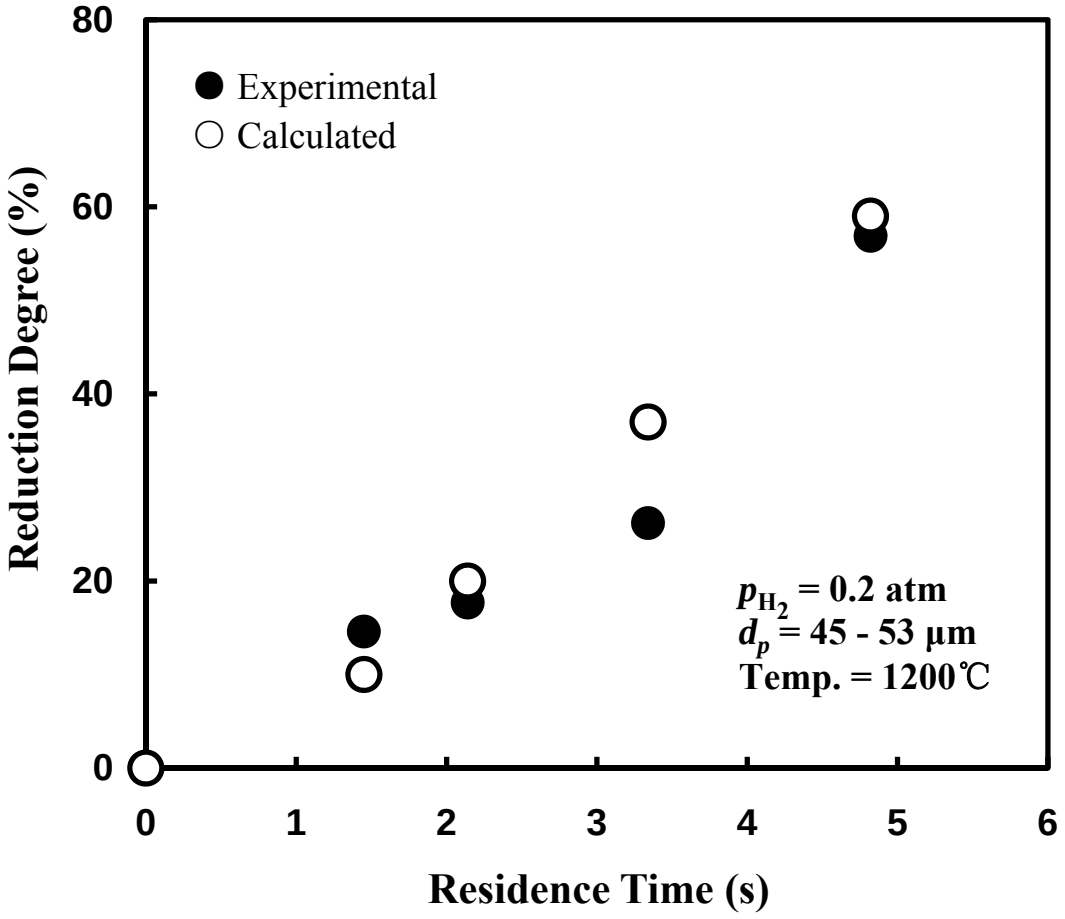

Figure 68. Comparison of experimental and calculated results

p_{H2} = 0.2 atm; d_p = 45 - 53 μm; Temp. = 1200℃

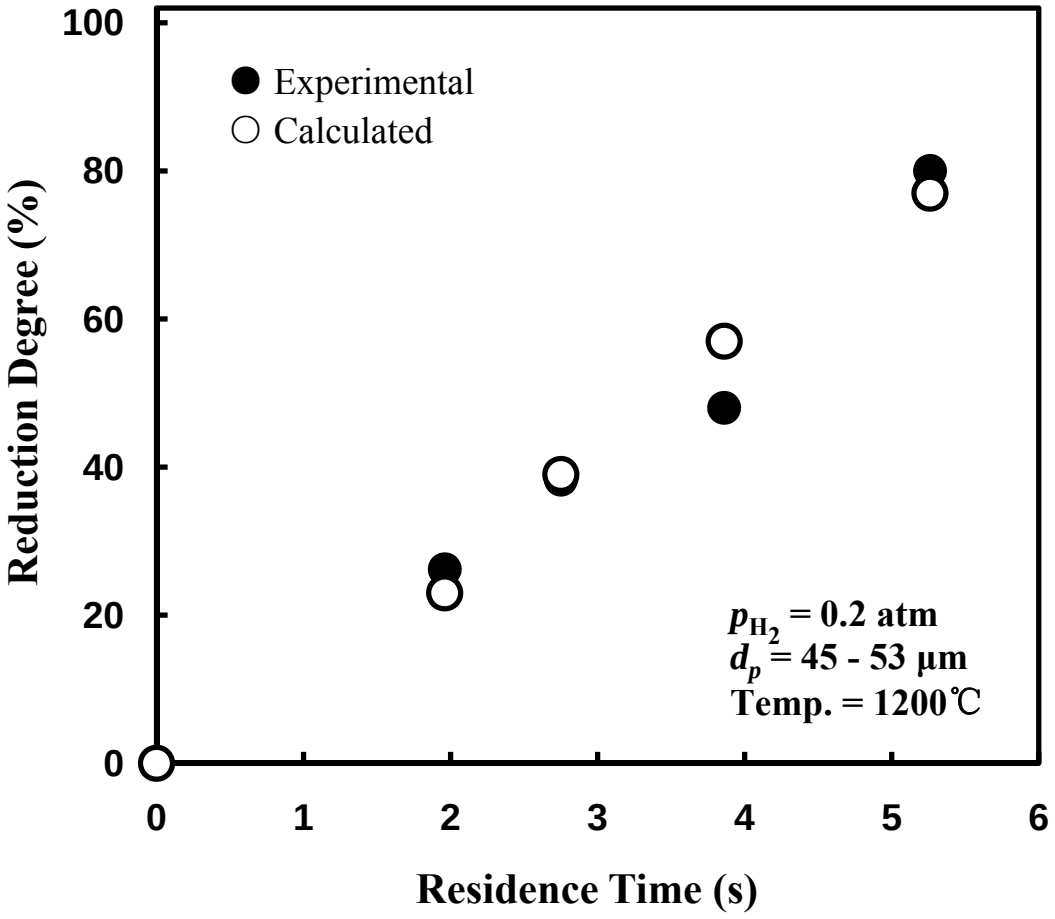

Figure 69. Comparison of experimental and calculated results

p_{H2} = 0.2 atm; d_p = 45 - 53 μm; Temp. = 1200℃

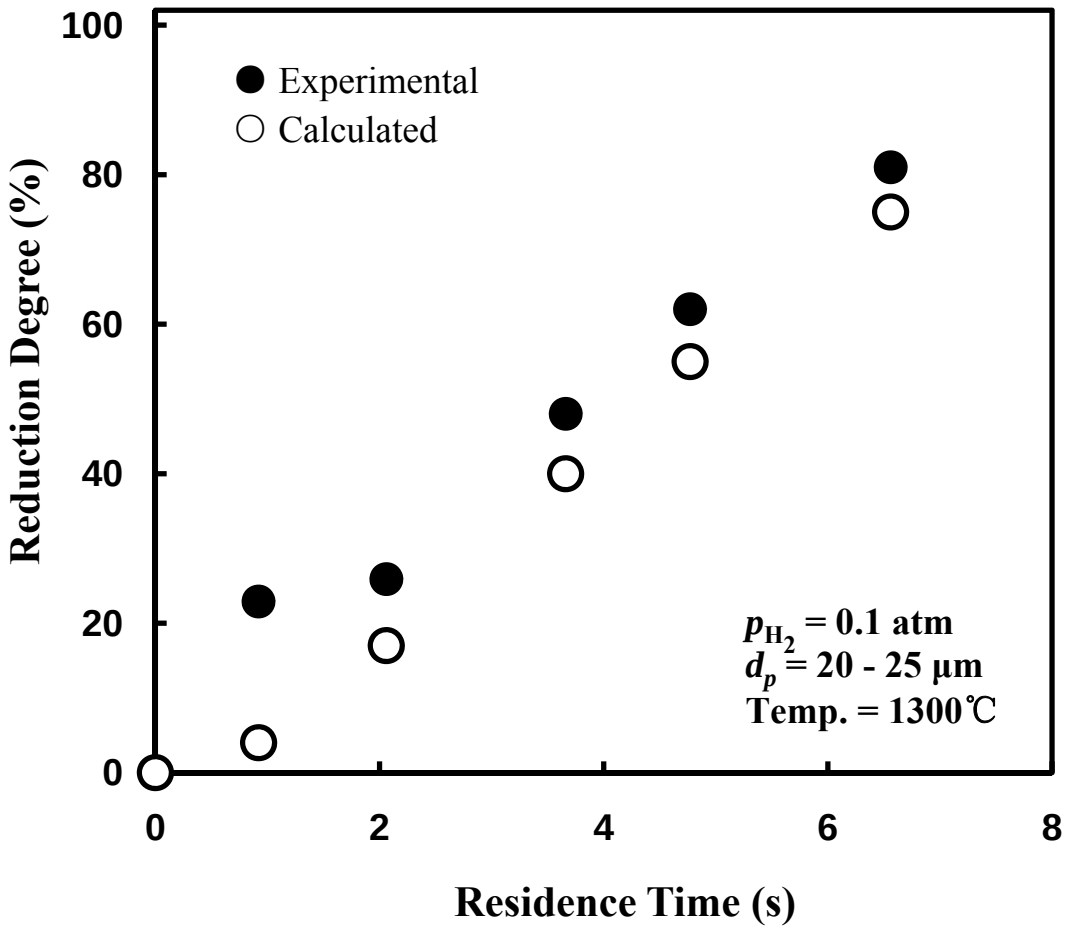

Figure 70. Comparison of experimental and calculated results

p_{H2} = 0.1 atm; d_p = 20 - 25 μm; Temp. = 1300℃

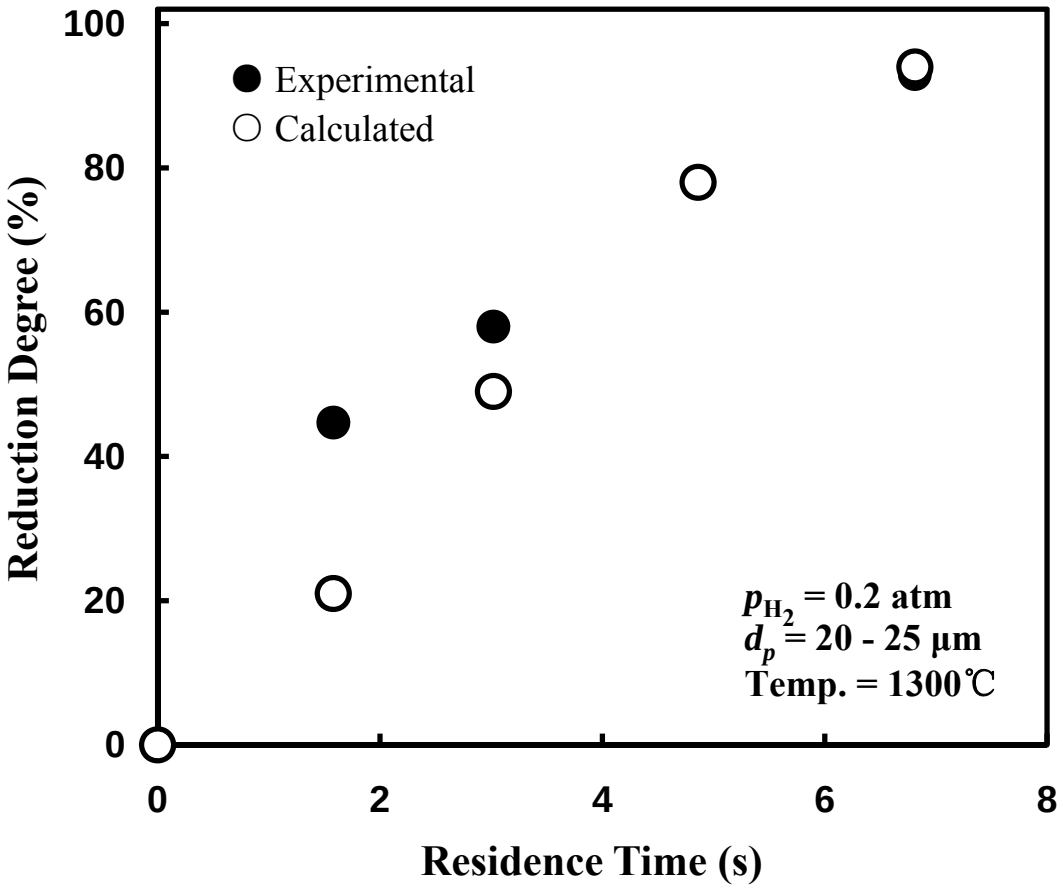

Figure 71. Comparison of experimental and calculated results

p_{H2} = 0.2 atm; d_p = 20 - 25 μm; Temp. = 1300℃

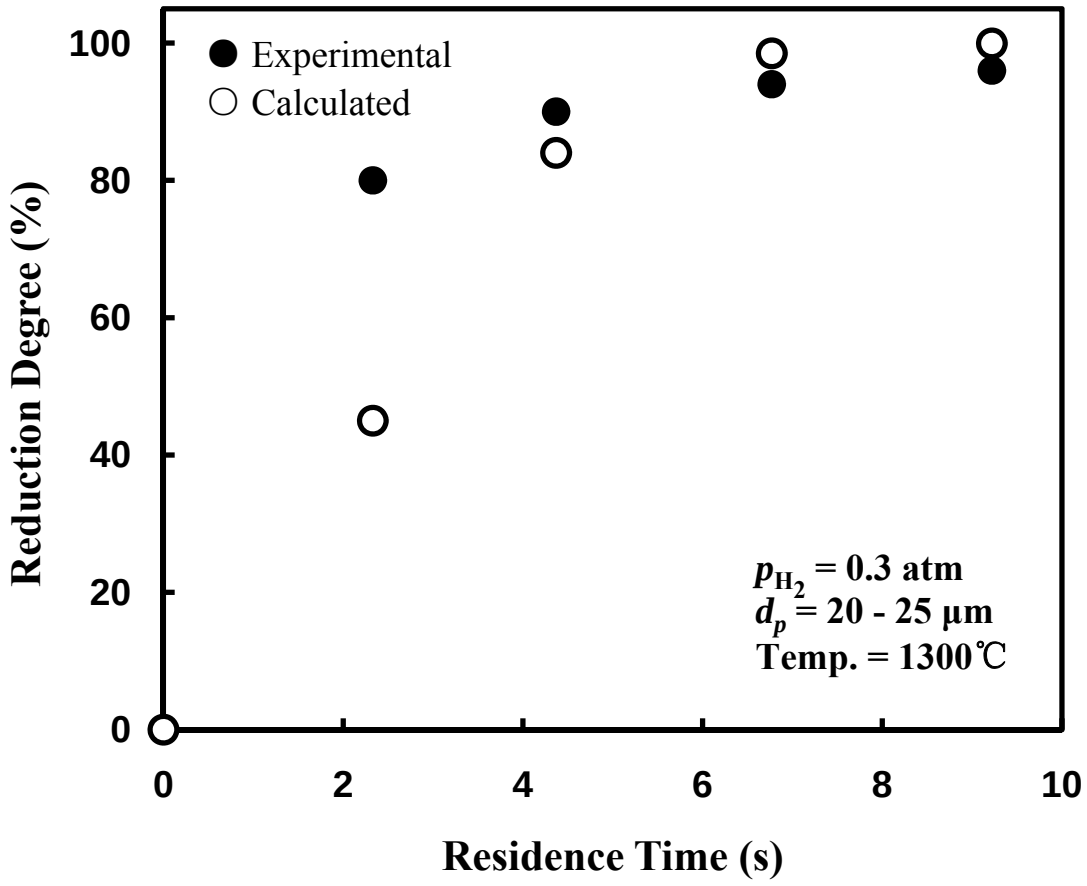

Figure 72. Comparison of experimental and calculated results

p_{H2} = 0.3 atm; d_p = 20 - 25 μm; Temp. = 1300℃

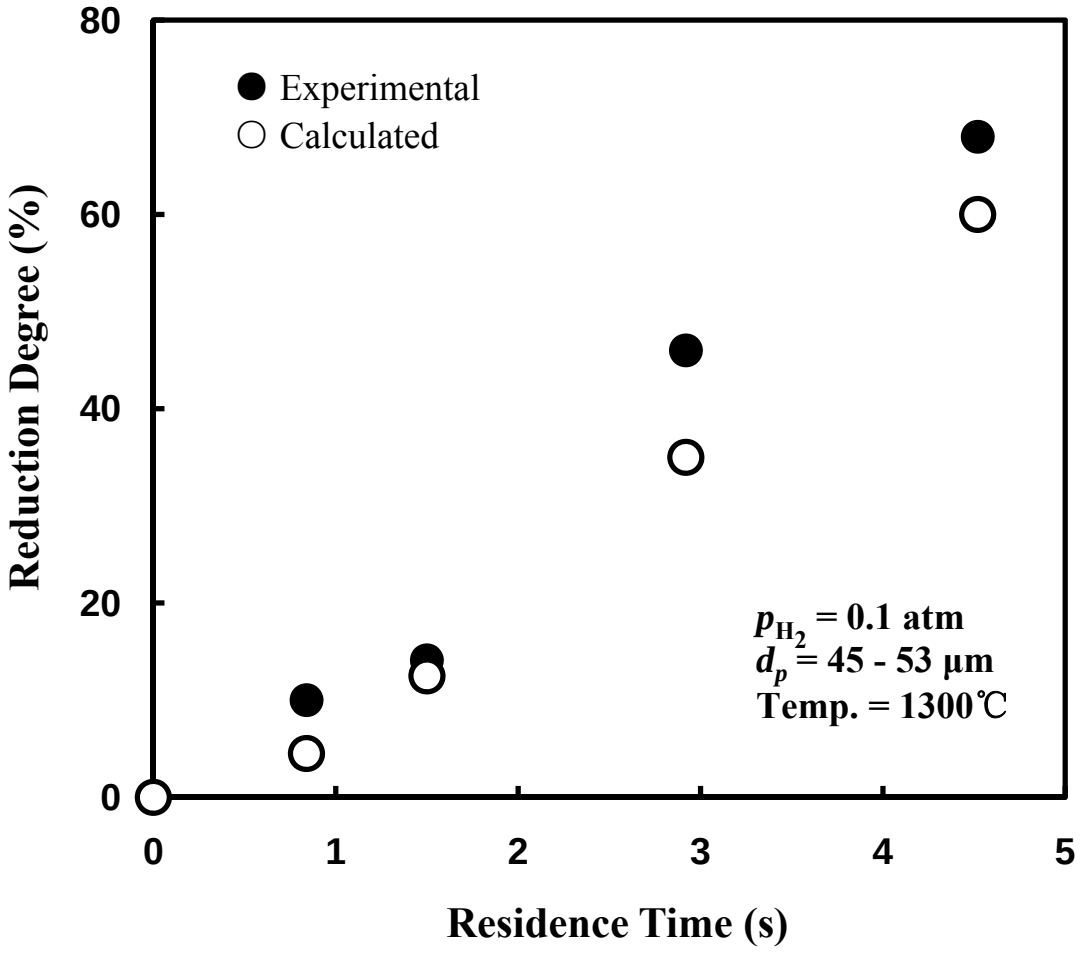

Figure 73. Comparison of experimental and calculated results

p_{H2} = 0.1 atm; d_p = 45 - 53 μm; Temp. = 1300℃

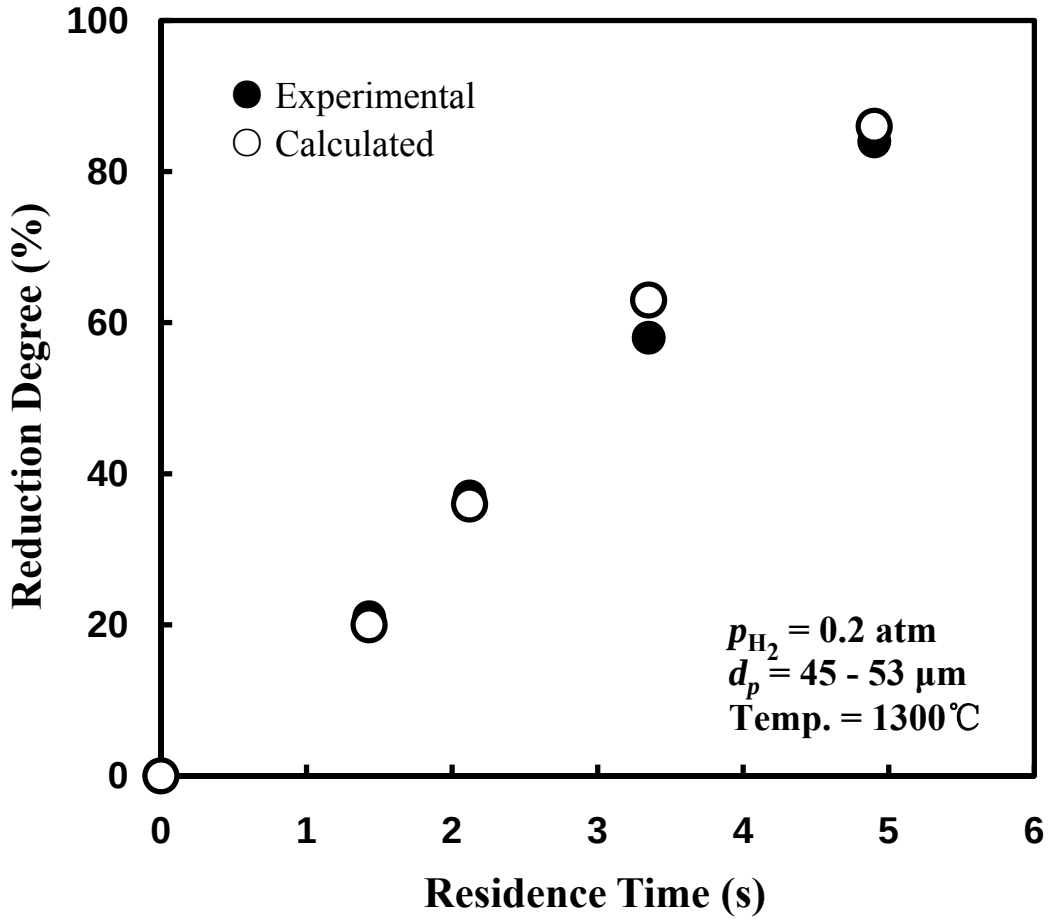

Figure 74. Comparison of experimental and calculated results

p_{H2} = 0.2 atm; d_p = 45 - 53 μm; Temp. = 1300℃

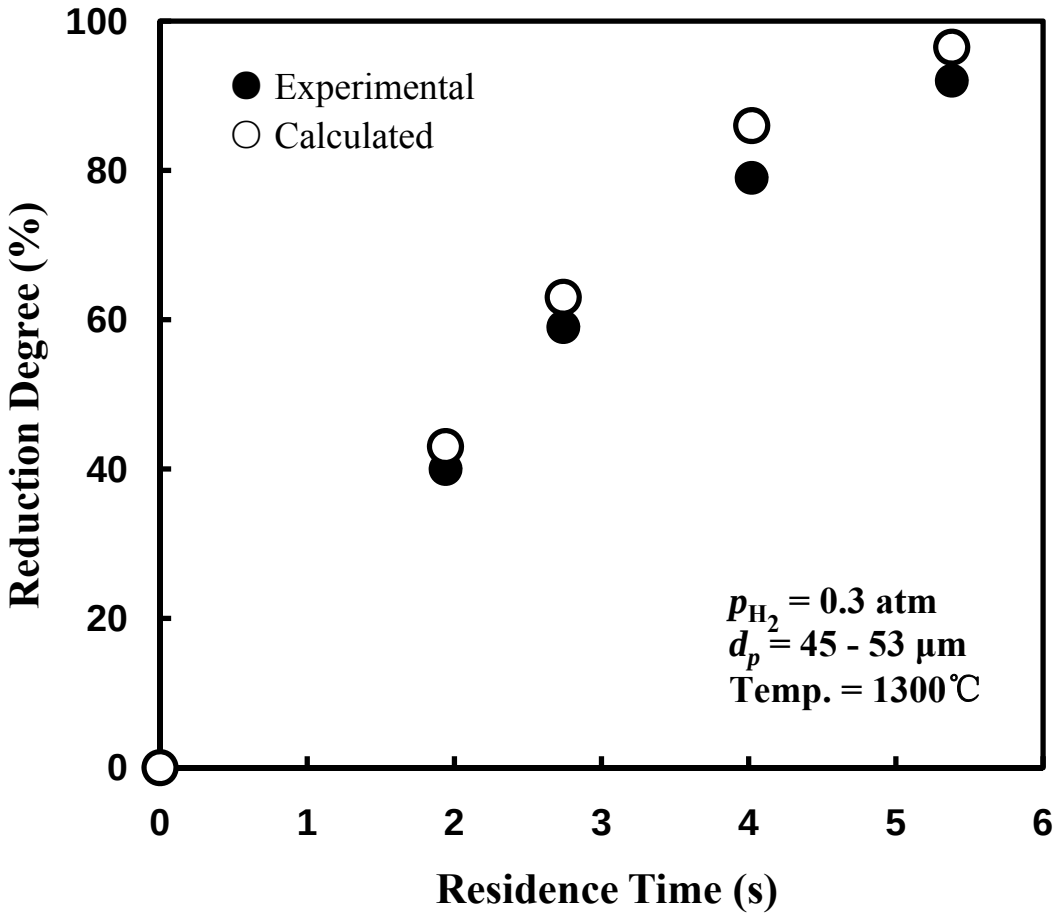

Figure 75. Comparison of experimental and calculated results

p_{H2} = 0.3 atm; d_p = 45 - 53 μm; Temp. = 1300℃

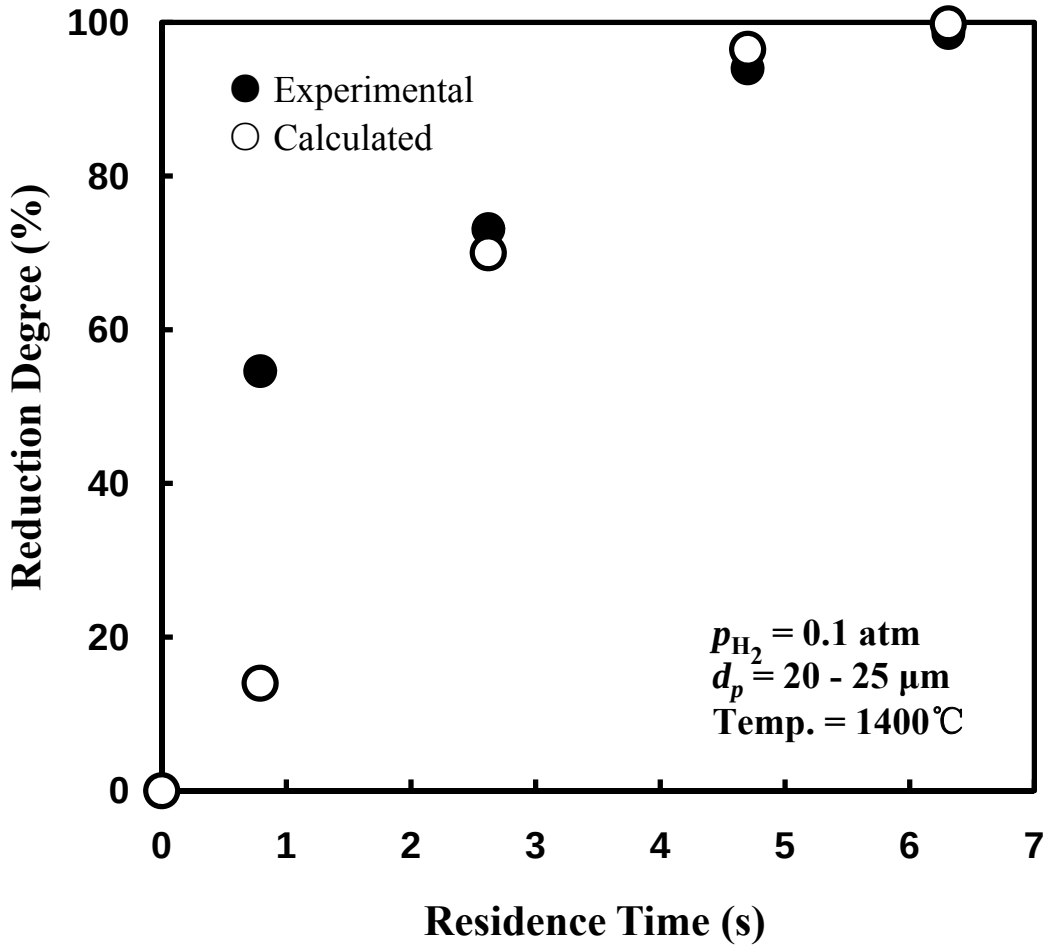

Figure 76. Comparison of experimental and calculated results

p_{H2} = 0.1 atm; d_p = 20 - 25 μm; Temp. = 1400℃

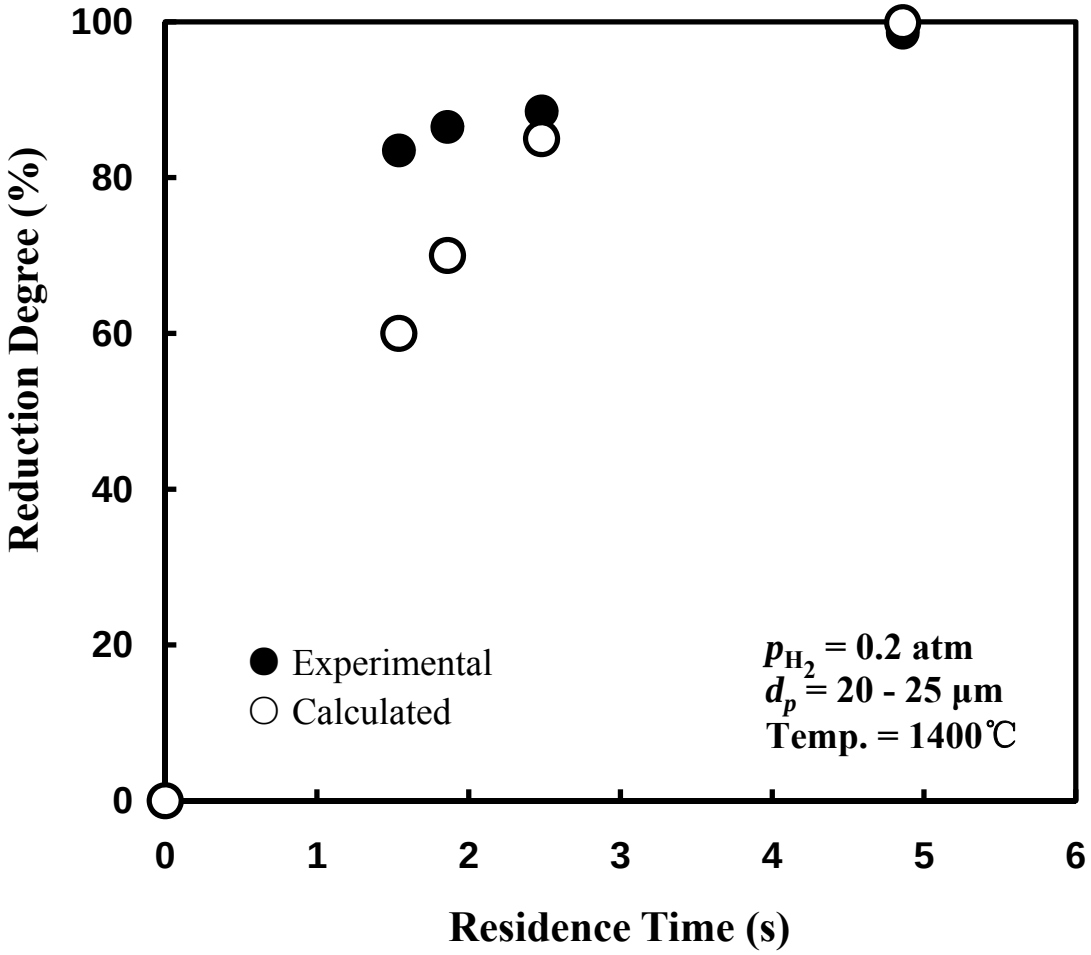

Figure 77. Comparison of experimental and calculated results

p_{H2} = 0.2 atm; d_p = 20 - 25 μm; Temp. = 1400℃

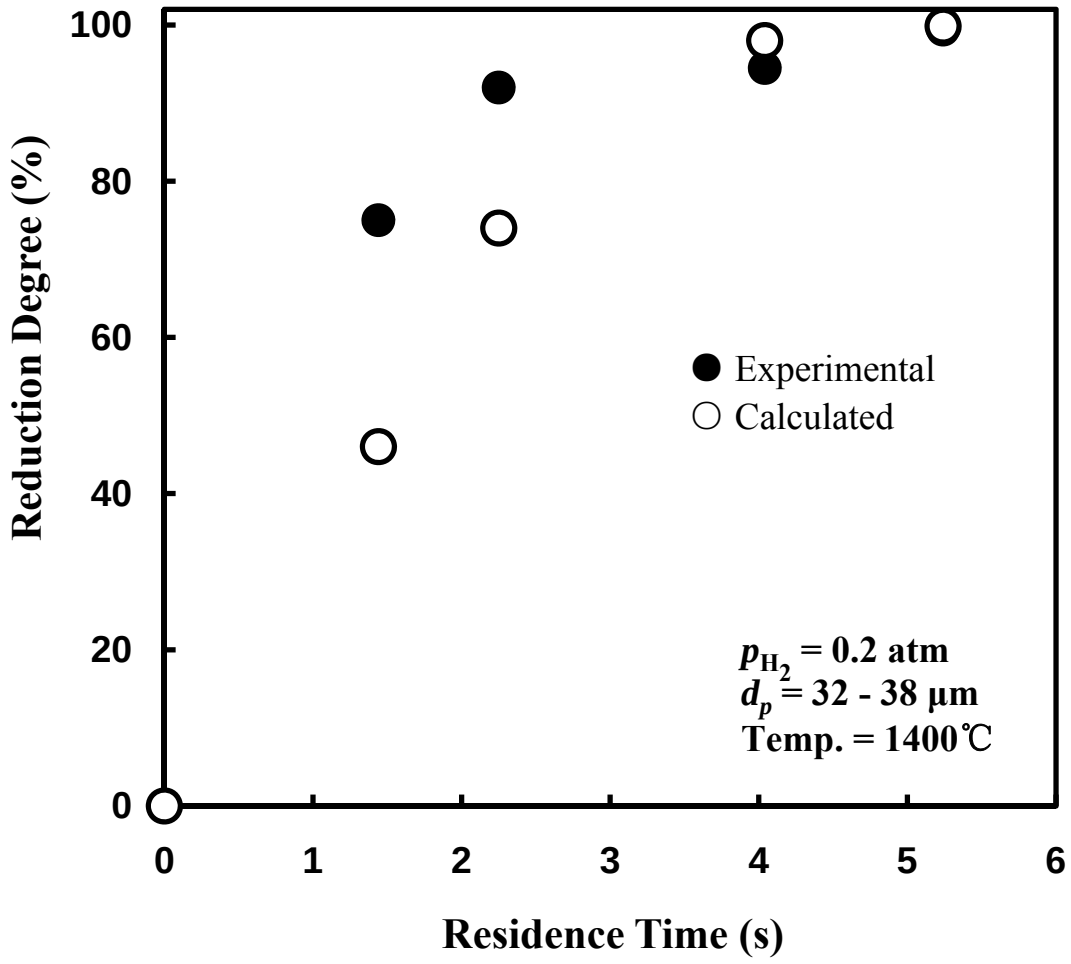

Figure 78. Comparison of experimental and calculated results

p_{H2} = 0.2 atm; d_p = 32 - 38 μm; Temp. = 1400℃

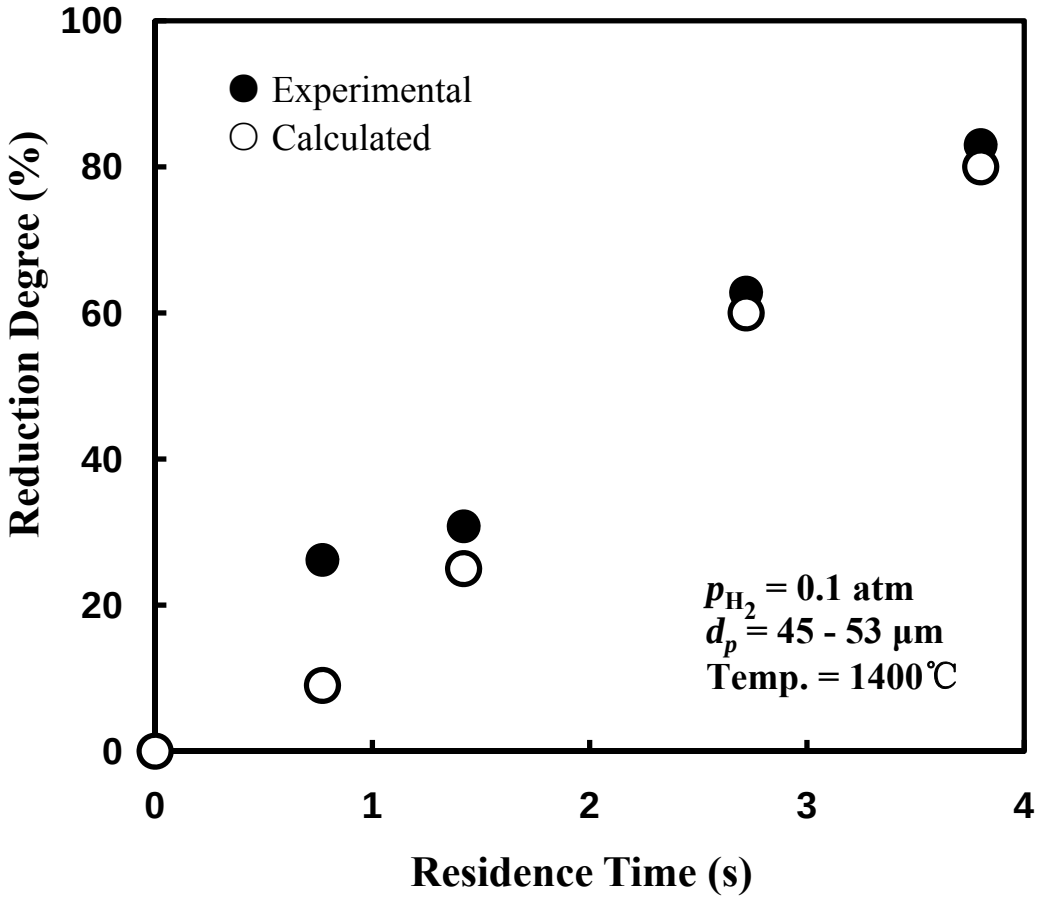

Figure 79. Comparison of experimental and calculated results

p_{H2} = 0.1 atm; d_p = 45 - 53 μm; Temp. = 1400℃

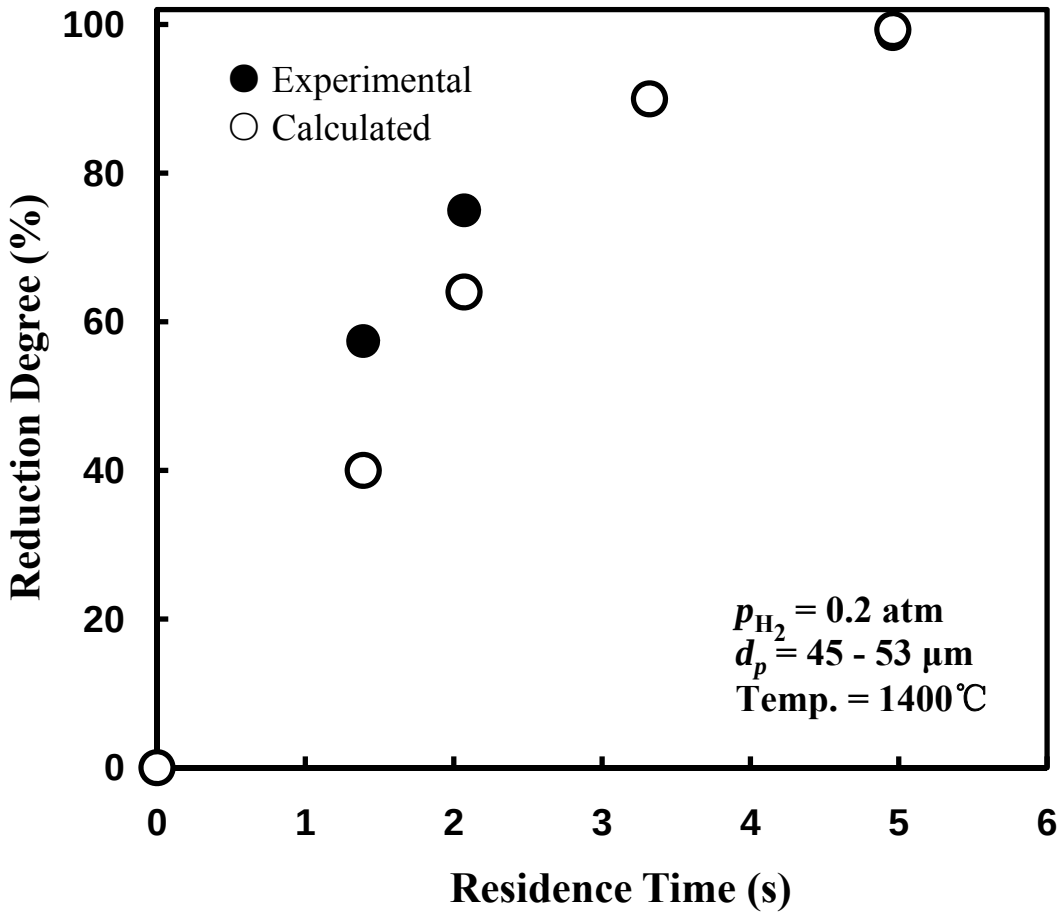

Figure 80. Comparison of experimental and calculated results

p_{H2} = 0.2 atm; d_p = 45 - 53 μm; Temp. = 1400℃

APPENDIX G

COMPLETE EXPERIMENTAL DATA

Table 2. Experimental data for reduction at 1150℃

Residence Time (s)	Particle Size (μm)	Feeding Rate (mg/min)	Excess Hydrogen (%)	Flowrate of H_2 (l/min)	Partial Pressure of H_2 (atm)	Reduction Degree (%)
4.93	20 - 25	599	200	1.933	0.85	54.6
7.39	20 - 25	298	200	0.962	0.85	72
9.27	20 - 25	176	200	0.568	0.85	92.8
12.17	20 - 25	60	200	0.200	0.85	98.4
3.34	32 - 38	595	200	1.920	0.85	62.7
4.07	32 - 38	358	200	1.156	0.85	77.8
4.92	32 - 38	169	200	0.545	0.85	88.1
5.58	32 - 38	60	200	0.200	0.85	96.7
2.23	45 - 53	556	200	1.796	0.85	65.7
2.51	45 - 53	330	200	1.064	0.85	73.1
2.97	45 - 53	60	200	0.194	0.85	88.9

Table 3. Experimental data for reduction of 20 - 25 μm particles at 1200℃

Residence Time (s)	Particle Size (μm)	Feeding Rate (mg/min)	Excess Hydrogen (%)	Flowrate of H_2 (l/min)	Partial Pressure of H_2 (atm)	Reduction Degree (%)
1.64	20 - 25	599	200	1.890	0.2	16.4
3.13	20 - 25	298	200	0.940	0.2	21
6.91	20 - 25	117	200	0.369	0.2	42.8
10.93	20 - 25	62	200	0.196	0.2	81
2.39	20 - 25	599	200	1.890	0.3	24.3
4.46	20 - 25	298	200	0.940	0.3	38.1
6.88	20 - 25	176	200	0.555	0.3	68
9.32	20 - 25	117	200	0.369	0.3	85.4
13.90	20 - 25	62	200	0.196	0.3	96.4

Table 4. Experimental data for reduction of 32 - 38 μm particles at 1200℃

Residence Time (s)	Particle Size (μm)	Feeding Rate (mg/min)	Excess Hydrogen (%)	Flowrate of H_2 (l/min)	Partial Pressure of H_2 (atm)	Reduction Degree (%)
1.53	32 - 38	595	200	1.877	0.2	10
2.80	32 - 38	291	200	0.918	0.2	17.9
4.17	32 - 38	169	200	0.533	0.2	27.3
5.36	32 - 38	115	200	0.363	0.2	45.5
7.34	32 - 38	62	200	0.196	0.2	72
2.17	32 - 38	595	200	1.877	0.3	34.4
3.77	32 - 38	291	200	0.918	0.3	42
5.37	32 - 38	169	200	0.533	0.3	60
8.53	32 - 38	62	200	0.196	0.3	88

Table 5. Experimental data for reduction of 45 - 53 μm particles at 1200℃

Residence Time (s)	Particle Size (μm)	Feeding Rate (mg/min)	Excess Hydrogen (%)	Flowrate of H_2 (l/min)	Partial Pressure of H_2 (atm)	Reduction Degree (%)
1.45	45 - 53	556	200	1.755	0.2	14.6
2.14	45 - 53	330	200	1.040	0.2	17.7
3.34	45 - 53	155	200	0.490	0.2	26.2
4.82	45 - 53	60	200	0.189	0.2	56.9
1.96	45 - 53	556	200	1.755	0.3	26.2
2.75	45 - 53	330	200	1.040	0.3	38.3
3.86	45 - 53	167	200	0.527	0.3	48
5.26	45 - 53	60	200	0.189	0.3	80

Table 6. Experimental data for reduction of 20 - 25 μm particles at 1300℃

Residence Time (s)	Particle Size (μm)	Feeding Rate (mg/min)	Excess Hydrogen (%)	Flowrate of H_2 (l/min)	Partial Pressure of H_2 (atm)	Reduction Degree (%)
0.92	20 - 25	542	200	1.650	0.1	22.9
2.06	20 - 25	233	200	0.709	0.1	25.9
3.66	20 - 25	117	200	0.356	0.1	48
4.77	20 - 25	90	200	0.274	0.1	62
6.56	20 - 25	62	200	0.189	0.1	81
1.58	20 - 25	599	200	1.823	0.2	44.7
3.02	20 - 25	298	200	0.907	0.2	58
4.86	20 - 25	176	200	0.536	0.2	78
6.81	20 - 25	117	200	0.356	0.2	93
2.33	20 - 25	599	200	1.811	0.3	80
4.37	20 - 25	298	200	0.918	0.3	90
6.77	20 - 25	176	200	0.533	0.3	94
9.22	20 - 25	117	200	0.369	0.3	96

Table 7. Experimental data for reduction of 32 - 38 μm particles at 1300℃

Residence Time (s)	Particle Size (μm)	Feeding Rate (mg/min)	Excess Hydrogen (%)	Flowrate of H_2 (l/min)	Partial Pressure of H_2 (atm)	Reduction Degree (%)
1.06	32 - 38	427	200	1.300	0.1	10
1.96	32 - 38	219	200	0.667	0.1	22.4
3.33	32 - 38	115	200	0.350	0.1	45
5.12	32 - 38	62	200	0.189	0.1	72
1.48	32 - 38	595	200	1.811	0.2	24
2.74	32 - 38	291	200	0.886	0.2	45
4.1	32 - 38	169	200	0.514	0.2	70
5.32	32 - 38	115	200	0.350	0.2	82
7.45	32 - 38	62	200	0.189	0.2	97
2.13	32 - 38	595	200	1.811	0.3	56
3.2	32 - 38	358	200	1.090	0.3	75
4.55	32 - 38	219	200	0.667	0.3	85
6.63	32 - 38	115	200	0.350	0.3	99

Table 8. Experimental data for reduction of 45 - 53 μm particles at 1300℃

Residence Time (s)	Particle Size (μm)	Feeding Rate (mg/min)	Excess Hydrogen (%)	Flowrate of H_2 (l/min)	Partial Pressure of H_2 (atm)	Reduction Degree (%)
0.84	45 - 53	504	200	1.534	0.1	10
1.5	45 - 53	271	200	0.826	0.1	14.1
2.92	45 - 53	110	200	0.295	0.1	46
4.52	45 - 53	62	200	0.118	0.1	68
1.43	45 - 53	556	200	1.693	0.2	21
2.12	45 - 53	330	200	1.003	0.2	37
3.35	45 - 53	167	200	0.472	0.2	58
4.90	45 - 53	60	200	0.183	0.2	84
1.94	45 - 53	556	200	1.693	0.3	40
2.74	45 - 53	330	200	1.003	0.3	59
4.02	45 - 53	167	200	0.472	0.3	79
5.38	45 - 53	60	200	0.183	0.3	92

Table 9. Experimental data for reduction at 1400℃

Residence Time (s)	Particle Size (μm)	Feeding Rate (mg/min)	Excess Hydrogen (%)	Flowrate of H_2 (l/min)	Partial Pressure of H_2 (atm)	Reduction Degree (%)
0.79	20 - 25	595	200	1.784	0.1	54.6
2.62	20 - 25	169	200	0.507	0.1	73.1
4.70	20 - 25	88	200	0.264	0.1	94
6.31	20 - 25	62	200	0.186	0.1	98.6
0.76	32 - 38	595	200	1.784	0.1	36.9
1.90	32 - 38	219	200	0.657	0.1	47.6
2.36	32 - 38	169	200	0.507	0.1	54.9
3.22	32 - 38	115	200	0.345	0.1	82.1
5.01	32 - 38	62	200	0.186	0.1	98
1.39	45 - 53	556	200	1.666	0.1	57.4
2.07	45 - 53	330	200	0.987	0.1	75
3.32	45 - 53	167	200	0.464	0.1	90
4.96	45 - 53	60	200	0.180	0.1	98.7

REFERENCES

Al-Kahtany, M. M. and Rao, Y. K., 1980. Reduction of magnetite with hydrogen: Part 1. Intrinsic kinetics. *Ironmaking and Steelmaking*, 7(2), pp. 49-58.

Chatterjee, A., 1993. *Beyond the blast furnace.* Boca Raton, FL: CRC press.

Choi, M. E. and Sohn, H. Y., 2010. Development of green suspension ironmaking technology based on hydrogen reduction of iron oxide concentrate: rate measurement. *Ironmaking and Steelmaking*, 37(2), pp. 81-8.

Choi, M. E., 2010. *Suspension hydrogen reduction of iron ore concentrate.* Ph. D. University of Utah.

Davis, E. G. and Feld, I. L., 1972. *Flash reduction of iron ore (Report No.: 7627)*. US Department of the Interior, Bureau of Mine, Washington, DC, USA.

Durst, F., Ray, S., Ünsal, B., and Bayoumi, O. A., 2005. The development lengths of laminar pipe and channel flows. *Transactions of the ASME*, 127 (6), pp. 1154 - 60.

El-Rahaiby, S. K. and Rao, Y. K., 1979. The kinetics of reduction of iron oxides at moderate temperatures. *Metallurgical Transactions. B*, 10B (2), pp. 257-69.

El-Rahaiby, S. K. and Rao, Y. K., 1980. Kinetics of reduction of wustite with helium-hydrogen gas mixtures at moderate temperatures. *Transactions of the Iron and Steel Institute of Japan*, 20(5), pp. 287-91.

Ezz, S. Y. M. and Wild, R., 1960. The gaseous reduction of fine iron ores. *Journal of Iron and Steel Institute*, 194, pp. 211-21.

Fruehan, R. J., 1998. Fruehan: blast-furnace output will continue to fall. *New Steel*, 14(5), pp. 34-6.

Hayashi, S. and Iguchi, Y., 1994. Hydrogen reduction of liquid iron oxide fines in gas-conveyed systems. *ISIJ International*, 34(7), pp. 555-61.

Hayashi, S. and Iguchi, Y., 1995. Influence of gangue species on hydrogen reduction rate of liquid wustite in gas-conveyed systems. *ISIJ International*, 35(3), pp. 242-9.

Hayes, P. C., 1979. The kinetics of formation of H_2O and CO_2 during iron oxide reduction. *Metallurgical Transactions B*, 10B (June), pp. 211-7.

Iguchi, Y., Ueda, Y., and Hayashi, S., 1994. Improvement in the reducibility of wustite by the intensified surface segregation of calcium ions by the double addition of CaO and SiO_2. *Metallurgical and Materials Transactions B*, 25(B), pp. 741-8.

International Organization for Standardization, 2006. ISO 5416, 3rd ed. *Direct reduced iron-Determination of metallic iron-Bromine-methanol titrimetric method*. Geneva, Switzerland: ISO.

Iguchi, Y. and Inouye, M., 1982. On the rate of the reduction of wustite, magnetite and hematite containing Al_2O_3, CaO and MgO. *Transactions ISIJ,* 22, pp. 679-87.

Lockwood Greene Technologies, 2000. Ironmaking process alternatives screening study. [Online]: U.S. Department of Energy. Available at: <http://www1.eere.energy.gov /industry/steel/pdfs/ironmaking_process.pdf> [Accessed 10 March 2010].

McCune, R. C. and Wynblatt, P., 1983. Calcium segregation to a magnesium oxide (100) surface. *Journal of American Ceramic Society*, 66, pp. 111-7.

Moinpour, M. and Rao, Y. K., 1988. Kinetics of reduction of hematite with helium-hydrogen gas mixtures at moderate temperatures. *Transactions of the Iron and Steel Institute of Japan*, 28(9), pp. 714-20.

Ozawa, M. and Tanaka, M., 1973. Reduction of fine iron ore in gas conveyed systems. *Transactions ISIJ*, 13, pp. 402-8.

Rao, Y. K., 1979. Mechanism and the intrinsic rate of reduction of metallic oxides. *Metallurgical Transactions B*, 10B (June), pp. 243-55.

Rao, Y. K. and Al-Kahtany, M. M., 1984a. Reduction of magnetite with hydrogen: Part 2. gas mixtures. *Ironmaking and Steelmaking*, 11(1), pp. 34-40.

Rao, Y. K. and Al-Kahtany, M. M., 1984b. Reduction of magnetite with hydrogen: Part 3. nucleation and growth. *Ironmaking and Steelmaking*, 11(2), pp. 88-94.

Ritt, A., 2000. Reaching for maximum flexibility. *New Steel*, 16(1), pp. 20-26.

Seetharaman, S. and Sohn, H. Y., 2005. The kinetics of metallurgical reactions. In: S. Seetharaman, ed. *Fundamentals of metallurgy*. Cambridge, ENGLAND: Woodhead Publishing Limited, pp. 299-310.

Shigematsu, N. and Iwai, H., 1989. Effect of CaO added with SiO_2 and/or Al_2O_3 on reduction rate of dense wustite hydrogen. *ISIJ, International,* 29(6), pp. 486-94.

Sohn, H. Y., 2007. Suspension ironmaking technology with greatly reduced energy requirement and CO_2 emission. *Steel Times International*, 31(4), pp. 68-72.

Sohn, H. Y., Choi, M. E., Zhang, Y., Ramos, Joshua E., 2009. Suspension reduction technology for ironmaking with low CO_2 emission and energy requirement. *Iron and Steel Technology (AISI Trans.)*, 6 (8), pp. 158-65.

Szekely, J. and Themelis, N. J., 1971. *Rate phenomena in process metallurgy.* New York: Wiley–Interscience.

Takeuchi, N., Nomura, Y., Ohno, K., Maeda, T., Nishioka, K., and Shimizu, M., 2007. Kinetics analysis of spherical wustite reduction transported with CH_4 gas. *ISIJ International*, 47(3), pp. 386-91.

Tasker, P. W., Colburn, E. A., and Mackrodt, W. C., 1985. Segregation of isovalent impurity cations at the surfaces of magnesia and calcium. *Journal of American Ceramic Society*, 68, pp. 74-80.

Themelis, N. J. and Gauvin, W. H., 1962a. Mechanism of reduction of iron oxides. *Canadian Mining and Metallurgical Bulletin*, 55, pp. 444-56.

Themelis, N. J. and Gauvin, W. H., 1962b. Reduction of iron oxide in gas-conveyed systems. *AIChE Journal*, 8, pp. 437-44.

Themelis, N. J. and Gauvin, W. H., 1963. A generalized rate equation for the reduction of iron oxides. *Transactions of the American Institute of Mining, Metallurgical and Petroleum Engineers*, 227, pp. 290-300.

Tsukihashi, F., Kato, K., Otsuka, K., and Soma, T., 1982. Reduction of molten iron oxide in CO gas conveyed system. *Transactions ISIJ,* 22, pp. 688-95.

Wimmers, O. J., Arnoldy, P., and Moulijn, J. A., 1986. Determination of the reduction mechanism by temperature-programmed reduction: application to small Fe_2O_3 particles. *Journal of Physical Chemistry*, 90(7), pp. 1331-7.

Worldsteel Committee on Economic Studies, 2010. *Steel Statistical Yearbook*. [online] Brussels: Worldsteel Association. Available at: <http://www.worldsteel.org /pictures/publicationfiles/SSY%202010.pdf> [Accessed 9 March 2011].